The activation of TP53 pathway is a therapeutic vulnerability in NUP98::KDM5A^{+} pediatric Acute Megakaryoblastic Leukemia

Dissertation

zur Erlangung des

Doktorgrades der Naturwissenschaften (Dr. rer. nat.)

der

Naturwissenschaftlichen Fakultät I –Biowissenschaften-
der Martin-Luther-Universität
Halle-Wittenberg

vorgelegt von

Herrn Luca Nunzio Cifarelli

Erstgutachter: Prof. Dr. Stefan Hüttelmaier

Zweitgutachterin: Prof. Dr. Dirk Heckl

Drittgutachter: PD Dr. Jessica Höll

Verteidigungsdatum: 16.12.2025

“Un paese ci vuole, non fosse che per il gusto di andarsene via. Un paese vuol dire non essere soli, sapere che nella gente, nelle piante, nella terra c'è qualcosa di tuo, che anche quando non ci sei, resta ad aspettarti.”

„Man braucht ein Land, und sei es nur, um wegzukommen. Ein Land bedeutet, nicht allein zu sein, zu wissen, dass in den Menschen, in den Pflanzen, in der Erde etwas von dir ist, dass es, auch wenn du nicht da bist, auf dich wartet.“

(Cesare Pavese, 1908-1950)

Table of Contents

Abstract ... 1

Zusammenfassung ... 3

1. Introduction ... 5

1.1. Hematopoiesis ... 5

1.1.1. From the classic hierarchy to the modern plastic model ... 5

1.1.2. Ontogeny of fetal and adult hematopoiesis ... 6

1.1.3. Characteristics of fetal and adult HSPCs ... 8

1.1.4. Molecular regulation of hematopoietic fate decision ... 9

1.2. Acute myeloid leukemia ... 10

1.2.1. Pathophysiology and classification ... 10

1.2.2. Pediatric acute myeloid leukemia ... 11

1.2.3. Therapies for pediatric AML ... 13

1.3. Acute megakaryoblastic leukemia ... 14

1.3.1. NUP98 fusion oncogenes ... 15

1.3.2. Mechanism of NUP98 fusion-mediated leukemogenesis ... 16

1.3.3. Potential therapeutic strategy for NUP98-rearranged leukemia ... 17

1.3.4. NUP98::KDM5A translocation ... 18

1.4. TRIP13 ... 20

1.4.1. Functions of TRIP13 ... 20

1.4.2. TRIP13 in cancer ... 22

2. Aims of the study ... 24

3. Material and methods ... 25

3.1. Materials ... 25

3.1.1. List of equipment and materials ... 25

3.1.2. Vectors ... 33

3.1.3. cDNAs ... 34

3.1.4. Oligonucleotides and primers ... 35

3.1.5. Cell culture media ... 38

3.1.5.1. Human cell lines ... 38

3.1.5.2. Murine primary cells ... 39

3.1.5.3. Human primary cells ... 39

3.1.6. Animal models ... 39

3.1.7. Softwares and online tools ... 39

3.2. Methods ... 40

3.2.1. Molecular biology and biochemistry 40
3.2.1.1. Cloning 40
3.2.1.2. sgRNA-negative selection screen 40
3.2.1.3. Western Blot 40
3.2.1.4. Co-Immunoprecipitation and Mass Spectrometry 41
3.2.2. Cell biology 41
3.2.2.1. Maintenance of cell lines and primary cells 41
3.2.2.2. Freezing and thawing of cells 41
3.2.2.3. Isolation of mFL-HSPCs 41
3.2.2.4. Isolation of mBM-HSPCs 42
3.2.2.5. Isolation of human HSPCs 42
3.2.2.6. Transfection 42
3.2.2.7. Virus concentration 43
3.2.2.8. Transduction 43
3.2.2.9. sgRNA-negative selection screen 43
3.2.2.10. Proliferation and rescue assays 44
3.2.2.11. Drug assays 44
3.2.2.12. Flow cytometry and Sorting 44
3.2.2.13. Apoptosis and Cell cycle assays 44
3.2.2.14. Cytospins 44
3.2.3. Animal Studies 44
3.2.3.1. Transplantations 45
3.2.3.2. Analysis of leukemic mice 45
3.2.4. Quantification and statistical analysis 45
3.2.4.1. sgRNA quantification: sgRNA negative selection screen 45
3.2.4.2. Gene Quantification: RNA-sequencing 45
3.2.4.3. Gene set enrichment analysis (GSEA) 46
3.2.4.4. Drug assays: Synergy effect 46
3.2.4.5. Mass Spectrometry 46
3.2.4.6. Statistical analysis 46
4. Results 47
4.1. Modeling NUP98::KDM5A^{+} AMKL 47
4.1.1. NUP98::KDM5A induces an aggressive leukemia in mFL-HSPCs 47
4.1.2. NUP98::KDM5A transforms only human fetal HSPCs 50
4.2. CRISPR-Cas9 screen reveals TRIP13 dependency in fetal NUP98::KDM5A^{+} leukemia 52
4.3. *TRIP13* is a molecular dependency in NUP98::KDM5A^{+} AMKL 55

4.3.1. *Trip13* loss induces higher cell death in a fetal context in vitro 55
4.3.2. *Trip13* knockout activates TP53 pathway in fetal NUP98::KDM5A$^+$ cells 56
4.3.3. TRIP13 interacts with PPM1D/WIP1 to repress TP53 pathway 58
4.4. Targeting the TRIP13/TP53-axis as a novel treatment approach for NUP98:: KDM5A$^+$ AMKL 61
4.4.1. Loss of *Trip13* shows sensitivity in NUP98::KDM5A$^+$ AMKL *in vivo* 61
4.4.2. Pharmacological TRIP13 inhibition as treatment of NUP98::KDM5A$^+$ AMKL *in vitro* ... 61
4.5. Pharmacological TP53 activation as a therapeutic strategy for NUP98::KDM5A$^+$ AMKL.. 65
5. Discussion 70
5.1. Modeling NUP98::KDM5A$^+$ leukemia remains a challenge 70
5.2. The fetal-enriched *TRIP13* gene is a molecular vulnerability of NUP98::KDM5A$^+$ leukemia 71
5.3. TRIP13 and PPM1D repress the TP53 pathway in NUP98::KDM5A$^+$ leukemia 73
5.4. TRIP13 protein interactome reveals several TP53 regulators 74
5.5. TP53 re-activation is a vulnerability in NUP98::KDM5A$^+$ leukemia 76
5.6. TP53 re-activation is a therapeutic approach for NUP98::KDM5A$^+$ leukemia 77
6. Conclusion 79
7. Outlook and future implications 80
8. References IV
9. Appendix XIX
9.1. List of figures XIX
9.2. List of tables XX
9.3. List of abbreviations XX
9.4. List of publications and conferences XXII
9.5. Curriculum Vitae XXIII
9.6. Declaration XXIV

Abstract

Chromosomal rearrangements have been identified as the main drivers of pediatric Acute Megakaryoblastic Leukemia (AMKL). The t(11;12) involving *NUP98* and *KDM5A/JARID1A* (NUP98::KDM5A) accounts for approximately 15% of pediatric AMKL cases and correlates with poor prognosis. An important aspect of AMKL is the strong enrichment in pediatric patients with frequent occurrence in infants (< 2 years of age). In this study, we aimed to unravel the contribution of cellular ontogeny in the initiation of NUP98::KDM5A-driven AMKL and highlight *TRIP13* as a fetal-enriched NUP98::KDM5A-specific vulnerability acting through TP53 pathway.

To investigate the important role played by the fetal cell-of-origin of NUP98::KDM5A-driven leukemia, we transduced murine hematopoietic stem and progenitor cells (HSPCs) originating from fetal liver (mFL-HSPCs) and bone marrow of adult mice (mBM-HSPCs) with a lentiviral vector overexpressing the cDNA encoding human NUP98::KDM5A. Our experimental setup revealed that fetal NUP98::KDM5A$^+$ cells acquire a more aggressive leukemic phenotype compared to adult NUP98::KDM5A$^+$ cells, despite similar transduction rates. Moreover, transcriptome analysis highlighted that the fetal gene signatures were maintained in fetal NUP98::KDM5A$^+$ cells rather than in adult NUP98::KDM5A$^+$ cells.

Based on these findings, we supposed that the fetal gene programs might have a catalytic effect on NUP98::KDM5A-mediated transformation. For this reason, we performed a CRISPR-Cas9 dropout screening targeting fetal expression signatures with a library probing 880 fetal enriched genes found to be deregulated when comparing fetal versus adult murine and human primary HSPCs. By comparing our findings with two other fetal liver-derived leukemia models – representing myeloid leukemia associated with Down Syndrome (ML-DS) and familial platelet disorder with predisposition to AML (FPD-AML) –, we identified *TRIP13* as a high-confidence candidate gene with exceptional dependency in fetal NUP98::KDM5A$^+$ AMKL. The comparing between human AML cell lines and NUP98::KDM5A-overexpressing human HSPCs originating from fetal liver (hFL-HSPCs) further confirmed the selective targeting of NUP98::KDM5A-driven cells by TRIP13 loss.

To explore the molecular mechanism of *TRIP13* sensitivity, we performed RNA-sequencing. Surprisingly, gene set expression analysis (GSEA) revealed only one highly significantly enriched pathway namely TP53 signaling. Functionally, loss of *Trip13* led to a dramatic upregulation of TP53 protein and cellular response in fetal NUP98::KDM5A$^+$ cells. Rescue experiments of *Trip13* knockout in fetal NUP98::KDM5A$^+$ cells further supported this finding: the massive depletion upon loss of *Trip13* was completely reverted by either re-expression of a human TRIP13 cDNA or by knockout of murine *TP53*. Of note, neither activation of TP53 signaling nor cell depletion was seen in healthy hematopoietic cells from fetal liver upon *Trip13* perturbation and DNA damage has been ruled out as the source of TP53 activation. We thus aimed to identify the underlying mechanisms of TRIP13-mediated TP53 regulation and identified WIP1/PPM1D, a direct regulator of TP53 activity and TP53 abundance through MDM2, as a direct binding partner of TRIP13 and as mediator of TRIP13-dependent TP53

control. Functionally, loss of *Ppm1d* phenocopied the effect of *Trip13* loss in fetal NUP98::KDM5A$^+$ cells.

Finally, we aimed to leverage TRIP13-mediated dependency on TP53 pathway therapeutically. To this end, we first explored *Trip13*-depletion in an *in vivo* setting. In a fluorescence-based competitive transplantation assay, *Trip13*-ablated leukemic blasts were significantly diminished in the bone marrow of recipient mice after 4 weeks. Next, fetal NUP98::KDM5A$^+$ cells were treated with the TRIP13 inhibitor DCZ0415. Similarly to genetic *TRIP13* ablation, fetal NUP98::KDM5A$^+$ cells showed a significantly higher sensitivity to the drug compared to models of ML-DS, FPD-AML, and healthy HSPCs. To exploit our mechanistic knowledge on TRIP13 ablation-mediated TP53 activation, we combined DCZ0415 with the MDM2 inhibitor Idasanutlin. In line with our mechanistic data, the combination of DCZ0415 with Idasanutlin showed a high synergistic effect.

Due to translational limitations of DCZ0415, we further explored the TP53 pathway to identify combinatorial dependencies enabling its reactivation and being exploitable with FDA-approved drugs. Using a CRISPR-Cas9 screening probing the gene-network and protein-network of TP53 in *Trip13*-depleted fetal NUP98::KDM5A$^+$ cells we found that loss of *Bcl-xl* synergizes with *Trip13* loss. Conversely, murine *TP53* or *Bbc3/Puma* ablation rescued the *Trip13* loss. Based on these findings, we reasoned that combined pharmacological inhibition of MDM2 (Idasanutlin) and BCL2/BCL-XL (Navitoclax), in conjunction with the broadly applicable chemotherapy sensitizer Azacytidine, may hold a novel treatment approach for NUP98::KDM5A$^+$ AMKL. Compared to modest response on single-agent treatments, this combination demonstrated highly synergistic induction of NUP98::KDM5A-leukemic cell death.

In conclusion, by exploring the contribution of the fetal cell-of-origin of NUP98::KDM5A-driven AMKL, our study uncovers TRIP13/PPM1D/TP53 axis as a molecular vulnerability, which we leveraged for a mechanism-driven treatment approach with Idasanutlin/Navitoclax /Azacytidine as a tailored therapeutic strategy for the treatment of high-risk pediatric AMKL.

Zusammenfassung

Chromosomale Umlagerungen wurden als Haupttreiber der pädiatrischen Akuten Megakaryoblastischen Leukämie (AMKL) identifiziert. Die t(11;12)-Translokation, die *NUP98* und *KDM5A/JARID1A* (NUP98::KDM5A) betrifft, macht etwa 15% der pädiatrischen AMKL-Fälle aus und korreliert mit einer schlechten Prognose. Ein wichtiger Aspekt der AMKL ist die starke Anreicherung bei pädiatrischen Patienten mit häufigem Auftreten bei Säuglingen (< 2 Jahre). In dieser Studie zielten wir darauf ab, den Beitrag der zellulären Ontogenese bei der Initiierung der NUP98::KDM5A-getriebenen AMKL zu entschlüsseln und *TRIP13* als eine fetal angereicherte, NUP98::KDM5A-spezifische Vulnerabilität hervorzuheben, die über den TP53-Signalweg wirkt.

Um die wichtige Rolle der fetalen Ursprungszelle der NUP98::KDM5A-getriebenen Leukämie zu untersuchen, transduzierten wir murine hämatopoetische Stamm- und Vorläuferzellen (HSPCs) aus der fetalen Leber (mFL-HSPCs) und dem Knochenmark erwachsener Mäuse (mBM-HSPCs) mit einem lentiviralen Vektor, der die cDNA für humanes NUP98::KDM5A überexprimiert. Unser experimenteller Aufbau zeigte, dass fetale NUP98::KDM5A$^+$ Zellen trotz ähnlicher Transduktionsraten einen aggressiveren leukämischen Phänotyp annehmen als adulte NUP98::KDM5A$^+$ Zellen. Darüber hinaus zeigte die Transkriptomanalyse, dass die fetalen Gensignaturen in fetalen NUP98::KDM5A$^+$ Zellen eher erhalten blieben als in adulten NUP98::KDM5A$^+$ Zellen.

Basierend auf diesen Erkenntnissen vermuteten wir, dass die fetalen Genprogramme einen katalytischen Effekt auf die NUP98::KDM5A-vermittelte Transformation haben könnten. Daher führten wir ein auf fetale Expressionssignaturen abzielendes CRISPR-Cas9-Dropout-Screening durch, mit einer Bibliothek, die 880 fetal angereicherte Gene untersuchte, die sich beim Vergleich fetaler *versus* adulter muriner und humaner primärer HSPCs als dereguliert erwiesen. Beim Vergleich unserer Ergebnisse mit zwei anderen aus der fetalen Leber abgeleiteten Leukämiemodellen – und zwar die myeloische Leukämie assoziiert mit Down-Syndrom (ML-DS) und die familiäre Thrombozytopenie mit Prädisposition für AML (FPD-AML) – identifizierten wir *TRIP13* als hochrangiges Kandidatengen mit außergewöhnlicher Abhängigkeit in fetaler NUP98::KDM5A$^+$ AMKL. Der Vergleich zwischen humanen AML-Zelllinien und NUP98::KDM5A-überexprimierenden humanen HSPCs aus der fetalen Leber (hFL-HSPCs) bestätigte weiter die selektive Targetierung von NUP98::KDM5A-getriebenen Zellen durch TRIP13-Verlust.

Um den molekularen Mechanismus der *TRIP13*-Sensitivität zu untersuchen, führten wir eine RNA-Sequenzierung durch. Überraschenderweise zeigte die Genset-Expressionsanalyse (GSEA) nur einen hochsignifikant angereicherten Signalweg, nämlich den TP53-Signalweg. Funktionell führte der Verlust von *Trip13* zu einer dramatischen Hochregulierung des TP53-Proteins und der zellulären Antwort in fetalen NUP98::KDM5A$^+$ Zellen. Rescue-Experimente des *Trip13*-Knockouts in fetalen NUP98::KDM5A$^+$ Zellen unterstützten diesen Befund weiter: Die massive Depletion nach Verlust von *Trip13* wurde entweder durch Re-Expression einer humanen TRIP13 cDNA oder durch Knockout des murinen TP53 vollständig revertiert.

Bemerkenswert ist, dass weder eine Aktivierung des TP53-Signalwegs noch eine Zelldepletion in gesunden hämatopoetischen Zellen aus der fetalen Leber nach *Trip13*-Störung beobachtet wurde, und DNA-Schäden als Quelle der TP53-Aktivierung ausgeschlossen wurden. Wir zielten daher darauf ab, die zugrundeliegenden Mechanismen der TRIP13-vermittelten TP53-Regulation zu identifizieren und identifizierten WIP1/PPM1D, einen direkten Regulator der TP53-Aktivität und TP53-Abundanz durch MDM2, als direkten Bindungspartner von TRIP13 und als Vermittler der TRIP13-abhängigen TP53-Kontrolle. Funktionell kopierte der Verlust von *Ppm1d* den Effekt des *Trip13*-Verlusts in fetalen NUP98::KDM5A$^+$ Zellen.

Schließlich zielten wir darauf ab, die TRIP13-vermittelte Abhängigkeit vom TP53-Signalweg therapeutisch zu nutzen. Zu diesem Zweck untersuchten wir zunächst die Trip13-Depletion in einem *in vivo* Setting. In einem fluoreszenzbasierten kompetitiven Transplantationsassay waren *Trip13*-ablatierte leukämische Blasten nach vier Wochen im Knochenmark der Empfängermäuse signifikant vermindert. Als nächstes wurden fetale NUP98::KDM5A$^+$ Zellen mit dem TRIP13-Inhibitor DCZ0415 behandelt. Ähnlich wie bei der genetischen TRIP13-Ablation zeigten fetale NUP98::KDM5A$^+$ Zellen eine signifikant höhere Empfindlichkeit gegenüber dem Medikament im Vergleich zu Modellen von ML-DS, FPD-AML und gesunden HSPCs. Um unser mechanistisches Wissen über die TRIP13-Ablations-vermittelte TP53-Aktivierung zu nutzen, kombinierten wir DCZ0415 mit dem MDM2-Inhibitor Idasanutlin. In Übereinstimmung mit unseren mechanistischen Daten zeigte die Kombination von DCZ0415 mit Idasanutlin einen hohen synergistischen Effekt.

Aufgrund der translationalen Einschränkungen von DCZ0415 untersuchten wir den TP53-Signalweg weiter, um kombinatorische Abhängigkeiten zu identifizieren, die seine Reaktivierung ermöglichen und mit FDA-zugelassenen Medikamenten nutzbar sind. Mittels eines CRISPR-Cas9-Screenings, das das Gen- und Protein-Netzwerk von TP53 in Trip13-depletierten fetalen NUP98::KDM5A$^+$ Zellen untersuchte, fanden wir heraus, dass der Verlust von *BCL-X$_L$* mit dem Verlust von *Trip13* synergistisch wirkt. Umgekehrt rettete die Ablation von murinem *TP53* oder *Bbc3/Puma* den *Trip13*-Verlust. Basierend auf diesen Erkenntnissen folgerten wir, dass die kombinierte pharmakologische Hemmung von MDM2 (Idasanutlin) und BCL2/BCL-X$_L$ (Navitoclax) in Verbindung mit dem breit anwendbaren Chemotherapie-Sensibilisator Azacytidin einen neuartigen Behandlungsansatz für NUP98::KDM5A$^+$ AMKL darstellen könnte. Im Vergleich zu einer moderaten Antwort auf Einzelwirkstoffbehandlungen zeigte diese Kombination eine hochsynergistische Induktion des Zelltods von NUP98::KDM5A-Leukämiezellen.

Zusammenfassend deckt unsere Studie durch die Untersuchung des Beitrags der fetalen Ursprungszelle der NUP98::KDM5A-getriebenen AMKL die TRIP13/PPM1D/TP53-Achse als molekulare Vulnerabilität auf, die wir für einen Mechanismus-basierten Behandlungsansatz mit Idasanutlin/Navitoclax/Azacytidin als maßgeschneiderte therapeutische Strategie für die Behandlung von pädiatrischer Hochrisiko-AMKL nutzten.

1. Introduction

1.1. Hematopoiesis

1.1.1. From the classic hierarchy to the modern plastic model

Blood is a highly regenerative and adaptable tissue, with millions of new blood cells replacing old ones every second throughout life (Rieger and Schroeder 2012).

Hematopoiesis is the process of the blood system, which generates all differentiated and functional blood cells, responsible to fulfill multiple tasks such as immune defense, gas transport, blood clotting and wound-healing (Orkin 1995). Due to a short life, mature fully differentiated blood cells of all lineages are regenerated by the hematopoietic system throughout life (Orkin and Zon 2008).

In the early 1960, transplantation experiments demonstrated the existence of an extraordinary cell (Wang, Doedens et al. 1997), which was capable of completely restoring the entire blood system (Till and Mc 1961, Becker, Mc et al. 1963, Wang, Doedens et al. 1997). This finding encouraged the development of clonal in vitro assays. Along with the advent of numerous cell surface antibodies and flow sorting (Morrison and Weissman 1994, Osawa, Hanada et al. 1996, Kondo, Weissman et al. 1997, Akashi, Traver et al. 2000, Kiel, Iwashita et al. 2005, Inlay, Bhattacharya et al. 2009), this has led to our current detailed view of the blood system as a developmental hierarchy, with the hematopoietic stem cells (HSCs) at the top and fully differentiated cells at the bottom (Orkin 2000) (Figure 1).

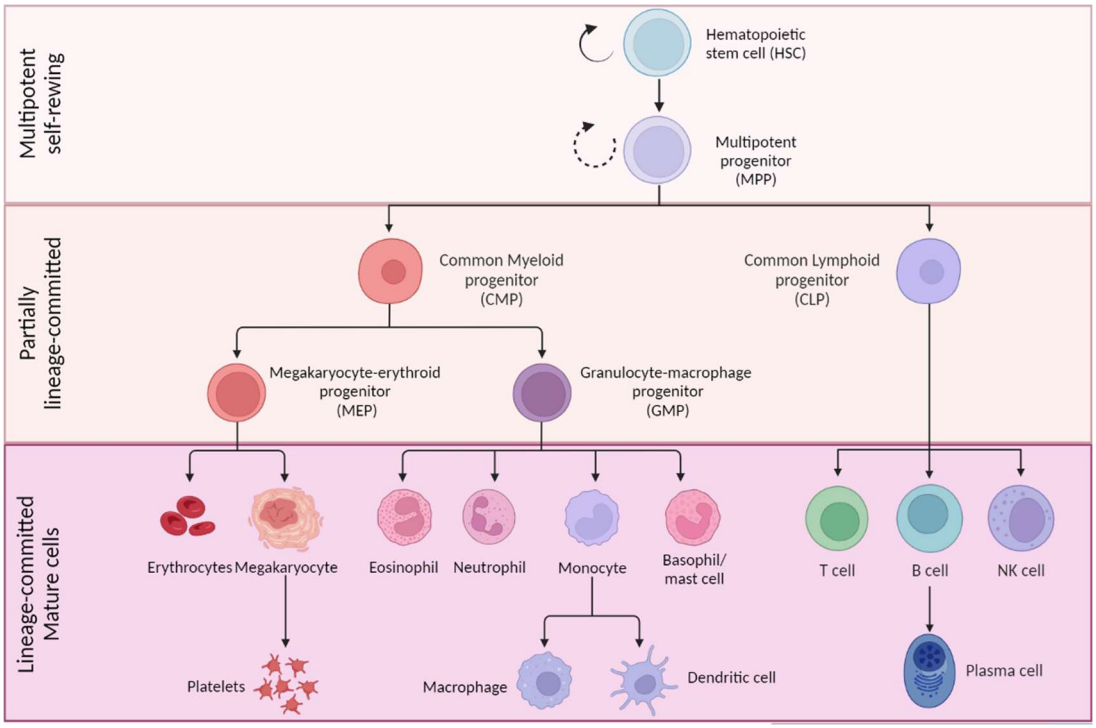

Figure 1 Tree-like hierarchy model representing the differentiation pathway of HSCs to originate the several fully differentiated mature cells, which constitute blood. Created in BioRender.com

HSCs have been defined on the basis of two essential abilities: multipotent differentiation and self-renewal, or generation of daughter stem cells (Orkin 2000). On the other hand,

progenitors are defined by limited lineage differentiation capacities and the absence of self-renewal (Cheng, Zheng et al. 2019).

The differentiation of HSCS into determined terminal mature cells is based on the tree-like hierarchy model (Figure 1). Along the tree-like hierarchy model, the differentiating cell reduces its multipotency, and acquires characteristics and functions of mature blood cells (Orkin 2000). Classically, HSC populations can be divided based on their reconstitution capacity into two subpopulations: long-term (LT)-HSCs and short-term (ST)-HSCs (Morrison, Wandycz et al. 1997, Pietras, Reynaud et al. 2015). LT-HSCs are a rare and quiescent population in the bone marrow (BM) and have a longer reconstitution capacity compared to ST-HSCs. LT-HSCs differentiate into ST-HSCs, which subsequently differentiate into multipotent progenitors (MPPs), losing their self-renewal ability (Morrison, Wandycz et al. 1997, Yang, Bryder et al. 2005). This stage defines the first lineage commitment, which bifurcates into lymphoid and myeloid common progenitors (CLPs and CMPs, respectively). The second bifurcation occurs at CMPs, which gives rise to granulocyte-monocyte and megakaryocyte-erythrocyte progenitors (GMPs and MEPs, respectively). On the other hand, CLPs further generate all lymphoid cells such as B-, T- and NK-cells (Kondo, Weissman et al. 1997, Akashi, Traver et al. 2000).

However, recent evidence suggests that the traditional model of hematopoietic differentiation oversimplifies a complex mechanism (Cheng, Zheng et al. 2019). Notably, single-cell omics analysis recently demonstrated the heterogeneity in the HSC population being more lineage-biased early on than initially thought (Wilson, Kent et al. 2015, Nestorowa, Hamey et al. 2016). Additional HSC populations have been identified (Benveniste, Frelin et al. 2010), and the MPP population has been further subdivided based on several distinct features (Wilson, Laurenti et al. 2008, Pietras, Reynaud et al. 2015). Myeloid progenitor populations have also been revealed to be more heterogeneous than initially believed, based on several new identified intermediate progenitors (Pronk, Rossi et al. 2007). The origin of megakaryocytes has been debated, with some studies suggesting a closer relationship between HSCs and megakaryocytes (Pronk, Rossi et al. 2007, Yamamoto, Morita et al. 2013). In line with the work discussed above, studies based on transcriptomes of HSCs and MEPs have challenged the classic view of MEPs as a true precursor for megakaryocytes, demonstrating that they were mainly differentiated from CMPs (Paul, Arkin et al. 2015, Nestorowa, Hamey et al. 2016).

Overall, hematopoietic differentiation nowadays results to be a much more continuous and biased process than initially described (Velten, Haas et al. 2017, Buenrostro, Corces et al. 2018), meaning that HSCs develop biases very early on toward certain cell lineages and differentiate continuously without going through multiple defined progenitor stages.

1.1.2. Ontogeny of fetal and adult hematopoiesis

The development of the human hematopoietic system during embryogenesis is a complex and dynamic process that occurs in multiple waves and anatomical sites, while the hematopoiesis in adults takes place in the BM (Dzierzak and Bigas 2018, Bigas, Galán Palma et al. 2022, Calvanese and Mikkola 2023).

In mammals, fetal blood development classically involves two waves: the primitive wave and the definitive wave (Jagannathan-Bogdan and Zon 2013). The first wave gives rise to primitive blood cells with the aim to facilitate tissue oxygenation as the embryo undergoes rapid growth (Orkin and Zon 2008). The latter wave produces self-renewing HSCs capable of giving rise to differentiated blood cells for the lifetime (Jagannathan-Bogdan and Zon 2013). However, the genesis of the human embryonic hematopoiesis cannot simply be explained by only two waves, since recent studies have shown the presence of a transient/intermediate wave (Dzierzak and Bigas 2018).

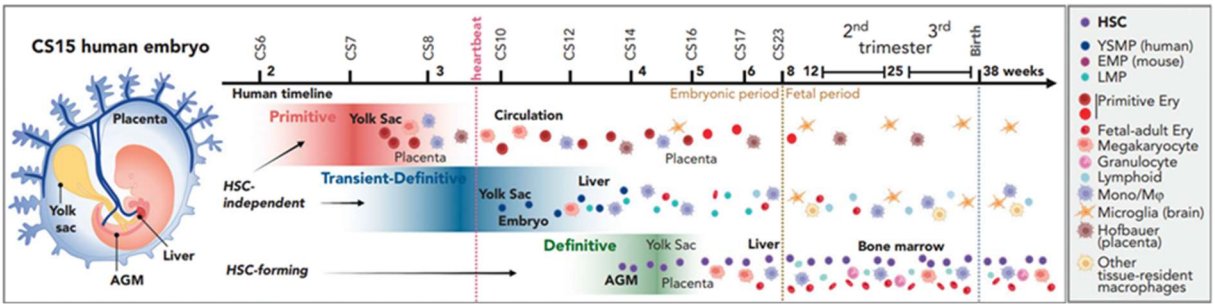

Figure 2 The developmental timeline of hematopoiesis in the CS15 (Carnegie stages 15) human embryo. Hematopoiesis in each location favors the production of specific blood lineages indicated in the right box. Adapted from Calvanese and Mikkola 2023 with permission.

During the first wave, the primitive blood-forming cells originate from the blood islands of the extraembryonic yolk sac at Carnegie stages 7-8 (CS7-8) of human development (Mikkola and Orkin 2006, Ivanovs, Rybtsov et al. 2017) and produce primitive erythroblasts, megakaryocytes, and macrophages (Palis 2016, Ivanovs, Rybtsov et al. 2017, Dzierzak and Bigas 2018, Iturri, Freyer et al. 2021). When the heartbeat begins (CS10), the primitive erythroblasts enter circulation to reach the allantois and placenta, where they enter in contact with macrophages and are replaced by fetal erythroid cells (Dzierzak and Bigas 2018, Calvanese and Mikkola 2023). However, the first wave is transitory and these primitive hematopoietic cells are not pluripotent and do not have self-renewal capability (Jagannathan-Bogdan and Zon 2013).

Next, the intermediate wave, named transient-definitive, gives rise to multipotent erythroid-myeloid progenitors (EMPs), which will then produce erythrocytes, macrophages, granulocytes and megakaryocytes, and immune-restricted progenitors (Palis 2016, Ottersbach 2019, Iturri, Freyer et al. 2021, Neo, Lie-A-Ling et al. 2021, Bigas, Galán Palma et al. 2022). However, this wave remains insufficiently characterized in human embryos, due to the inaccessibility and unavailability of these samples (Bigas, Galán Palma et al. 2022, Calvanese and Mikkola 2023).

At CS13 the last wave generates definitive HSCs, which are detected in the intraembryonic aorta-gonad-mesonephros (AGM) region, where HSCs emerge at CS14 to CS16 on the intra-aortic hematopoietic clusters (IAHC) (Ivanovs, Rybtsov et al. 2017, Dzierzak and Bigas 2018, Ottersbach 2019). Then, they colonize the placenta followed by the fetal liver at CS17 (Palis 2016, Dzierzak and Bigas 2018, Neo, Lie-A-Ling et al. 2021, Bigas, Galán Palma et al. 2022, Calvanese and Mikkola 2023), which are major sites of their expansion and maturation. Shortly

before birth, HSCs migrate first to the spleen and they finally home to the BM, which remains the dominant site of HSC-derived hematopoiesis after birth and throughout adulthood (Neo, Lie-A-Ling et al. 2021) (Figure 2).

The cellular origin of HSCs has been difficult to prove due to the intermixing of populations via circulation (Neo, Lie-A-Ling et al. 2021, Calvanese and Mikkola 2023). Several studies have confirmed that the HSCs from the second and third waves emerge *de novo* via an endothelial-to-hematopoietic transition (EHT) from a subpopulation of endothelial cells named hemogenic endothelium (HE) (Garcia-Alegria, Menegatti et al. 2018, Ottersbach 2019, Dignum, Varnum-Finney et al. 2021, Wu and Hirschi 2021). HE cells can give rise to different types of hematopoietic cells, such as EMPs and the first adult-type HSCs (Dignum, Varnum-Finney et al. 2021, Weijts, Yvernogeau et al. 2021). The cell origin of the primitive HSCs remains still a subject of debate, although a previous study proposed that they originate from a HE-like intermediate named Hemogenic angioblast (Garcia-Alegria, Menegatti et al. 2018, Ottersbach 2019, Neo, Lie-A-Ling et al. 2021).

Recently, transgenic mouse knockout and various lineage-tracing approaches based on single cell technologies have interrogated the contribution of different lineages to the heterogeneity and developmental trajectories of fetal and adult hematopoiesis (Garcia-Alegria, Menegatti et al. 2018, Dignum, Varnum-Finney et al. 2021, Iturri, Freyer et al. 2021, Neo, Lie-A-Ling et al. 2021, Patel, Christodoulou et al. 2022). These studies suggested that MPPs or ST-HSCs predominantly sustain adult hematopoiesis, while LT-HSCs are the main drivers of the immune and blood system in fetal and early postnatal life (Roy, Wang et al. 2021, Patel, Christodoulou et al. 2022, Sommarin, Olofzon et al. 2023).

1.1.3. Characteristics of fetal and adult HSPCs

Since the hematopoiesis takes place in different locations or niches during the development, fetal and adult blood cells result to be different in cell cycle status, molecular profile, and composition of progenitor cells (Figure 3) (Orkin and Zon 2008, Ivanovs, Rybtsov et al. 2017, Roy, Wang et al. 2021, Sommarin, Olofzon et al. 2023).

In contrast to mostly quiescent adult HSCs, fetal HSCs are actively cycling and show higher proliferative capacity so that they are able to fully reconstitute the whole hematopoietic system (Bowie, Kent et al. 2007, Popescu, Botting et al. 2019, Ranzoni, Tangherloni et al. 2021). Transcriptomic, epigenetic, proteomic, and functional studies have shown that there are differences in gene and protein expression between fetal and adult HSCs (Popescu, Botting et al. 2019, Ranzoni, Tangherloni et al. 2021, Roy, Wang et al. 2021, Camiolo, Mullen et al. 2024). These differences include an increase in the expression of genes associated with leukemia and a decrease in the expression of genes that play a role in repairing DNA damage, maintaining genomic integrity, and remodeling chromatin (Rossi, Bryder et al. 2005, Nijnik, Woodbine et al. 2007). Metabolic studies have also shown that fetal and adult HSPCs depend on different metabolic processes, the first relying on anabolic conditions and the latter depending on glucose metabolism (Camiolo, Mullen et al. 2024). Overall, these differences might lead to an increased susceptibility of fetal HSPCs to develop leukemia (Camiolo, Mullen et al. 2024).

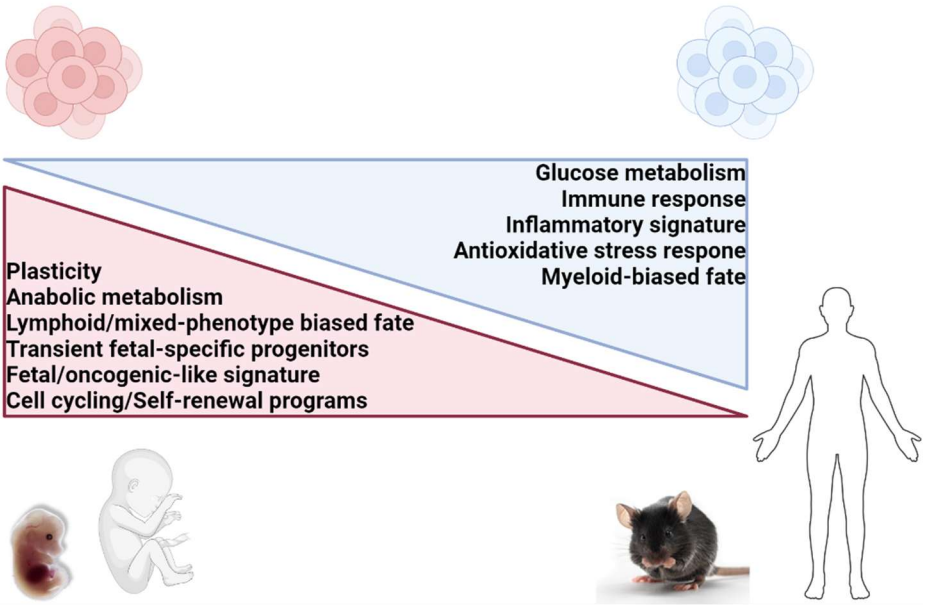

Figure 3 The unique features of fetal and adult HSPCs identified by transcriptomic, epigenetic, proteomic, and functional studies. Adapted from Camiolo, Mullen et al. 2024 with permission using BioRender.com.

1.1.4. Molecular regulation of hematopoietic fate decision

To constantly renew the blood system, the appropriate number of specific cells must be produced at the right time and location. This requires making the right decisions in HSC/HSPCs about whether to remain inactive or proliferate, self-renew or differentiate, choose a specific lineage, survive or die, and stay in place or migrate (Rieger and Schroeder 2012). The precise timing and order of these decisions in each cell are crucial for normal blood cell production, both under normal or altered conditions. The hematopoiesis is balanced by a tightly regulated combination of transcription factors (TFs) (Orkin and Zon 2008) and cytokines, which precisely activates the signaling pathway leading to differentiation of HSCs/HSPCs to mature blood cells (Zhu and Emerson 2002, Zhang and Lodish 2008, Seita and Weissman 2010).

Cytokines are important regulators of blood cell production and can influence the choice of lineage by affecting the survival, growth, maturation, and activation of different types of blood cells (Zhang and Lodish 2008).

TFs can also direct lineage choice and even reprogram cells that have already committed to a specific lineage, allowing them to switch to a different one (Rieger and Schroeder 2012). A core group of TFs has been identified to play an essential role in the development of the hematopoietic system (Dzierzak and Bigas 2018). While TAL1/SCL, LMO2, and FLI1 TFs regulate the primitive hematopoiesis, it has been found that RUNX1 and GATA2 TFs regulate the definitive hematopoiesis (Dzierzak and Bigas 2018). When activated or inactivated, TFs trigger the transcription of target genes (Rieger and Schroeder 2012). RUNX1 and GATA2 control several pathways, such as NOTCH, ETS/EGR or BMP pathway (Dzierzak and Bigas 2018). The NOTCH signaling pathway is required for HSC specification within the AGM region and is very tightly regulated, since it is important for both hematopoietic and arterial fates (Dzierzak and Bigas 2018, Bigas, Galán Palma et al. 2022). The Wnt/β-Catenin pathway plays a crucial role for HSC generation (Dzierzak and Bigas 2018, Bigas, Galán Palma et al. 2022). The BMP pathway and inflammatory signals also exert important functions in the hematopoietic

development (Dzierzak and Bigas 2018, Bigas, Galán Palma et al. 2022). Through interaction with chromatin remodeling complexes, TFs can also cause changes in the chromatin structure, affecting cell commitment to a specific lineage (Orkin and Zon 2008). Ultimately, epigenetic changes caused by modifications to chromatin and DNA may determine which lineage a cell commits to (Rieger and Schroeder 2012).

Nevertheless, it is also worth keeping in mind that hematopoiesis is not a closed circuit, but is regulated by the microenvironment or niche in a more complex context (Jagannathan-Bogdan and Zon 2013). The niche plays an important role in the maintenance and maturation of HSCs, since the contact between HSCs and osteoblasts in the BM niche or endothelial cells in the vascular niche determines the activation of signaling pathways, which can lead to maturation of the HSCs or to their proliferation (Jagannathan-Bogdan and Zon 2013).

Subtle changes and misregulation of individual TFs will directly impact on normal differentiation and can lead to leukemia (Rosenbauer, Owens et al. 2006). A notable characteristic of TFs in the blood system is that most of them are associated with chromosomal abnormalities or somatic mutations in human hematopoietic malignancies (Orkin and Zon 2008). Overall, disruptions of normal cell fate decisions underlie hematological disorders (Bowman, Busque et al. 2018).

1.2. Acute myeloid leukemia

1.2.1. Pathophysiology and classification

Disturbance in the processes of hematopoiesis can lead to the development of hematologic malignancies. Accumulation of not fully differentiated cells (blasts) in the BM, as well as in the peripheral blood, leads to altered physiological hematopoiesis known as leukemia (Papaemmanuil, Gerstung et al. 2016, Döhner, Estey et al. 2017). Based on the onset of the symptoms and percentage of blasts, leukemia can be classified as acute or chronic and myeloid or lymphoid, according to the hematopoietic lineage affected.

Acute myeloid leukemia (AML) represents a clinically, cytogenetically, and molecularly heterogeneous hematologic disease characterized by uncontrolled proliferation of undifferentiated immature myeloid progenitor cells (Bonnet and Dick 1997). AML accounts for 25 percent of all adult leukemias in the Western world, occurring primarily at older age, with a median age of sixty-nine years (Siegel, Naishadham et al. 2013).

Since the accumulation of leukemic blasts in the BM goes at the expense of normal cells, most patients present symptoms such as anemia, fever, increased infection rate due to displacement of physiologic hematopoiesis (Pelcovits and Niroula 2020, Newell and Cook 2021, Stubbins, Francis et al. 2022).

Recently, the classification of AML has been changed being no longer based on the morphological, but on the molecular and genetic criteria of the disease. According to the World Health Organization (WHO), the new AML classification takes into account clinical, molecular/genetic, and pathological parameters (Khoury, Solary et al. 2022). The prevailing classification approach comprises two main groups: 1. AML with AML-defining genetic alterations and 2. AML defined by cell differentiation (Khoury, Solary et al. 2022). The first

group is mainly based on the established diagnostic criteria for AML with chromosomal translocation such as PML::PARA and RUNX1::RUNX1T1, but also includes somatic mutations such as NPM1 and CEBPA (Khoury, Solary et al. 2022). The second group is based on immunophenotyping and detection of markers and includes, for example, acute megakaryoblastic leukemia (AMKL) and acute erythroid leukemia (Khoury, Solary et al. 2022). For the majority of AML subtypes, the presence of more than 20% of blasts is required to diagnose this hematological disease (Döhner, Estey et al. 2017). However, in most cases this is criterion no longer required for diagnosing the subset of AML with defining genetic alterations (Khoury, Solary et al. 2022).

The advent of next-generation sequencing technology revealed the heterogenous mutational profile of AML (Ley, Miller et al. 2013, Papaemmanuil, Gerstung et al. 2016). Many of these mutations have been found to influence disease prognosis, and the presence of cooperating co-mutations may have an additional modifying effect (DiNardo and Cortes 2016). Thus, AML has been deeply characterized at the genomic level and prognostic correlations have been established. The role of many of the defining genetic features has also been functionally verified. Yet, there are many mutations of unknown significance. Further, increasing accessibility of transcriptional-, epigenetic- and proteomic-characterization is expected to further refine the classification in the future.

1.2.2. Pediatric acute myeloid leukemia

Acute leukemias, accounting for 1 out of 3 cancers diagnosed in children up to 14 years of age, represent the most common form of childhood malignancies (Siegel, Miller et al. 2020), with the most frequent being acute lymphoblastic leukemia (ALL) followed by AML. Compared to ALL, pediatric AML occurs in ~15% of the acute leukemia cases (standardized annual incidence: 7 per 1 million children) and is associated with poor outcomes (Elgarten and Aplenc 2020, Reinhardt, Antoniou et al. 2022), when compared to other childhood cancers.

Collaborative efforts through cooperative group trials have significantly advanced our understanding of pediatric AML biology and improved patient outcomes over the past decades (Conneely and Stevens 2021). However, relapse remains a persistent challenge leaving clinicians limited treatment options. While AML is more prevalent and extensively studied in older adults, comprehensive studies in pediatric AML are rare due to low numbers of patients (Conneely and Stevens 2021). For this reason, the field of pediatric AML has progressed by translating insights from adult studies (Conneely and Stevens 2021, Obszański, Kozłowska et al. 2022).

However, despite similar phenotype and classification, many differences exist between pediatric and adult AML, mostly due to age and genetic landscape (Figure 4) (Papaemmanuil, Gerstung et al. 2016, Bolouri, Farrar et al. 2018, Marceau-Renaut, Duployez et al. 2018).

Advances in sequencing technology have shed light onto the pathogenesis of pediatric AML, revealing novel fusion genes, focal deletions, and recurrent mutations unique to pediatric AML, some of which are associated with particularly poor prognosis (Papaemmanuil, Gerstung et al. 2016, Bolouri, Farrar et al. 2018, Cheng, Yung et al. 2023). In contrast to adults, pediatric patients have a strongly increased incidence of chromosomal abnormalities, while only 20%

show a normal karyotype (Aung, Mills et al. 2021). In particular, rearrangements involving the KMT2A locus (formerly MLL1, 11q23) are highly frequent in pediatric de novo AML (Creutzig, van den Heuvel-Eibrink et al. 2012, Reimer, Knöß et al. 2017). In contrast, the number of somatic mutations in pediatric patients is lower than in adult patients (5–6 somatic mutations per pediatric sample compared to 10–13 per adult genome) (Papaemmanuil, Gerstung et al. 2016, Bolouri, Farrar et al. 2018). Pediatric patient genetics are enriched for mutations in *FTL3*, *NPM1*, *WT1*, *CEBPA* and *KIT, RUNX1, CBFB, NUP98* and *KMT2A* rearrangements, as well as structural aberration including trisomy 8 and *UBTF* tandem duplication, which occur rarely or with very low frequency in adults (Aung, Mills et al. 2021, Umeda, Ma et al. 2024). In contrast, mutations in *TP53* and epigenetic regulators, such as *DNMT3A, IDH1/2* and *TET2*, are rarely detected in pediatric patients, while being commonly present in adults (Aung, Mills et al. 2021, Cheng, Yung et al. 2023). Consistent with the observations made in adult patients, *TP53* alterations are independent prognostic factors associated with tumor aggressiveness and very poor survival (Cheng, Yung et al. 2023).

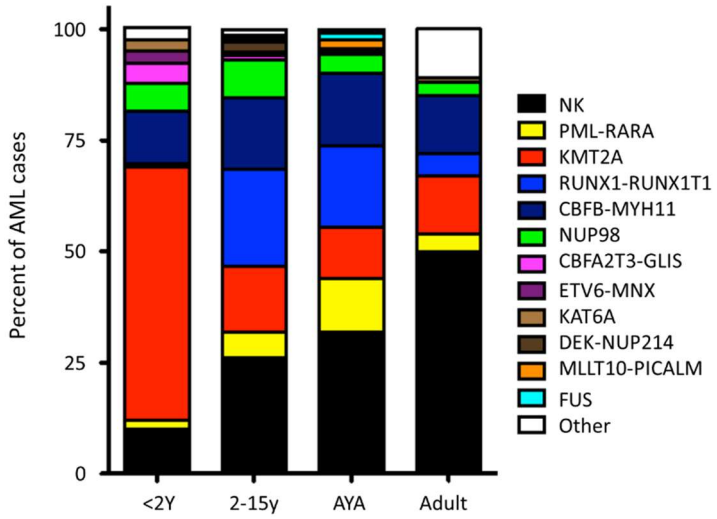

Figure 4 Leukemic fusions in AML by age. The approximate frequency of recurrent fusions in AML in infants (defined as patients < 2 years of age), young children (2–15 years), adolescents and young adults, (AYA; 15–39 years), and adults (> 40 years). NK, normal karyotype. Compiled data from Creutzig, van den Heuvel-Eibrink et al. 2012 and Bolouri, Farrar et al. 2018 with permission.

However, the reasons underlying the differences between pediatric and adult AML remain widely unknown. Studies suggest that these might rely on the ontogenic changes in the HSPCs (Lopez, Noguera et al. 2019, Okeyo-Owuor, Li et al. 2019). For this reason, it is currently believed that most pediatric leukemias originate before birth (Mack, Zhang et al. 2021). Furthermore, several studies have demonstrated that fetal HSCs are resistant to many leukemic oncogenes detected in adult AML (Okeyo-Owuor, Li et al. 2019, Li, Kong et al. 2020). Nonetheless, both intrinsic properties of fetal HSCs, which facilitate the different mutational landscape, and environmental influence of the niche have been proposed to explain such differences between fetal and adult HSCs (Calvi and Link 2015). Understating the fetal-intrinsic properties, as well as different epigenetic status, will provide new insights into the development of future therapies (Schwarzer, Emmrich et al. 2017, Bolouri, Farrar et al. 2018).

1.2.3. Therapies for pediatric AML

Recent studies indicate that the overall survival (OS) rate of children with AML has significantly improved, with up to 75% of affected children now surviving the disease due to the advancements in supportive care (Getz, Szymczak et al. 2021, Yang, Jaing et al. 2021, Reinhardt, Antoniou et al. 2022). Despite the high rate of complete first remission (90%), nearly 50% of pediatric patients relapse with severe reduction of the OS rate (40%) for the relapsed patient population (Rasche, Zimmermann et al. 2018, Chen and Glasser 2020).

Due to the genetic heterogeneity of AML, the high relapse rate and the therapy-related toxicity, the treatment of AML remains challenging and little progress has been made in therapeutic treatments over the past 40 years (Chen and Glasser 2020, Conneely and Stevens 2021, Reinhardt, Antoniou et al. 2022). The current backbone of pediatric AML treatment remains a combination of cytarabine and anthracyclines, a regimen used more than five decades, and/or an allogenic stem cell transplant (Lichtman 2013, Estey 2018, Conneely and Stevens 2021). However, this therapy is associated with significant acute toxicities and long-term consequences for the patients (Conneely and Stevens 2021).

As traditional chemotherapy for pediatric AML is reaching its limits, novel therapeutic strategies are urgently required to improve outcomes (Chen and Glasser 2020, Conneely and Stevens 2021, Reinhardt, Antoniou et al. 2022). Despite genetic differences between pediatric and adult AML, treatments developed for adults are often applied to children (Obszański, Kozłowska et al. 2022). However, recognizing the heterogeneity and molecular vulnerabilities of pediatric AML has shown its power to result in novel targeted therapies (Bhansali, Pratz et al. 2023). Pediatric AML treatment is risk-stratified, allowing for tailored therapeutic approaches based on relapse risk (Conneely and Stevens 2021, Obszański, Kozłowska et al. 2022). This stratification considers multiple factors, including the genetic profiles, initial treatment response assessed by minimal residual disease, and the context of AML development (Daver, Wei et al. 2020, Awada, Mustafa Ali et al. 2022). Significant advancements include refined risk stratification methodologies and targeted therapies that focus on aberrant signaling, epigenetic regulation, immune system reactivation, and novel metabolic pathway inhibition (Chen and Glasser 2020, Conneely and Stevens 2021). These innovations include liposomal formations of chemotherapeutic agents, small molecule inhibitors, epigenetic therapy, the antibody-drug conjugates (ADCs) and immunotherapy (Chen and Glasser 2020, Conneely and Stevens 2021).

Amongst the most prominent ones here to mention are: (1) CPX-351, a liposomal formulation of cytarabine and daunorubicin at the optimal 5:1 molar ratio, has shown promising results in a phase I/II study in relapsed/refractory pediatric AML (Cooper, Absalon et al. 2020). (2) The first-generation FLT3 inhibitors, Midostaurin and Sorafenib, which are multi-kinase inhibitors, and the second-generation agents, Quizartinib and Gilteritinib, which are more FLT3-specific with reduced off-target activity (Chen and Glasser 2020, Conneely and Stevens 2021). Additionally, clinical trials are planned to test inhibitors targeting other kinases such as CDK4/6 and MEK in both adult and pediatric AML patients (Schmoellerl, Barbosa et al. 2020, Pikman, Tasian et al. 2021). In preclinical studies, the BCL-2 inhibitor Venetoclax has shown synergistic effects when combined with other agents (Pullarkat, Lacayo et al. 2021, Stubbins, Francis et al. 2022).

Furthermore, targeting dysregulated epigenetic pathways, for example with histone deacetylase inhibitors or small molecules targeting Menin to inhibit KMT2A fusions, represents a promising strategy for improving pediatric AML treatment outcomes in the future (Chen and Glasser 2020, Conneely and Stevens 2021, Bhansali, Pratz et al. 2023).
To reduce the adverse effects of chemotherapy and to circumvent chemoresistance, several immunotherapeutic approaches are currently under investigation (Chen and Glasser 2020, Conneely and Stevens 2021, Tabata, Chi et al. 2021, Bhansali, Pratz et al. 2023). Gemtuzumab Ozogamicin is a Food and Drug Administration (FDA)-approved ADC targeting CD33, a marker highly expressed in AML (Chen and Glasser 2020, Conneely and Stevens 2021). Similarly, CD123 and mesothelin have emerged as promising targets for ADCs (Chen and Glasser 2020, Conneely and Stevens 2021). Chimeric antigen receptor (CAR) T-cells or NK-cells, targeting antigens, such as CD123, CD33, CLL-1 or NKG2D are under development to add cellular immunotherapy to the treatment of (pediatric) AML (Conneely and Stevens 2021, Tabata, Chi et al. 2021).
Despite these recent and coming improvements in the treatment options and prognosis, there is a pressing need to further explore targeted treatments that avoid excessive toxicity to the affected children(Reinhardt, Antoniou et al. 2022).
However, larger clinical studies in pediatric populations are necessary to establish these molecular-targeted therapies as effective complements to standard chemotherapy (Conneely and Stevens 2021). The boost in clinical trials, particularly in immunotherapy, BCL-2 inhibitors, and hypomethylating agents, reflects growing interest in these innovative treatments. This trend holds promise for significantly improving pediatric AML outcomes in the near future.

1.3. Acute megakaryoblastic leukemia

AMKL is a morphologically defined subgroup of AML characterized by abnormal megakaryoblasts expressing platelet-specific surface lineage markers (CD41, CD42, and CD61) (Gruber and Downing 2015).
Pediatric AMKL was initially subdivided in two major groups according to the presence or absence of Trisomy 21 (Down-syndrome, DS) and thus referred to as DS- or non-DS-AMKL (the latter one referred to as AMKL in this thesis) (Gruber and Downing 2015). In the recent WHO classification, the latter forms a subtype of myeloid neoplasms associated with germline predisposition, known nowadays as myeloid leukemia associated with Down syndrome (also referred to in this thesis as ML-DS) (Khoury, Solary et al. 2022).
While AMKL is rare in adults, with a frequency of only 1% of AML cases (Pagano, Pulsoni et al. 2002), it occurs more frequently in children [usually, 2 years of age (de Rooij, Masetti et al. 2016)], often after progression from myelodysplastic syndromes, and represents 4%-15% of pediatric AML cases (Gruber and Downing 2015, de Rooij, Branstetter et al. 2017).
Although it represents a heterogeneous group, pediatric AMKL is both biologically and clinically distinct, displaying an inferior outcome compared to ML-DS. Hence, pediatric AMKL is considered as high-risk leukemic group (Athale, Razzouk et al. 2001, de Rooij, Masetti et al. 2016).
AMKL is characterized by a limited number of specific genetic abnormalities, subdividing the malignancies in distinct subsets. RNA and exome sequencing in a large pediatric cohort have

shed light on the genomic landscape of pediatric AMKL (Hsiao, Yang et al. 2005, Gruber, Larson Gedman et al. 2012, Thiollier, Lopez et al. 2012, de Rooij, Branstetter et al. 2017). More than 70% of AMKL patients harbor oncogenic gene fusions, which are recurrent and mutually exclusive (de Rooij, Branstetter et al. 2017). These include CBFA2T3::GLIS2 (~18%), KMT2A rearrangements (MLLr/KMT2Ar; ~17%), HOX rearrangements (HOXr; ~15%), NUP98::KDM5A (~11%), and RBM15::MKL1 (~10%) (Figure 5) (de Rooij, Branstetter et al. 2017). Despite the efforts made in the detection and identification of chimeric oncogenes, the etiology of 30-40% of cases remains insufficiently understood (de Rooij, Branstetter et al. 2017).

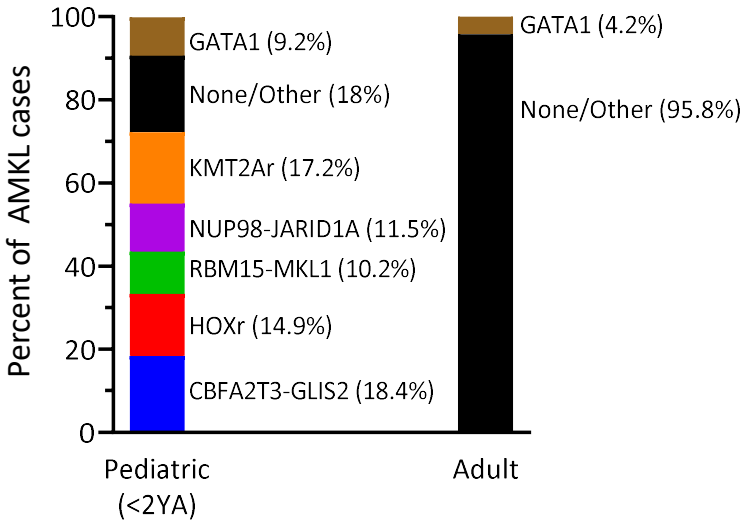

Figure 5 Pediatric and adult AMKL patients are genomically distinct. Bar plot showing the distribution of recurrent chromosomal translocation and GATA1 mutations in adult and pediatric AMKL cases. Adapted from de Rooij, Branstetter et al. 2017 with permission.

AMKL patients display variable outcomes based on the chromosomal translocation: AMKL patients harboring chromosomal translocations such as CBFA2T3::GLIS2, KMT2Ar, and NUP98::KDM5A typically experience poor outcomes with lower event-free survival (EFS) compared to ML-DS and pediatric AML, despite intensified treatment (de Rooij, Masetti et al. 2016, de Rooij, Branstetter et al. 2017). On the other hand, AMKL patients carrying GATA1 mutations but lacking a fusion gene have a similar outcome observed in ML-DS, thus appearing biologically and clinically similar to the latter one.

The current treatment protocols are based on intensive chemotherapy using an anthracycline and cytarabine backbone, including stem cell transplantation in selected cases (de Rooij, Hollink et al. 2013). However, improvement of clinical outcome has reached a plateau, highlighting the need to develop novel therapeutic options to improve survival (Noort, Wander et al. 2021).

1.3.1. NUP98 fusion oncogenes

The Nucleoporin 98 (NUP98) protein is a member of the nuclear pore complex (NPC), which facilitates the bidirectional transport of macromolecules between the nucleus and the cytoplasm (Radu, Moore et al. 1995). Beyond its role in the NPC, NUP98 associates with the Anaphase-Promoting Complex (APC) (Jeganathan, Malureanu et al. 2005) and interacts with

the chromatin to actively regulate gene expression independently of the NPC (Capelson, Liang et al. 2010, Capitanio, Montpetit et al. 2017). Structurally, the N-terminus of NUP98 consists of a series of intrinsically disordered phenylalanine-glycine (FG) or glycine-leucine-phenylalanine-glycine (GLFG) amino acids residues separated by a Gle2-binding-sequence (GLEBS) domain, while the C-terminal portion contains RNA-binding and autoproteolytic cleavage sites (APD) (Figure 7).

NUP98 translocations are recurrently detected in diverse hematopoietic malignancies. While relatively rare in adult AML, they are overrepresented in childhood AML, with a frequency between 10-15% of cases (Gough, Slape et al. 2011). Notably, AML patients harboring these translocations often have a poor prognosis and frequently carry additional mutations, suggesting a potential functional cooperation with NUP98-fusions (Gough, Slape et al. 2011).

All NUP98 translocations share a common N terminus characterized by the FG/GLFG repeats of NUP98 (N-NUP98), which is fused in-frame with the C-terminal of more than 30 different fusion partners (Gough, Slape et al. 2011, Bertrums, Smith et al. 2023). C-terminal fusion partners of N-NUP98 in AML are proteins typically involved in epigenetics and transcriptional control (Michmerhuizen, Klco et al. 2020). A recent study investigating the role of the NUP98 moiety in cellular transformation demonstrated that an artificial fusion protein (art-KDM5A), comprising a synthetic N-terminal GLFG repeat sequence fused to the C-terminal portion of KDM5A, could recapitulate a phenotype similar to that observed with the native NUP98::KDM5A fusion protein (Terlecki-Zaniewicz, Humer et al. 2021). Nevertheless, the specific contribution of the individual moieties still requires further investigation.

1.3.2. Mechanism of NUP98 fusion-mediated leukemogenesis

Given the involvement of endogenous NUP98 in transcriptional control and the structural and functional diversity of C-terminal fusion partners among NUP98-fusion proteins, it has been hypothesized that chromatin targeting of NUP98-fusion proteins depends on the NUP98 N-terminus, while the C-terminal fusion partners might mediate specific gene regulatory functions that drive leukemogenesis (Franks, McCloskey et al. 2017). However, several NUP98-fusions, which lack partner genes with annotated DNA-binding or chromatin-interaction domain, such as NUP98::DDX10, still result in aberrant expression of defined genes (Yassin, Abdul-Nabi et al. 2010, Schmoellerl, Barbosa et al. 2020). This suggests that chromatin targeting of NUP98, common to all distinct fusion partners, is essential for leukemogenesis (Franks, McCloskey et al. 2017, Schmoellerl, Barbosa et al. 2020).

NUP98 fusion oncoproteins exploit the functions of wild-type NUP98 and especially the transcriptional and/or chromatin-modifying activities of the partner genes to drive malignancies.

Several studies have shown that NUP98 fusions sustain self-renewal of HSPCs and enhance the expression of HOXA cluster genes, recapitulating principal aspects of the human disease (Wang, Cai et al. 2007, Wang, Song et al. 2009, Gough, Lee et al. 2014). A recent study demonstrated that NUP98-fusions share several highly overexpressed target genes crucial for their oncogenic activity (Schmoellerl, Barbosa et al. 2020).

Based on phase separation approaches, it has been suggested that the transformation mechanism behind NUP98 fusions is more complex and broader than believed (Terlecki-Zaniewicz, Humer et al. 2021). NUP98 belongs to the group of FG nucleoporins, which contain intrinsically disordered regions (IDRs). Thanks to the low-affinity interactions, IDR-containing proteins forms biomolecular condensates, membraneless structures, which control several biological processes. A recent study has demonstrated that the IDR within NUP98::HOXA9 is essential for leukemogenesis and activation of the oncogenic gene-expression program, facilitating the binding of transcription factors and/or promoting long-distance looping between enhancers and oncogene promoters (Ahn, Davis et al. 2021).

Furthermore, NUP98-fusion proteins exert their oncogenic activity in the context of large protein complexes, particularly histone-modifying chromatin complexes.

A chromatin-immunoprecipitation study has shown that the NUP98::NSD1 fusion interacts with Wdr8 to recruit the Wdr82–Set1A/COMPASS (complex of proteins associated with Set1) complex, which, due to its methylase function, deposits an activating mark on histone H3 lysine 4 (H3K4me3) across the *HOXa* cluster and at the *Meis1* promoter (Franks, McCloskey et al. 2017). Recent studies have also demonstrated that the KMT2A/NSL complex interacts with several NUP98-fusion proteins through direct binding between MLL1 and the FG/GLFG repeats of NUP98. (Xu, Valerio et al. 2016, Heikamp, Henrich et al. 2022).

A number of additional proteins have indeed been shown to interact in complex with the FG/GLFG repeat domains of NUP98 fusions, and many of these cofactors contribute to the activation and repression of genes, such as CREBBP/EP300 (Wang, Song et al. 2009).

Both chromatin-binding and IDR-containing domains have previously been shown to be essential for tumorigenicity, which supports the hypothesis of chromatin deregulation as a general mechanism of transformation.

1.3.3. Potential therapeutic strategy for NUP98-rearranged leukemia

Although the molecular mechanism of NUP98 fusion protein-mediated leukemogenesis is not fully described, recent studies have suggested potential therapeutic approaches (Xu, Valerio et al. 2016, Schmoellerl, Barbosa et al. 2020, Heikamp, Henrich et al. 2022). One possible strategy is to target epigenetic modulators, such as histone acetyltransferase and histone deacetylase inhibitors (Michmerhuizen, Klco et al. 2020). Previous studies have proposed the inhibition of MLL1 interaction with Menin and NUP98, leveraging the critical role of KMT2A/MLL1 in NUP98-fusion-dependent leukemogenesis (Xu, Valerio et al. 2016, Heikamp, Henrich et al. 2022). Another potential approach is to pharmacologically inhibit transcriptional targets, such as CDK6, given its high expression and direct regulation by NUP98-fusions (Schmoellerl, Barbosa et al. 2020). Thus, a few venues towards the development of specific treatment options for NUP98-rearranged leukemias have been suggested, but a better understanding of therapeutic vulnerabilities in NUP98-rearranged leukemia is still urgently needed to improve patient outcomes.

1.3.4. NUP98::KDM5A translocation

The t(11;12)(p15;p12) involving *NUP98* and *KDM5A* (NUP98::KDM5A), also known as *JARID1A or RBP2*, produces a gene rearrangement that encodes a fusion protein composed by N-NUP98 fused in-frame with the histone lysine demethylase KDM5A (Figure 7).

Although the frequency of NUP98 translocations is rare in adult AML, NUP98::KDM5A rearrangement is overrepresented in childhood AML, found primarily in ~15% AMKL and 12% infant AML cases (de Rooij, Branstetter et al. 2017, Masetti, Guidi et al. 2019, Noort, Wander et al. 2021). Patients carrying NUP98::KDM5A translocation show an inferior EFS and OS compared to patients without NUP98::KDM5A (Figure 6) (Noort, Wander et al. 2021).

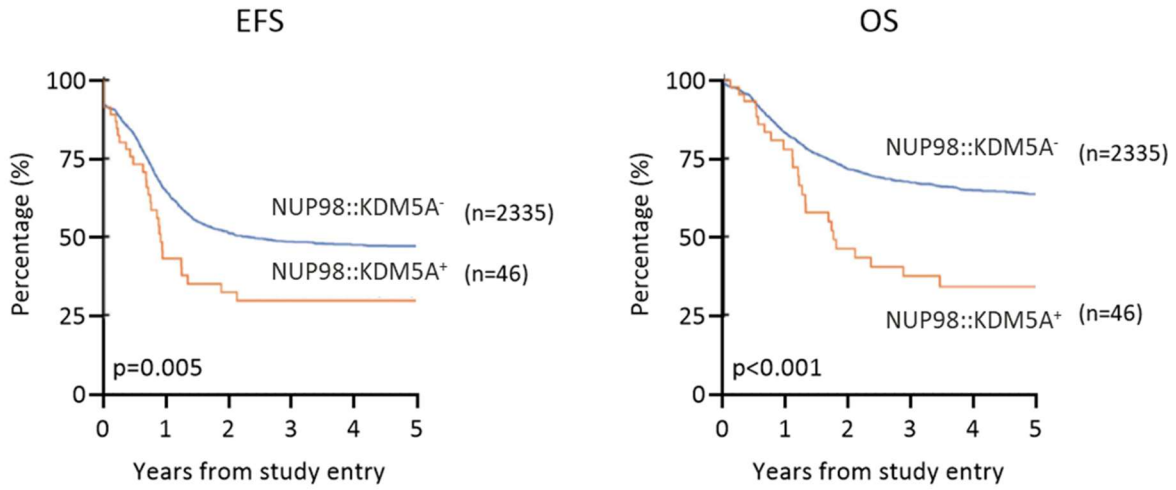

Figure 6 Survival of NUP98::KDM5A⁺ AML: Kaplan-Meier survival curve of event-free survival (EFS) (left) and overall survival (OS) of NUP98::KDM5A⁺ versus NUP98::KDM5A⁻ patients. Adapted from Noort, Wander et al. 2021 with permission.

Given that *NUP98* is located 3Mb from the 11p telomere and *KDM5A* is located at the telomeric end of 12p13, the NUP98::KDM5A fusion is cryptic and therefore undetectable with conventional karyotyping. NUP98::KDM5A is mutually exclusive with other type-II aberrations (de Rooij, Hollink et al. 2013, Noort, Wander et al. 2021). Interestingly, chromosome 13 aberrations are highly enriched in NUP98::KDM5A⁺ AMKL patients (Bertrums, Smith et al. 2023) and *RB1* (Retinoblastoma Binding transcriptional Corepressor 1) gene is often co-mutated (de Rooij, Masetti et al. 2016). In addition, other chromosomal abnormalities are associated with NUP98::KDM5A, in particular trisomy 21, hyperdiploidy and a complex karyotype (de Rooij, Masetti et al. 2016). NUP98::KDM5A overexpressing leukemia cells show a strong upregulation of *HOXA* and *HOXB* cluster genes, which has also been found in other NUP98-rearranged leukemia (de Rooij, Hollink et al. 2013).

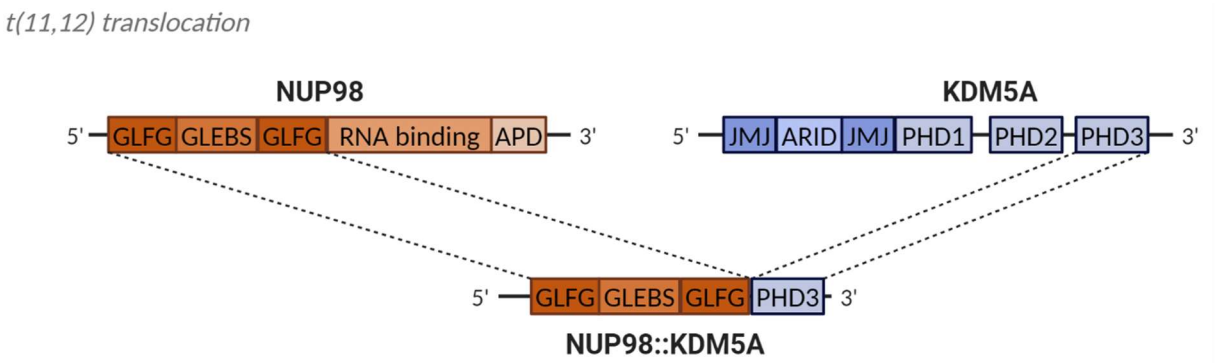

Figure 7 Structure of NUP98, KDM5A, and NUP98::KDM5A proteins. GLFG, GLFG repeats; GLEBS, Gle2-binding domain; RNA binding, RNA binding domain; APD, autoproteolytic domain; JMJ, Jumonji domain; ARID, AT-rich interactive domain; PHD1/2/3, plant homeodomains 1/2/3. Created in BioRender.com

The histone lysine demethylase KDM5A contains two Jumonji catalytic domain (JMJ), one ARID DNA-binding domain and three plant homeodomain (PHD) fingers. The third PHD finger of KDM5A recognizes various histone 3 lysin 4 methylation (H3K4me) states, with a preference for H3K4me3. Once engaged as a fusion protein partner, KDM5A lost its demethylase activity since only the third PHD finger is kept. This probably led to the retainment of the methylation status of H3K4, resulting in sustained upregulation of HOX genes and other transcription factors, thus favoring a stem cell phenotype (de Rooij, Hollink et al. 2013). A previous study investigated the role of KDM5A moiety in the transformation process and demonstrated that loss of the third PHD domain impaired leukemogenesis, while deletions in *KDM5A* sequence before or after had no effect on transformation (Wang, Song et al. 2009). Of note, mutations on H3K4me3-engaging residues abrogate the binding of NUP98::KDM5A to the *Hoxa* promoter affecting the enforced expression, thus preventing the leukemic transformation of HSPCs (Wang, Song et al. 2009).

Due to limited access to primary material and the lack of cell lines expressing NUP98::KDM5A, modeling NUP98::KDM5A fusion to understand its molecular mechanism of transformation has been challenging. By altering proliferation, differentiation, maturation, and self-renewal, NUP98::KDM5A fusion protein is sufficient to induce leukemic transformation in different cellular and animal models (Wang, Song et al. 2009, Cardin, Bilodeau et al. 2019). A previous study showed that the overexpression of NUP98::KDM5A fusion oncoprotein in mBM-HSPCs has led to uncontrolled proliferation of transformed cells with myeloblast phenotype and induced to AML *in vivo* (Wang, Song et al. 2009). Similarly, human HSPCs isolated from cord blood and lentivirally transduced with a cDNA encoding for NUP98::KDM5A not only showed maturation arrest but also recapitulated the AMKL phenotype *de novo* and other leukemia subtypes in xenograft models (Wang, Song et al. 2009, Cardin, Bilodeau et al. 2019).

However, the detailed molecular mechanism of leukemic transformation driven by NUP98::KDM5A remains unclear.

1.4. TRIP13

Located on chromosome 5p15.33, thyroid hormone receptor interacting protein 13 (TRIP13) belongs to the AAA (ATPase family Associate with diverse cellular Activities) + ATPase superfamily. It is comprised of 14 exons and encodes a protein with 432 amino acids. The TRIP13 protein harbors a non-catalytic NH_2 terminal domain, which may function as a recruiter for interaction partners, followed by a single ATPase domain at the C-terminus. Like the majority of ATPases, it is assembled into a homohexamer to exert its biological function (Figure 8) (Chen, Jomaa et al. 2014). The TRIP13 protein interacts with thyroid hormone receptors, but also with a variety of HORMA domain-containing proteins, which act downstream, upon a change of their conformation (Li, Sarangi et al. 2022).

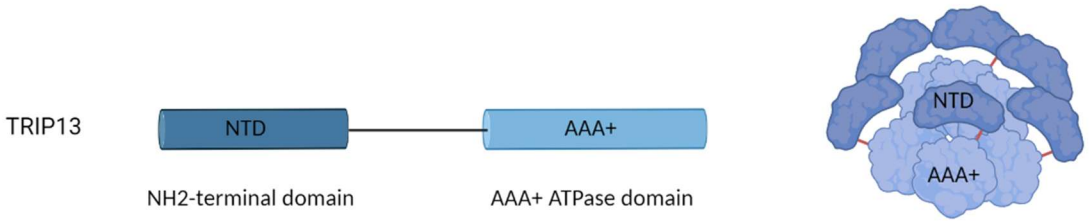

Figure 8 A schematic representation of the domain organization of TRIP13: NH2-terminal domain (NTD) and AAA+ ATPase domain. Adapted from Vader 2015 with permission using BioRender.com

1.4.1. Functions of TRIP13

TRIP13 is involved in various cellular processes during mitosis and meiosis (Figure 9).
During mitosis, unattached kinetochores promote the formation of the mitotic checkpoint complex (MCC), which is formed by MAD2/MAD2L1, BUBR1, BUB3 and CDC20 (Musacchio 2015). MCC is a downstream of the spindle assembly checkpoint (SAC) and the capture of CDC20 in the MCC prevents the activation of the anaphase promoting complex/cyclosome (APC/C) (Sudakin, Chan et al. 2001). TRIP13, together with the MAD2-binding protein MAD2BP/MAD2L1BP (p31Comet), disassembles the MCC, promoting inactivation of SAC (Vader 2015). Subsequently, MAD2L1BP binds the closed conformation of MAD2 (C-MAD2) by displacing BUBR1 and BUB3, TRIP13 converts C-MAD2 into the open conformation of MAD2 (O-MAD2) (Mapelli and Musacchio 2007). The conformational change of MAD2 determines a different binding affinity for CDC20 (Musacchio and Salmon 2007). This unleashes CDC20, which is free to interact with APC/C allowing its activation, SAC silencing and anaphase onset (Figure 9). Overall, in this process TRIP13 recruitment is essential for providing energy for the MCC disassembly upon ATP hydrolysis (Teichner, Eytan et al. 2011).

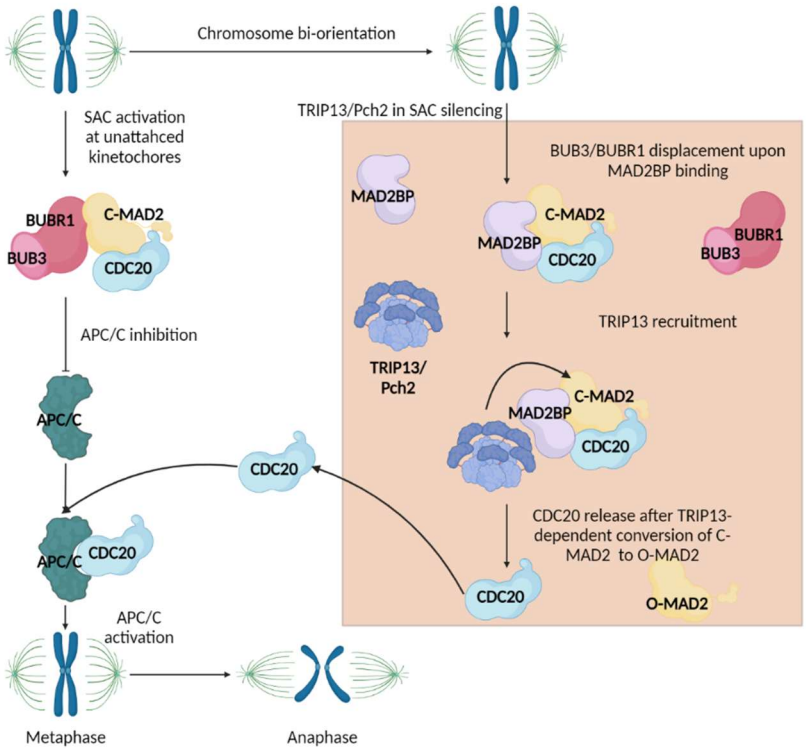

Figure 9 Model describing the role of TRIP13/Pch2 in the regulation of the spindle assembly checkpoint (SAC). Upon SAC activation at unattached kinetochores, C-MAD2 together with BUB3 and BUBR1 sequesters CDC20 into the mitotic checkpoint complex (MMC) to inhibit APC/C. During SAC silencing, MAD2BP (p31COMET) displaces BUBR and BUB3 and TRIP13/Pch2 is recruited. Thanks to the ATP hydrolysis, TRIP13/Pch2 changes the conformation status of C-MAD2 in O-MAD2, allowing the release of CDC20, which can be free to interact with APC/C, promoting mitotic progression. Adapted from Vader 2015 with permission using BioRender.com

During meiotic G2/prophase, TRIP13 influences several events such as crossover (CO) and synaptonemal complex (SC) formation, checkpoint controls, and DNA strand break (DSB) repair (Vader 2015). Several studies suggest that the SC component Zip1 is required and might be responsible of pch2/TRIP13 recruitment to synapsed chromosomes allowing the TRIP13-dependent removal of Hop1 (HORMAD1/2) from the chromosome (San-Segundo and Roeder 1999, Börner, Barot et al. 2008). However, the dynamic of this regulation requires further investigation, given that the direct interaction between these two proteins has not yet been described (Cardoso da Silva and Vader 2021). Besides the mechanism described above, TRIP13 could contribute to the establishment of the DSB repair process deciding between the homology-directed repair (HDR) pathway and nonhomologous end-joining (NHEJ) pathway. Upon DSB formation, TRIP13, together with ATM, determines the interhomolog biased homologues recombination (HR) (Ho and Burgess 2011, Cardoso da Silva and Vader 2021). In addition, TRIP13 modulates the activities of HORMAD1/2, which is required for meiotic chromosome organization and pairing, DSB formation, and interhomolog HR (Figure 10). TRIP13 removes HORMAD1/2 from chromosomes and facilitates its phosphorylation, which is mediated by ATM/ATR (Figure 10) (Ho and Burgess 2011, Lo, Chuang et al. 2014). Finally, TRIP13 and HORMAD1/2 affect SPO11-dependent meiotic DSB formation (Vader 2015).

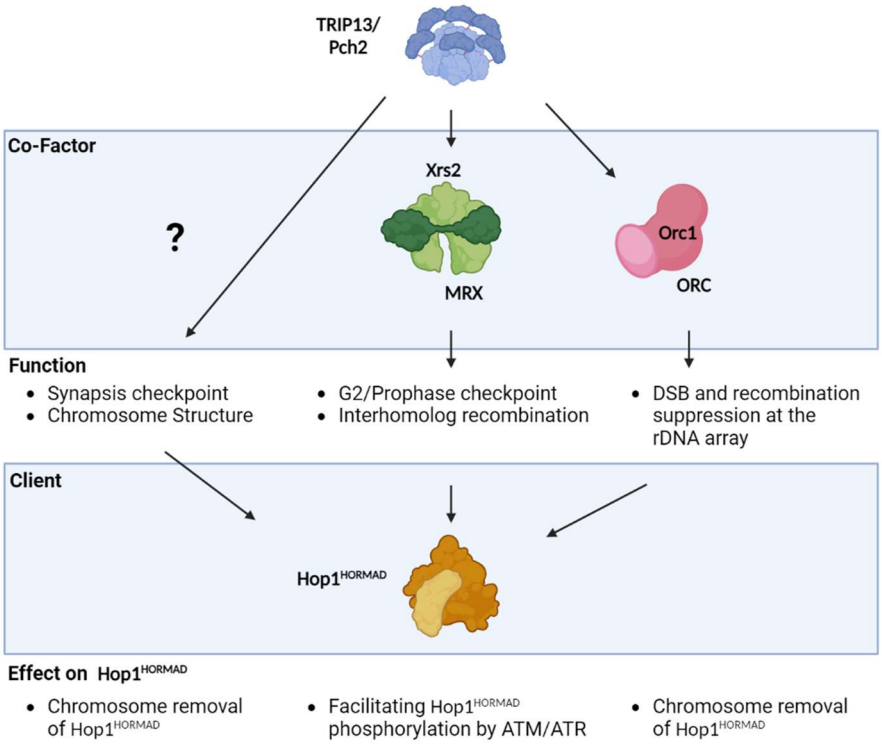

Figure 10 Model describing the role of TRIP13/Pch2 in meiotic G2/prophase. During meiosis TRIP13/Pch2 interacts with multiple cofactors to regulate the universal downstream protein HORMAD/Hop1. Adapted from Vader 2015 with permission using BioRender.com

A recent study using a quantitative proteomics approach with a proximity-labeling method showed the involvement of TRIP13 in DSB repair process at different levels (Jeong, Wie et al. 2022). Upon induction of DNA damage, TRIP13 is immediately recruited and interacts directly with MRE11 and RAD50, two members of the MRN complex. In addition, TRIP13 mediates the interaction between MDC1 with the MRN complex, activating the ATM signaling pathway. However, the depletion of TRIP13 inhibits the activation of the DNA damage signaling and the recruitment of downstream proteins affecting HDR, rather than NHEJ (Jeong, Wie et al. 2022). Moreover, the SILAC method revealed that TRIP13 interacts with MRE11 even in absence of DNA damage (Jeong, Wie et al. 2022). Nevertheless, this mechanism needs to be further explored.

In budding yeast, Pch2/TRIP13 is enriched in the nucleolus, where the ribosomal DNA is present, and directly interacts with Orc1/ORC to suppress meiotic recombination between repetitive sequences within the ribosomal DNA (Figure 10) (Cardoso da Silva and Vader 2021).

1.4.2. TRIP13 in cancer

In the last decades, the oncogenic properties of TRIP13 have attracted considerable attention. Due to its crucial role in the regulation of spindle assembly checkpoint, altered expression can potentially lead to chromosome segregation errors promoting aneuploidy, chromosome instability (CIN) and, at last, to tumorigenesis (Tao, Yang et al. 2017, Levine and Holland 2018). Notably, *TRIP13* overexpression has been identified in several tumors and associated with inferior OS, poor prognosis and drug resistance (Banerjee, Russo et al. 2014, Lu, Qian et al. 2019).

The first report about the oncogenic role of *TRIP13* was on head and neck cancer in 2014 (Banerjee, Russo et al. 2014), followed by several studies, which have confirmed the tumorigenic effect in other tumors. Given its essential function in the regulation of SAC and DNA damage repair, the oncogenic activity of *TRIP13* can affect several spindle proteins and several signaling pathways. Studies on a variety of malignancies have demonstrated that overexpression of *TRIP13* promotes cell proliferation, invasion, migration and epithelial-mesenchymal transition. Based on its AAA+ ATPase property, TRIP13 modulates and regulates several molecular processes by interacting with different partners. For example, TRIP13 regulates proliferation and invasion of melanoma cancer cells through activation of AKT signaling pathways (Lu, Mengxuan et al. 2022). On the other hand, these processes in ovarian cancer cells are mediated by a TRIP13-dependent activation of the NOTCH signaling pathway (Yu, Chen et al. 2022), in breast cancer cells through Wnt/Beta-catenin signaling pathway (Liu, Zhang et al. 2022) or through a c-Myc circuit (Banerjee, Russo et al. 2014, Zhou, Zhang et al. 2017, Zhang, Zhu et al. 2019, Li, Liu et al. 2021). Moreover, findings in thyroid cancer and glioblastoma reported that *TRIP13* overexpression and its co-expressed genes are associated with several cancer-related pathways such as TP53 signaling pathway (Chen, Lin et al. 2021). Notably, TRIP13 was able to modulate *TP53* in thyroid cancer cells, through a direct interaction with tetratricopeptide repeat protein 5 (TTC5), a known TP53 cofactor (Yu, Xiao et al. 2019).

Recent studies have implicated that overexpression of TRIP13 exhibited less sensitivity to anticancer drugs (Banerjee, Russo et al. 2014, Tao, Yang et al. 2017). Multiple myeloma (MM) and squamous cell carcinoma of the head and neck cells (SCCHN) showed high expression levels of *TRIP13* exhibiting less sensitivity to bortezomib and cisplatin respectively (Banerjee, Russo et al. 2014, Tao, Yang et al. 2017), potentially due to the correlation between TRIP13 overexpression and numerous apoptotic related pathways such as TP53 and PARP signaling pathways (Zhou, Zhang et al. 2017). Of note, TRIP13 overexpression favors the survival of genomically instable cells through DNA damage repair mechanisms (Jeong, Wie et al. 2022). By interacting with KU70 and KU80 TRIP13 activates DNA-PKc promoting DNA repair of chronic lymphocytic leukemia (CLL) and SCCHN cells (Banerjee, Russo et al. 2014, Zhou, Zhang et al. 2017). Moreover, a previous study has demonstrated that TRIP13, regulating the protein level of MAD2L1 via proteasome degradation, mediates the in-/activation of SAC and Bortezomib-resistance, which is rescued upon inhibition of PI3K/AKT signaling pathway by elevating MAD2L1 protein level (Tao, Yang et al. 2017).

Taken together, these studies suggest that TRIP13 is a novel potential biomarker for diagnosis and a possible novel therapeutic target for human cancer. In this direction, a small new inhibitor of TRIP13 (DCZ0415) has recently been identified showing promising results in the treatment of MM (Wang, Huang et al. 2020), perihilar cholangiocarcinoma (Li, Liu et al. 2021) and colorectal cancer (Agarwal, Afaq et al. 2022), where DCZ0415 inhibits the NF-kB signaling pathway promoting apoptosis and cell cycle arrest. These results were further improved when combined with additional drugs such as PARP inhibitors in hepatocellular carcinoma (Xu, Ma et al. 2022). However, the molecular structure requires improvements due to low water-solubility and permeability though cell membrane (Li, Liu et al. 2021). Nevertheless, more efforts need to be made for the development of TRIP13 inhibitors.

2. Aims of the study

Hematological malignancies arise from alterations in oncogenic drivers triggering enhanced proliferation, blocked differentiation, immune escape resulting in overgrowth of normal hematopoiesis. Pediatric AMKL as a subform of AML is characterized by the presence of very specific fusion oncogenes that lead to this uncontrolled proliferation which in case of AMKL affects immature megakaryoblasts (Gruber and Downing 2015). The NUP98::KDM5A fusion is detected in ~15% of pediatric AMKL cases but is very rare in adults (de Rooij, Branstetter et al. 2017, Masetti, Guidi et al. 2019, Noort, Wander et al. 2021). Pediatric NUP98::KDM5A$^+$ AMKL patients have poor prognosis and lower survival rate. For this reason, NUP98::KDM5A$^+$ AMKL is classified as a high-risk leukemia (Noort, Wander et al. 2021) and targeted therapies would be desirable to offer new treatment options for the affected children.

Noteworthy, NUP98::KDM5A fusion occurs at high frequency in very young children (< 2 years of age), suggesting its origin to derive from fetal hematopoiesis, which is in line with recent findings proposing that initiating mutations of pediatric leukemias are acquired in utero (de Smith and Spector 2024).

Fetal and adult HSPCs differ in proliferative capacity and differentiation programs, reside in different niches and subsequently by their transcriptional, epigenetic, and proteomic programs (Camiolo, Mullen et al. 2024). These distinctions, coupled with fewer driver mutations required in pediatric leukemias, indicate a crucial role of the fetal context in leukemia initiation (Camiolo, Mullen et al. 2024).

Recent studies have provided new insights into the biological, epigenetic and mechanistic properties of pediatric leukemias (Lopez, Noguera et al. 2019, Schmoellerl, Barbosa et al. 2020). Despite advances in our understanding of the molecular mechanisms underlying NUP98::KDM5A-driven AMKL, effective treatment strategies remain limited.

Given the high-risk classification of NUP98::KDM5A$^+$ AMKL and the current treatment limitations, there is an urgent need to develop tailored therapies for pediatric NUP98::KDM5A$^+$ AMKL patients (Michmerhuizen, Klco et al. 2020) and its fetal origin my reveal targetable weaknesses.

This thesis investigates the contribution of the fetal gene signatures in NUP98::KDM5A-driven leukemogenesis and the ability to exploit them therapeutically. To this end, we generated murine NUP98::KDM5A models from fetal liver and BM HSPCs. Based on potential fetal origin of NUP98::KDM5A-driven AMKL, we hypothesize an involvement of fetal gene programs, which we interrogated by using a CRISPR-Cas9 dropout screening to identify molecular dependencies. By elucidating the molecular mechanisms and dependencies of NUP98::KDM5A-driven AMKL, this study aims to contribute to developing effective, tailored therapies for this high-risk pediatric leukemia subtype.

3. Material and methods

3.1. Materials

3.1.1. List of equipment and materials

Table 1: List of technical devices

Technical devices	Product name	Supplier	Ref. number
Autoclave	Systec VX-150	Omnilab	101291150
Cell culture hood	Heraeus Biohazard Cabinet Hera Safe KS12	Thermo Fisher Scientific	40461432
Incubators	Forma™ Steri-Cult™ CO2 Incubator		3307TS
	BBD 6220		51020241
Water bath	GFL 1083	GFL	1083
Centrifuge	Megafuge 8R	Thermo Fisher Scientific	15287539
	Multifuge 1S-R		75004331
	Varifuge 3.0RS		1703315
	MiniSpin	Eppendorf	5452000010
	MyFuge	Biozym	55C1008-B-E
	Micro Star 17	VWR-avantor	521-1646
Ultracentrifuge	Sorvall LYNX 4000	Thermo Fisher Scientific	7500658
Centrifuge	Thermo ScientificTM CytospinTM 4		A78300003
Microscope	Axiovert 40 CFL		10326743
	Axiovert 40 C	Zeiss	NA
	Axiovert 25		NA
Couting chamber	Neubauer counting Chamber	Marienfeld-Superior	0640110
Flow Cytometer	FACS Aria II	BD Biosciences	
	CytoFLEX S	Beckman Coulter	C01159
Nucleoporator	4D-Nucleofector Core Unit		AAF-1003B
	4D-Nucleofector Y Unit	Lonza	AAF-1003Y
	4D-Nucleofector X Unit		AAF-1003X
Precision Balance	PNJ 3000-2M	Kern&Sohn	3000-2M
	CP2201	Sartorius	NA

pH meter	SevenEasy pH-meter	Mettler Toledo	51302803
Shaker	Infors HT Multitron Standard	INFORS HT	
	Vortex-Genie® 2	Roth	P505.1
	Thermomixer F1.5	Eppendorf	5384000012
Rotator	Disc-Mixer RS-RD 5	PHOENIX	PHOE_14007
	Stuart Scientific SRT1 Roller Mixer	Stuart Scientific	R000100771
Luminometer	GloMax Navigator	Promega	GM2000
UV Table	Blue Light LED Illuminator	Analytikjena	846-057-570
	Quantum	Vilber	
UV-Nanospectrometer	NanoDrop™ One/OneC Microvolume UV-Vis Spectrophotometer	Thermo Fisher Scientific	ND-ONE-W
	Qubit4		Q33238
Thermocycler	MiniAmp Thermal Cyclers		A37835
	Mastercycler personal	Eppendorf	NA
	96 Universal Gradient	Peqlab	PQ95-06002
	PowerPac 200 Power Supply		NA
Gel chambers for agorose gels	Mini-SUB® Cell GT and Wide Mini-SUB® Cell		1704405
Western blot equipment	Mini-PROTEAN® Comb, 10-well, 1.5 mm, 66 µl		1653365
	Mini-PROTEAN® Combs, 15-well, 1.5 mm, 40 µl		1653366
	Mini-PROTEAN® Short Plates		1653308
	Mini-PROTEAN® Spacer Plates with 1.5 mm Integrated Spacers	Bio-Rad	1653312
	15-Well Comb, 14 cm wide, 0.75 mm thick, fixed-height comb		1704445
	Trans-Blot® Turbo™ Transfer System		1704150
	Mini-PROTEAN® Tetra Cell		1658000
	PowerPac HC Power Supply		1645052
Gel imaging system	ChemiDoc MP Imaging System		17001402
Ice machine	IceMachine	Ziegra	213036

Refrigerator	Liebherr Premium NoFrost, 4°C and -20°C	Liebherr	
	Ultra Low Freezer MDF-U73VC VIP	Sanyo	MDF-U73V
Irradiator	Faxitron MultiRad160	Faxitron Bioptic	

All plastic wares (Filters, Pipettes, Tips, Plates, Dishes, Flasks, Syringes) were obtained from Sarstedt, Biozym or Greiner Bio-One.

Table 2: List of molecular biology reagents

Molecular Biology	Product name	Supplier	Ref. number
Bacteria	XL-1 Blue competent bacteria	Agilent Technologies MfG GmbH&Co.KG	200236
Bacterial media	LB-Medium (Luria/Miller)	Roth	X968
	LB-Agar (Luria/Miller)		X969.2
	Super-Optimal Broth Medium (SOB)		AE27.1
	SOC-Medium		
Buffers, reagents and kits- to work with DNA	6x DNA loading dye	Thermo Fisher Scientific	R0611
	GeneRuler DNA ladder mix		SM0331
	Tris-Acetat-EDTA-Buffer, 50x		B49
	Ethanol absolut	Sigma	24105-2,5L-M
	2-propanol		33539-1L-M
	Ampuwa free distilled water	HSK Handels GmbH	4801694
	Universal-Agarose, peqGOLD	VWR	732-2789P
DNA isolation	PureLink™ HiPure Plasmid Maxiprep Kit	Thermo Fisher Scientific	K210007
	GeneJET Plasmid Miniprep Kit		K0503
	GeneJET Gel Extraction Kit		K0692
	QIAamp DNA Micro Kit	Qiagen	56304
Genomic DNA isolation	QIAamp DNA Blood Mini Kit		51104
	AllPrep DNA/RNA Mini Kit		80204
DNA quantification	Qubit dsDNA HS Assay Kit	Thermo Fisher Scientific	Q32854

RNA isolation	Quick RNA MicroPrep Kit	Zymo Research	R1050
RNA quantification	Qubit RNA HS Assay Kit		Q32852
Cloning	T4 DNA Ligase	Thermo Fisher Scientific	EL0011
	Fast AP alkaline phosphatase		EF0651
	T4 Polynucleotide Kinase		EK0031
	Restriction enzymes	New England Biolabs	
	NEBNext High Fidelity 2x Master Mix		M0541L

Table 3: List of proteomics reagents

Proteomics	Product name	Supplier	Ref. number
Buffers, reagents and kits- to work with proteins	RIPA Lysis Buffer	Thermo Fisher Scientific	89901
	Restore PLUS Western blot stripping Buffer		46430
	Tween 20	Calbiochem	655204
	Powdered Milk	Roth	T145.2
	TEMED	Bio-Rad	161-0800
	4x Laemmli Sample Buffer		1610747
	Clarity Max Western ECL Substrate		1705062
	Trans-Blot Turbo RTA Mini 0.2 µm PVDF Transfer Kit, for 40 blots #1704272		1704272
	10x TBS		170-6435edu
	Trans-Blot Turbo 5x Transfer Buffer		10026938
	Ammonium Persulfate (APS) 10g		1610700
	TGX Stain-Free™ FastCast™ Acrylamide Kit, 10%		1610183
	Methanol	Roth	4627
	Rotiphorese® 10x SDS-PAGE buffer		3060

Table 4: List of cell culture reagents

Cell culture	Product name	Supplier	Ref. number

Reagents for cell culture	Lenti-X-Concentrator	Takara	631231
	RetroNection GMP grade	Takara	T202
	Erythrocyte Lysis buffer	c-c-Pro	PL-29-L
	dimethyl sulfoxide (DMSO)	Roth	A994.2
	EDTA 1kg	Roth	X986.2
	PEI	Polysciences	23966
	Cell Dissociation Buffer, enzyme-free, PBS	Gibco by Life technologies	13151-014
	Caffeine	Sigma Aldrich	BCCC8969
	APC BrdU Flow Kit	BS biosciences	552598
	APC Annexin V apoptosis Detection Kit II	BS biosciences	560209
	CellTiter-Glo Luminescent Cell viability Assay	Promega	G7571
	FBS	Gibco by Life technologies	16000044
	Penicillin/ streptomycin		15140-122
	Sodium pyruvate		11360070
	L-Glutamine		25030-081
	NEAA		11140-050
	Opti-MEM		31985062
	Phosphate Saline Buffer		BE17-516F
	0.5% Trypsin-EDTA (10X)		15400-054
Media	DMEM		11965-092
	RPMI		21875-034
	IMDM		12440-053
	Stemspan SFEM	StemCellTechnologies	9650
Cytokines	Recombinant Human TPO	Peprotech	300-18
	Recombinant Human SCF		300-07
	Recombinant Human Flt3-Ligand		300-19
	Recombinant Human IL-6		200-06
	Recombinant Murine TPO		315-14
	Recombinant Murine SCF		250-03

	UM171	Stemcell Technologies	72914
	StemRegenin 1		72344
	Polybrene	Sigma Aldrich	TR-1003-G
	DAPI		D9542

Table 5:List of antibiotics

Antibiotics	Product name	Supplier	Ref. number
Cloning	Ampicilline (Final concentration 100µg/mL)	Applichem	69-52-3
Cas9 expression selection	Blasticidine (Final concentration 10µg/mL)	InvivoGen	ant-bl-1
	Puromycin (Final concentration 1µg/mL)		ant-pr-1
Gene expression induction	Doxycycline hyclate (Final concentration 0.5µg/mL)	Sigma	D9891-1G
Post transplantation	Ciprofloxacin (Final concentration 50µg/mL)	Fresenius KABI	15LF506R1

Table 6: Drugs used for *in vitro* experiments

Drugs	Product name		Supplier	Ref. number
TRIP13 inhibitor	DCZ0415	(Wang, Huang et al. 2020)	MedChemExpress	HY-15676
MDM2 inhibitor	Idasanutlin (RG7388)	(Konopleva, Martinelli et al. 2020)		HY-130603
BCL2/BCL-XL inhibitor	Navitoclax (ABT-263)			HY-10087
	5-Azacytidine (Azacitidine)			HY-10586

Table 7: Antibodies used for flow cytometry and Western Blot

Antibodies	Product name	Clone	Supplier	Ref. number
Fetal liver cell isolation	Anti-mouse TER-119 Biotin	TER-119	BD biosciences	553672
	EasySep™ Mouse Streptavidin RapidSpheres™ Isolation Kit		Stemcell Technologies	19860
Flow Cytometry	Pacific Blue Anti-mouse Lineage Cocktail		Biolegend	133310

Anti-mouse TER-119 APC/Cyanine7	TER-119	BD biosciences	560509
Anti-mouse CD41 APC/Cyanine7	MWReg30	Biolegend	133928
Anti-mouse CD16/32 APC/Cyanine7	S17011E		156612
Anti-mouse CD117 (c-kit) APC/Cyanine7	2B8		105826
Anti-mouse CD117 APC	2B8	BD biosciences	553356
Anti-mouse/rat Ly-6G/Ly-6C (Gr-1) APC	RB6-8C5	Biolegend	108412
Anti-mouse/rat CD42d APC	1C2		148505
Anti-mouse/rat CD42d PerCP/Cyanine5.5			148507
Anti-mouse CD34 PerCP/Cyanine5.5	HM34		128607
Anti-mouse Ly-6G/Ly-6C PerCP/Cyanine5.5	RB6-8C5	BD Biosciences	552093
Anti-mouse CD71 PerCP/Cyanine5.5	CY1G4	BD Biosciences	567256
Anti-mouse Ly-6A/E PE/Cy7	D7		561021
Anti-CD11b PE/Cy7	M1/70	Biolegend	552850
Anti-mouse CD41 PE/Cy7	MWReg30		133915
Anti-Human CD38 PE/Cy7	HB7	BD Biosciences	335825
Anti-Human CD15 V500	HI98		561585
Anti-Human CD42b APC	HIP1		551061
Anti-Human CD90 APC	5E10		559869
Anti-Human CD34 PE/Cy7	581	Beckman Coulter	A21691
Anti-Human CD41 PE/Cy7	P2		6607115
Anti-Human CD235a APC-A750	11E4B-7-6 (KC16)		A89314
Anti-Human CD33 PerCP/Cyanine5.5	D3HL60.251		A70198
Anti-Human CD117 APC-A750	104D2D1		B92450

	Anti-Human CD14 APC	RMO52		IM2580
	Annexin-V APC		BD Biosciences	550475
	Anti-BrdU APC	BU20A	Biolegend	339807
	Anti-BrdU PE/Cyanine7	3D4	Biolegend	364118
Immuno-precipitation	Pierce Anti-HA Magnetic Beads		Thermo Fisher Scientific	88837
Western Blot	TRIP13 Antibody (C-4)		Santa Cruz	sc-514314
	β-Tubulin Antibody			2146S
Primary antibodies	Phospho-Histone H2A.X (Ser139) (20E3) Rabbit mAb			9718T
	HAUSP (D17C6) XP Rabbit mAb			4833T
	CRM1 Antibody (H-7)		Cell Signaling	sc-74455
	p53 (D2H9O) Rabbit mAb			32532S
	Vinculin (E1E9V) XP Rabbit mAb			13901S
	GAPDH (14C10) Rabbit mAb			2118S
	Anti-HA tag antibody [HA.C5]			ab18181
	Anti-p53 antibody [PAb 240]			ab26
Secondary antibodies	Rabbit Anti-mouse IgG H&L		abcam	ab46540
	Goat Anti-Rabbit IgG H&L (HRP)			ab6721

Table 8: Cell lines used for *in vitro* experiments

Human cell lines	Product name	Cytogenetics	Supplier	Ref. number
Non-Leukemia	HEK 293T	61-73<3n>XXX	DSMZ	ACC 635
cell lines	HT1080	46<2n>XY		ACC 315
Leukemia cell lines	K562	61-68<3n>XX		ACC 10
	HEL	63(60-64)<3n>XYY		ACC 11
	CMK	85-90<4n>XY		ACC 392
	OCI-AML3	48(45-50)<2n>X/XY		ACC 582

	KASUMI-1	45<2n>X		ACC 220
	M07E	46(45-46)<2n>XX		ACC 104
	ML2	92(84-94)<4n>XX		ACC 15
	NOMO1	46-47<2n>XX		ACC 542

Table 9: Vectors used for the experiments

Vector list	Name	Features	Addgene Ref.
	psPAX2		12260
	pMD2.G		12259
Constitutive cDNA overexpression with reporter	SIN40C.SFFV.MCS.IRES.GFP		169280
	SIN40C.SFFV.MCS.IRES.dTomato		169279
	SIN40C.SFFV.3HA-NUP98::KDM5A.IRES.GFP		
	SIN40C.SFFV.3HA-TRIP13.IRES.GFP		
shRNA or miRNA overexpression with reporter	SIN40C.SFFV.mTagBFP.miR30n		169281
	SIN40C.SFFV.dTomato.miR30n		169277
sgRNA	SGL40C.EFS.E2Crimson	(Labuhn et al., 2018)	100894
	SGL40C.EFS. dTomato		89395
Inducible cDNA overexpression	SIN40C.TRE.MCS.IRES.dTomato.PGK.sfGFP.P2A.Tet3G		169283
	SIN40C.TRE.3HAxNUP98::KDM5A.IRES.dTomato.PGK.sfGFP.P2A.Tet3G		
	SIN40C.TRE.3HAxTRIP13.IRES.dTomato.PGK.sfGFP.P2A.Tet3G		

3.1.2. Vectors

SIN40C.SFFV.MCS.IRES.GFP/dTomato: constitutive cDNA overexpression vector driven by the SFFV promoter. cDNAs encoding NUP98::KDM5A and TRIP13 were cloned upon AgeI and MluI digestion.

SGL40C-NL-SL-EFS-dTomato/E2Crimson (Reimer, Knöß et al. 2017, Labuhn, Adams et al. 2018): This vector encodes the invariable part of the gRNA against Target genes under control of a hU6 promotor and a reporter fluorescent protein (dTomato/E2Crimson) under the control of

an EFS promoter. The sgRNA of the target gene of interest was cloned into the backbone as a double stranded oligonucleotide by a BmsBI digestion.
SIN40C.SFFV.dTomato/mTagBFP2.miR30n: this vector encodes the 5p and 3p arms of the miR30n miRNA, allowing the cloning of a shRNA specific stem loop (see 3.1.5) upon BsmBI digestion.
SIN40C.TRE.MCS.IRES.dTomato.PGK.sfGFP.P2A.Tet3G: All-in-one inducible overexpression vector, with expression of insert of interest driven by the Tet Regulatory Element and constitutive expression of the Tet3G regulator, whose activation can be regulated upon doxycycline addition or removal.

3.1.3. cDNAs

NUP98::KDM5A encoding cDNA was designed based on report in human patients (de Rooij, Hollink et al. 2013). TRIP13 encoding cDNA was designed based on Ensembl genome browser. All cDNAs were tagged at the 5' terminus with three HemoAgglutinin tag (3xHA), flanked with AgeI at 5' terminus and MluI at 3' terminus, codon optimized and ordered from pTwistAmp. Plasmid were retransformed and cDNA were subcloned used the restriction enzymes AgeI and MluI into the backbone vectors for constitutive expression: NUP98::KDM5A cDNA in SIN40C.SFFV.GFP.IRES.MCS and TRIP13 in cDNA in SIN40C.SFFV.MCS.IRES.dtomato.

NUP98::KDM5A:

TACCCCTATGATGTGCCCGACTACGCTTACCCTTACGACGTGCCAGATTACGCCTATCCATACGACGTCCCCGAC
TATGCTGGTGGATCTGGCGGCGGAGGCAGCTTCAACAAGAGCTTCGGCACACCTTTTGGAGGCGGCACAGGC
GGCTTTGGCACCACATCTACCTTCGGCCAGAATACCGGCTTCGGAACCACTAGCGGCGGAGCCTTTGGCACATC
TGCCTTTGGCTCCAGCAACAACACCGGCGGACTGTTCGGCAACAGCCAGACAAAACCTGGCGGCCTGTTTGGC
ACCTCCAGCTTTTCTCAGCCTGCCACCAGCACCAGCACAGGCTTTGGCTTTGGAACAAGCACCGGCACCGCCAA
CACACTGTTTGGAACAGCCTCTACCGGCACCAGCCTGTTCAGCAGCCAGAACAATGCCTTCGCTCAGAACAAGC
CCACAGGCTTCGGCAACTTCGGCACCTCTACAAGCAGCGGAGGCCTGTTCGGAACTACCAACACCACCAGCAAT
CCCTTCGGCAGCACAAGCGGCTCCCTGTTTGGACCCAGCAGCTTTACAGCCGCTCCTACAGGCACCACCATCAA
GTTCAATCCTCCAACCGGCACAGACACCATGGTCAAAGCTGGCGTGTCCACCAACATCAGCACCAAGCACCAGT
GCATCACCGCCATGAAGGAATACGAGAGCAAGAGCCTGGAAGAACTGCGGCTGGAAGATTACCAGGCCAACA
GAAAGGGCCCTCAGAATCAAGTCGGAGCCGGCACAACCACCGGACTGTTTGGTAGCTCTCCTGCCACCTCTAGC
GCCACTGGCCTGTTTAGCTCCAGCACCACCAATAGCGGCTTCGCCTACGGACAGAACAAGACCGCCTTTGGAAC
CTCCACCACCGGATTCGGCACAAACCCAGGCGGACTTTTTGGCCAGCAGAACCAGCAGACCACCTCTCTGTTTA
GCAAGCCTTTCGGCCAGGCCACCACCACACAGAACACTGGCTTCAGCTTTGGCAACACCTCCACAATCGGCCAG
CCTAGCACCAATACCATGGGGCTGTTTGGCGTGACCCAGGCTTCTCAACCAGGCGGGCTCTTTGGGACCGCCAC
AAATACCTCTACAGGGACCGCATTCGGAACCGGAACAGGGCTGTTCGGACAGACAAACACCGGATTTGGCGCC
GTGGGCAGCACACTCTTCGGAAACAACAAGCTGACCACCTTCGGCTCTAGCACCACAAGCGCCCCATCCTTCGG
TACAACATCTGGCGGGCTTTTCGGCTTCGGGACTAACACCAGCGGCAACTCCATCTTTGGCAGCAAGCCTGCTC
CTGGCACACTCGGAACAGGACTTGGCGCTGGATTTGGCACAGCCCTTGGAGCTGGACAGGCATCCCTGTTCGG
GAACAATCAGCCCAAGATCGGCGGACCACTTGGCACCGGCGCTTTTGGAGCACCTGGCTTCAATACCACCACCG
CCACACTCGGTTTTGGAGCCCCTCAAGCTCCTGTGGCTCTGACCGATCCTAATGCCTCTGCTGCTCAGCAGGCCG
TTCTGCAGCAGCACATCAACAGCCTGACATACAGCCCCTTCGGCGACAGCCCTCTGTTCAGAAACCCCATGAGC
GACCCCAAGAAGAAAGAAGAGGACGACTCCATGGAAGAGAAGCCCCTGAAAGTGAAGGGCAAAGACAGCAG
CGAGAAGAAGCGCAAGCGGAAGCTGGAAAAGGTCGAGCAGCTGTTCGGCGAGGGCAAGCAGAAGTCCAAAG

AACTGAAGAAGATGGACAAGCCCCGGAAGAAGAAGCTGAAACTGGGCGCCGACAAGAGCAAAGAGCTGAAC
AAACTGGCCAAGAAGCTCGCCAAAGAGGAAGAGAGGAAGAAAAAGAAAGAGAAGGCCGCTGCCGCCAAGGT
GGAACTGGTCAAAGAGTCCACCGAGAAGAAACGCGAGAAAAAGGTGCTGGACATCCCCTCTAAGTACGATTG
GAGCGGAGCCGAGGAAAGCGACGACGAAAACGCTGTGTGCGCTGCCCAGAATTGCCAGAGGCCATGCAAGG
ATAAGGTGGACTGGGTGCAGTGTGACGGCGGCTGTGATGAGTGGTTCCACCAAGTGTGCGTGGGCGTGTCAC
CTGAGATGGCCGAGAACGAGGACTACATCTGCATCAACTGCGCCAAAAAGCAGGGCCCCGTGTCTCCTGGACC
TGCTCCTCCACCTAGCTTCATCATGAGCTACAAGCTGCCTATGGAAGATCTGAAAGAGACAAGCTGA

TRIP13:

TACCCTTACGATGTGCCCGACTACGCTTACCCCTACGACGTGCCAGATTATGCCTATCCTTATGACGTCCCCGAC
TATGCCGGCGGATCTGGCGGCGGAGGATCTGATGAAGCTGTGGGCGATCTGAAGCAGGCCCTGCCTTGTGTG
GCCGAGTCTCCTACAGTGCACGTGGAAGTGCACCAGAGAGGCAGCAGCACCGCCAAGAAAGAGGACATCAAT
CTGAGCGTGCGGAAGCTGCTGAACCGGCACAATATCGTGTTCGGCGACTACACCTGGACCGAGTTCGACGAGC
CTTTCCTGACCAGAAACGTGCAGAGCGTGTCCATCATCGACACCGAGCTGAAAGTGAAGGACAGCCAGCCTAT
CGACCTGAGCGCCTGTACTGTGGCCCTGCACATCTTCCAGCTGAACGAGGATGGCCCCAGCAGCGAGAACCTG
GAAGAGGAAACCGAGAACATCATTGCCGCCAACCACTGGGTGCTGCCTGCCGCCGAATTTCACGGACTGTGGG
ATAGCCTGGTGTACGATGTGGAAGTGAAGTCCCATCTGCTGGACTACGTGATGACCACACTGCTGTTCAGCGA
CAAGAACGTGAACAGCAACCTGATCACCTGGAACCGGGTCGTCCTGCTGCATGGACCTCCAGGCACAGGCAAG
ACAAGCCTGTGTAAAGCCCTGGCTCAGAAGCTGACCATCCGGCTGAGCAGCAGATACAGATACGGCCAGCTGA
TCGAGATCAACAGCCACAGCCTGTTCAGCAAGTGGTTCAGCGAGAGCGGCAAGCTGGTCACCAAGATGTTCCA
GAAGATCCAGGACCTGATCGACGACAAGGACGCCCTGGTGTTCGTGCTGATCGATGAGGTGGAAAGCCTGAC
AGCCGCCAGAAATGCCTGTAGAGCCGGAACCGAACCTAGCGACGCCATCAGAGTGGTCAATGCCGTGCTGACC
CAGATCGACCAGATCAAGAGACACAGCAACGTGGTCATCCTGACCACCAGCAACATCACCGAGAAGATCGACG
TGGCCTTCGTGGACAGAGCCGACATCAAGCAGTACATCGGCCCTCCATCTGCCGCCGCTATCTTCAAGATCTAC
CTGTCCTGCCTGGAAGAACTGATGAAGTGCCAGATCATCTACCCCAGACAGCAGCTCCTGACACTGCGCGAGCT
GGAAATGATCGGCTTCATCGAGAACAACGTGTCCAAGCTGAGCCTGCTGCTGAATGACATCAGCAGAAAGAGC
GAGGGCCTGAGCGGCAGAGTGCTGAGAAAGCTGCCTTTTCTGGCCCACGCACTGTACGTGCAGGCCCCTACAG
TGACCATCGAGGGATTTCTGCAGGCACTGAGCCTGGCCGTGGACAAGCAGTTCGAGGAAAGAAAGAAGCTGG
CCGCCTACATCTGA

3.1.4. Oligonucleotides and primers

All oligonucleotides were synthesized by IDT and purchased dried and standard desalted. All oligonucleotides were dissolved in water at 100 µM.

Table 10 : sequencing primers used to assess inserted cDNAs and sgRNAs after cloning

Name	Target	Sequence
DH037_mU6_Seq		TTTGCTGTACTTTCTATAGTG
DH077_SFFV_fwd_Seq	SFFV promoter	ATCAGCCTGCTTGTCGCTTC
DH078_IRES_rev_Seq	IRES	CATATAGACAAACGCACACCG
DH079_PPT_fw	PPT	GGT ACA GTG CAG GGG AAA GAA TA
DH038-H1_SEQ		TTTGCATGTCGCTATGTGTTC
DH080_PRE_rev	WPRE	AAAGCAGCGTATCCACATAGC
DH119_hU6_Seq	hU6 promoter	

Table 11 : Single strand oligonucleotides for sgRNA cloning. All sgRNA were design using CCTop - CRISPR/Cas9 target online predictor (Stemmer, Thumberger et al. 2015). Overhangs for BsmBI cloning are included (CACC/AAAC)

Name	Species	FW_Sequence	REV_Sequence
sgTrp53.4	Murine	CACCGAGGAGCTCCTGACACTCGGA	AAACTCCGAGTGTCAGGAGCTCCTC
sgTrip13.1		CACCGGATAGCCTCGTGTATGATG	AAACCATCATACACGAGGCTATCC
sgTrip13.2		CACCGCTACTCGGATAGCATCTGA	AAACTCAGATGCTATCCGAGTAGC
sgTrip13.3		AAACTCAGATGCTATCCGAGTAGC	AAACTCAGGTAAATTCCTAGTTC
Ing5_1		CACCgCCTGCACTCACCATCTCGT	AAACACGAGATGGTGAGTGCAGGc
Ing5_2		CACCGAAAGCAGAGATCGACATCC	AAACGGATGTCGATCTCTGCTTTC
Ehmt2_1		CACCGTGAGCTACACGAAAGTCG	AAACCGACTTTCGTGTAGCTCAC
Ehmt2_2		CACCGAGTGATGCGGCCCCGACA	AAACTGTCGGGGCCGCATCACTC
Nr3c1_1		CACCgATTATGGGGTGCTGACGTG	AAACCACGTCAGCACCCCATAATc
Nr3c1_2		CACCgTGTCCATGGGACTGTATAT	AAACATATACAGTCCCATGGACAc
Nfyc_1		CACCGAAATCCGAAACTTAACAG	AAACCTGTTAAGTTTCGGATTTC
Nfyc_2		CACCgAGTACTGGACAGGCTCCGC	AAACGCGGAGCCTGTCCAGTACTc
Bcl2l12_1		CACCgAGGCTCGGAACCATAGCAG	AAACCTGCTATGGTTCCGAGCCTc
Bcl2l12_2		CACCgCCCTGTCCCAACTCCACCC	AAACGGGTGGAGTTGGGACAGGGc
Ppm1d_1		CACCgTAGCTCCACAAGTCACCTA	AAACTAGGTGACTTGTGGAGCTAc
Ppm1d_2		CACCGAATGGCCAAAGACTATGAC	AAACGTCATAGTCTTTGGCCATTC
Ppif_1		CACCGATGTCGTGCCAAAGACTGC	AAACGCAGTCTTTGGCACGACATC
Ppif_2		CACCgCGCTCGTGTACTTGGACGT	AAACACGTCCAAGTACACGAGCGc
Bak1_1		CACCGAACTCTGTGTCGTAGCGC	AAACGCGCTACGACACAGAGTTC
Bak1_2		CACCgTGGTACCTGGAGGCGATCT	AAACAGATCGCCTCCAGGTACCAc
Ago2_1		CACCgCTGTCCGACTTGTAAACAC	AAACGTGTTTACAAGTCGGACAGc
Ago2_2		CACCGATACCTGTTCACTCTCCGA	AAACTCGGAGAGTGAACAGGTATC
Ak6_1		CACCGTTATACGACGGCTACGATG	AAACCATCGTAGCCGTCGTATAAC
Ak6_2		CACCgCTATATGAAACCAGCGTTC	AAACGAACGCTGGTTTCATATAGc
Dhrs2_1		CACCgACTGGTACATAAGCCACTC	AAACGAGTGGCTTATGTACCAGTc
Dhrs2_2		CACCGGGAGCCAGTGAACAGATC	AAACGATCTGTTCACTGGCTCCC
Dvl2_1		CACCgCGAATCTGTCGTATCACTG	AAACCAGTGATACGACAGATTCGC
Dvl2_2		CACCGAATACCTAGAAAGGCGTTT	AAACAAACGCCTTTCTAGGTATTC
Tpt1_1		CACCgCAGCCCGTCCGCGATCTCC	AAACGGAGATCGCGGACGGGCTGc
Tpt1_2		CACCgCCGATGAGCGAGTCATCGA	AAACTCGATGACTCGCTCATCGGc
Rbbp4_1		CACCGTAAGTGCCCACTGAGATT	AAACAATCTCAGTGGGCACTTAC
Rbbp4_2		CACCGCCACTGGGCAGTTAAGCT	AAACAGCTTAACTGCCCAGTGGC

Prkag1_1		CACCGTGTCAAATACCACCAACT	AAACAGTTGGTGGTATTTGACAC
Prkag1_2		CACCGAGACTTAGACATGAATTC	AAACGAATTCATGTCTAAGTCTC
Cops5_1		CACCgTGTGTACTAACATCAATCC	AAACGGATTGATGTTAGTACACAc
Cops5_2		CACCgAATCCTGGCGGCGAAACCC	AAACGGGTTTCGCCGCCAGGATTc
Psmf1_1		CACCgATCCTTAGACTCATACCGG	AAACCCGGTATGAGTCTAAGGATc
Psmf1_2		CACCgCAAACGGCTACTATGCCTT	AAACAAGGCATAGTAGCCGTTTGc
Psma7_1		CACCGTATCTCGGCCCTAATTGT	AAACACAATTAGGGCCGAGATAC
Psma7_2		CACCgATACAGACGTTATCGTCCA	AAACTGGACGATAACGTCTGTATc
Ewsr1_1		CACCgATGGACAACAGAGTAGCTA	AAACTAGCTACTCTGTTGTCCATc
Ewsr1_2		CACCgCTACCATCAAACCATTCCA	AAACTGGAATGGTTTGATGGTAGc
Prkcd_1		CACCgAGATTATCGGCCGCTGCAC	AAACGTGCAGCGGCCGATAATCTc
Prkcd_2		CACCGAGTCTGTCGGAATATACC	AAACGGTATATTCCGACAGACTC
Mapkap1_1		CACCGCAGTACACGAGTGAAGGAC	AAACGTCCTTCACTCGTGTACTGC
Mapkap1_2		CACCgCTTGGAGTACTCATTAAAG	AAACCTTTAATGAGTACTCCAAGc
Ercc2_1		CACCGCAGACTCGGGCCAGCGTCA	AAACTGACGCTGGCCCGAGTCTGC
Ercc2_2		CACCgCGCTGATAGGCCACAATCA	AAACTGATTGTGGCCTATCAGCGc
Hdac2_1		CACCgCTTGATATACTCATCGCTG	AAACCAGCGATGAGTATATCAAGc
Hdac2_2		CACCgCATCTATACCATCTCTCAT	AAACATGAGAGATGGTATAGATGc
Setd2_1		CACCgCTGCATTCGCTTAATATCC	AAACGGATATTAAGCGAATGCAGc
Setd2_2		CACCGTATGTATCTTCCCGATGT	AAACACATCGGGAAGATACATAC
Brd1_1		CACCGGGATATACGGAGCGCACA	AAACTGTGCGCTCCGTATATCCC
Brd1_2		CACCGGCTCAATGAATACCGTGT	AAACACACGGTATTCATTGAGCC
Tpp2_1		CACCGATACACGGCTAAGCACTA	AAACTAGTGCTTAGCCGTGTATC
Tpp2_2		CACCGTTACTGTTGGAAATAACCG	AAACCGGTTATTTCCAACAGTAAC
Usp10_1		CACCgTCGTGAGAGATATCCGCCC	AAACGGGCGGATATCTCTCACGAc
Usp10_2		CACCgAGTCATCGAACCTAGTGAG	AAACCTCACTAGGTTCGATGACTc
Rpa3_1		CACCGTTACCACAGTATATCGAC	AAACGTCGATATACTGTGGTAAC
Rpa3_2		CACCGCTTGACGAGGAAATCTCT	AAACAGAGATTTCCTCGTCAAGC
Pbk_1		CACCGGCTCAGTACCAATATAAC	AAACGTTATATTGGTACTGAGCC
Pbk_2		CACCGAATGACTTAATAGAAGAG	AAACCTCTTCTATTAAGTCATTC
Csnk2a1_1		CACCGGACATGACAATTATGATC	AAACGATCATAATTGTCATGTCC
Csnk2a1_2		CACCGACATTGTAAAAGACCCTG	AAACCAGGGTCTTTTACAATGTC
Taf7_1		CACCgAGAATATGCCGCTACGGTG	AAACCACCGTAGCGGCATATTCTc
Taf7_2		CACCGAAGCTGTCAGTACTCGTT	AAACAACGAGTACTGACAGCTTC
Smc4_1		CACCgAGCATGGAATCAATAACAT	AAACATGTTATTGATTCCATGCTc

Smc4_2		CACCgAGAAGCAGTAGTTAAGTTA	AAACTAACTTAACTACTGCTTCTc
Pttg1ip_1		CACCgCAGCATACGCCCCAGCGAG	AAACCTCGCTGGGGCGTATGCTGc
Pttg1ip_2		CACCCGCAGGAACCTCCGAGAGT	AAACACTCTCGGAGGTTCCTGCG
Fancb.1		CACCGTCACCGATCCACTCAATAG	AAACCTATTGAGTGGATCGGTGAC
Fancb.3		CACCGCAGCTGGTCTCTAGTAGCG	AAACCGCTACTAGAGACCAGCTGC
Fanci.3		CACCGAAATGGTTAAGTTAGACC	AAACGGTCTAACTTAACCATTTC
Brip1.2		CACCGCAGACGAACTCTATCACG	AAACCGTGATAGAGTTCGTCTGC
Pus7.1		CACCGTACGTCGTAAAGCATGAGC	AAACGCTCATGCTTTACGACGTAC
Pus7.3		CACCGTAGTGCATAAACTCGCCGC	AAACGCGGCGAGTTTATGCACTAC
Ube2c.1		CACCGTATAGCACACATCTCGTAG	AAACCTACGAGATGTGTGCTATAC
Ube2c.3		CACCGCTGTTAAGAAAGATCACGG	AAACCCGTGATCTTTCTTAACAGC
Ube2t.3		CACCGTCCAGGTTTGTGTCGCTGT	AAACACAGCGACACAAACCTGGAC
Fancb.1		CACCGTACTGAAACCCCGTTCTGG	AAACCCAGAACGGGGTTTCAGTAC
Fancb.3		CACCGCTTTCAATAGGTCATTG	AAACCAATGACCTATTGAAAGC
Fanci.3		CACCGATCCCCGAGAAGCCGTGAT	AAACATCACGGCTTCTCGGGGATC
Brip1.2		CACCGTCAGACAACCTGTTCAAGT	AAACACTTGAACAGGTTGTCTGAC
Pus7.1		CACCGCCCTGCTACCACCCCAACG	AAACCGTTGGGGTGGTAGCAGGGC
Pus7.3		CACCGTGCTGCCCACTTACGGTGC	AAACGCACCGTAAGTGGGCAGCAC
Ube2c.1		CACCGGCTGATTTGCGAGCTCGT	AAACACGAGCTCGCAAATCAGCC
Ube2c.3		CACCGGAAGTTATCATTCCTGAG	AAACCTCAGGAATGATAACTTCC
Ube2t.3		CACCGCCAGCACGTGATGCCCGG	AAACCTATTGAGTGGATCGGTGAC
sgLuc		CACCGAGTTCACCGGCGTCATCGTC	AAACGACGATGACGCCGGTGAACTC
sgTRIP13.1	human	CACCGTTGTCATCACATAATCG	AAACCGATTATGTGATGACAAC
sgTRIP13.2		CACCGTGCATGCACTCAAATCGAT	AAACATCGATTTGAGTGCATGCAC
sgTRIP13.3		CACCGGGCTAACGCTTTACACA	AAACTGTGTAAAGCGTTAGCCC

Table 12: primers used to assess the sgRNA cutting efficiency

Name	Species	FW_Sequence	REV_Sequence
sgTrp53.4_TIDE	Murine	AGGGTCTCAGAAGTTTGAGG	ATGTGAGGGAAGAGAGTTCC
sgTrip13.1_TIDE		gaactccaggcctcaatgag	ctgattgacactgagaggcc
sgTrip13.2_TIDE		ctgagccctctcacttggtg	tccaacagggaacatcgctc

3.1.5. Cell culture media

3.1.5.1. Human cell lines

Human 293T: DMEM supplemented with 10% FBS advanced, 1xNEAA, 1xSodium pyruvate, 1xPenicillin/Streptomycin.

Human HEL, NOMO-1, THP-1 and ML-2: RPMI 1640 supplemented with 10% FBS, 1xNEAA, 1xSodium pyruvate, and 1xPenicillin/Streptomycin.
Human CMK, HT93 and M-07E: RPMI 1640 supplemented with 20% FBS, 1xNEAA, 1xSodium pyruvate, and 1xPenicillin/Streptomycin. 10ng/mL IL-3 were added to M-07E.

3.1.5.2. Murine primary cells

mFL-HSPCs were cultured in pre-stimulation medium composed by: DMEM supplemented with 10% FBS, 1% penicillin/streptomycin, 1% sodium pyruvate, 1% L-glutamine, 1% nonessential amino acids, 25ng/mL murine TPO and 25ng/mL murine SCF.
mBM-HSPCs were cultured in pre-stimulation medium composed by: IMDM supplemented with 10% FBS, 1% penicillin/streptomycin, 1% sodium pyruvate, 1% L-glutamine, 1% nonessential amino acids, 50ng/mL murine TPO and 50ng/mL murine SCF.
After 24 hours post-transduction, mFL-HSPCs and mBM-HSPCs were cultured in selection medium promoting megakaryocytic differentiation composed by: DMEM and IMDM, respectively, supplemented with 10% FBS, 1% penicillin/streptomycin, 1% sodium pyruvate, 1% L-glutamine, 1% nonessential amino acids, 15ng/mL murine TPO and 15ng/mL murine SCF.

3.1.5.3. Human primary cells

Human fetal and adult PB $CD34^+$ HSPCs: cells were cultured in pre-stimulation medium composed by: Stemspan SFEM II supplemented with 1% penicillin/streptomycin, 0.75 µM Stemregenin, 35nM UM171, 100ng/ml human FLT3L, 50ng/ml human TPO, 100ng/ml human SCF, 20ng/ml human IL6. After 24 hours post-nucleoporation, hFL-HSPCs and adult PB $CD34^+$ HSPCs cells were cultured in selection medium promoting megakaryocytic differentiation composed by: Stemspan SFEM II, respectively, supplemented with 10% FBS, 1% penicillin/streptomycin, 15ng/mL human TPO and 15ng/mL human SCF.

3.1.6. Animal models

C57BL/6N: females mice used as transplant recipients or for timed breedings of $Cas9^{eth}$ embryos.
B6J.129(Cg)-Gt(ROSA)26Sor$^{tm1.1(CAG-cas9*,-EGFP)Fezh}$/J: male mice used for for timed breedings of $Cas9^{eth}$ embryos with females C57BL/6N mice.

3.1.7. Softwares and online tools

- CCTop - CRISPR/Cas9 target online predictor (Stemmer, Thumberger et al. 2015) (https://cctop.cos.uni-heidelberg.de)
- Snapgene 4.1.9 (Snapgene.com)
- Clone Manager (Sci-Ed software)
- Primers3plus (primer3plus.com)
- BLAST (NCBI)
- Ensembl (Sievers, Wilm et al. 2011)
- StepOne™ software (Life Technologies, Thermo Fisher)
- CytExpert (Beckman Coulter)
- Kaluza 2.1 (Beckman Coulter)
- Graphpad Prism version 8 (San Diego, CA)

- GSEA (Broad Institute, UC San Diego) (Mootha, Lindgren et al. 2003, Subramanian, Tamayo et al. 2005)
- Image Lab 6.0 (Bio-Rad)
- STRING (Szklarczyk, Kirsch et al. 2023)
- BioRender (BioRender.com)

3.2. Methods

3.2.1. Molecular biology and biochemistry

3.2.1.1. Cloning

For restriction enzyme cloning, corresponding insert/backbone vectors were digested with the corresponding restriction enzymes and gel-purified with GeneJET Gel Extraction Kit. For shRNA cloning, matching oligonucleotides (see Table 11) were hybridized and phosphorylated.
For cDNA cloning cDNA sequences were obtained from a G-Block or plasmid (restriction enzyme digestion) or PCR product (see Table 8), gel-purified and ligated into digested and dephosphorylated SIN40C vector (see Table 9). Ligation was carried out at room temperature for 60minutes. Ligation mixtures were transformed into competent XL-1 blue bacteria by a heat shock of 45 s at 42°C and subsequent incubation in SOC media at 37°C and 200 rpm for 30 min. Bacteria were then suspended on LB-agar plates supplemented with ampicillin and incubated over night at 37°C. Growing colonies were picked, expanded and used for plasmid-DNA preparation. Plasmid-DNA was analyzed by a control digestion and subsequent Sanger sequencing by Seqlab Microsynth with specific oligos (see Table 10).

3.2.1.2. sgRNA-negative selection screen

Genomic DNA was isolated at day 2 post-transduction and at the end timepoint from a suitable cell amount to ensure proper representation (1000x coverage), using the QIAamp DNA Blood Mini Kit (Qiagen). The sgRNA amplicon was PCR-amplified (see Table 13) using primers containing the p5 and p7 adaptor sequences (Gialesaki, Bräuer-Hartmann et al. 2023), gel-purified. sgRNA quantification was assessed by next generation sequencing (NGS; single-end) on an Illumina HiSeq 2500 (see 3.2.4.1).

Table 13: PCR protocol for amplicon sequencing

	Temperature	Time	Cycle
Initial Denaturation	98°C	2 minutes	1
Denaturation	98°C	10 seconds	30
Annealing	62°C	30 seconds	
Extension	72°C	30 seconds	
Final Extension	72°C	5 minutes	1

3.2.1.3. Western Blot

To measure protein expression, cells were sorted and lysed in Pierce RIPA buffer. Protein concentration was calculated based on lysed cell number and equal amounts per sample were separated by SDS-PAGE. Proteins were transferred on polyvinylidene difluoride (PVDF) membrane, blocked with 5% milk for 1 hour at room temperature and incubated with primary

antibodies over night at 4°C. Blots were further incubated with an HRP-conjugated secondary antibody for 1 hour at room temperature and developed using Clarity Max Western ECL Substrate.

3.2.1.4. Co-Immunoprecipitation and Mass Spectrometry

To identify protein-protein interaction partners of TRIP13, Co-immunoprecipitation of TRIP13 was performed on OCI-AML3 cells using Anti-HA antibody coupled to magnetic beads (Pierce Anti-HA Magnetic Beads). All steps e.g cell lysis, nuclear extraction and washing, followed standard protocols. After cell lysis and affinity pulldown, proteins were eluted and subjected to proteolysis with trypsin according to the FASP (filter-aided sample preparation) protocol (Wiśniewski et al., 2009). Downstream steps were performed in collaboration with Professor Andrea Sinz´ lab by Dr. Christian Ihling. Samples were analyzed by LC/MS/MS using a U3000 nano-HPLC system coupled to a Q-Exactive Plus mass spectrometer. After desalting the samples on the trapping column (Acclaim PepMap 100, 300 µm × 5 mm, 5µm, 100 Å, Thermo Fisher Scientific), peptides were separated on the separation column (µPAC 50 cm, C18) using a linear gradient from 3% to 40% B (solvent A: 0.1% (v/v) formic acid in water, solvent B: 0.08% (v/v) formic acid in acetonitrile) with a constant flow rate of 300 nl/min over 180 min. Data were acquired in data-dependent MS/MS mode with higher-energy collision-induced dissociation (HCD), and normalized collision energy set to 28%. Each high-resolution full scan (m/z 375 to 1799, R = 140,000 at m/z 200) in the orbitrap was followed by high-resolution product ion scans (R = 17,500) of the 10 most intense signals in the full-scan mass spectrum (isolation window 2 Th). The target value of the automated gain control was set to 3,000,000 (MS) and 200,000 (MS/MS); maximum accumulation times were set to 100 ms (MS) and 150 ms (MS/MS). Precursor ions with charge states <2+ or >6+ were excluded from fragmentation. Dynamic exclusion was enabled (duration 60 seconds, window 3 ppm).

3.2.2. Cell biology

3.2.2.1. Maintenance of cell lines and primary cells

Cells were maintained at 37°C with 5% CO_2 in their corresponding appropriate medium (see 3.1.2.) and optimal density. Suspension cells were split by medium change every two to three days to maintain optimal cell density. Adherent HEK293T cells were split after aspirating the medium, washing the cells with PBS and trypsinization for 1 minute at RT. Detached cells were seeded in an appropriate amount of medium.

3.2.2.2. Freezing and thawing of cells

For long-term storage, cells were frozen in FBS supplemented with 10% DMSO in cryotubes in 1°C containers at –80°C and then stored in liquid nitrogen. For reuse, cells were rapidly thaw in water bath at 37°C, washed in prewarmed medium to remove DMSO and lastly resuspended with corresponding medium and appropriate cell density.

3.2.2.3. Isolation of mFL-HSPCs

Murine fetal HSPCs were isolated from liver of heterozygous Cas9 knock-in 13.5 embryos. First, fetal livers were passed through a 20G and 23G needle ten times each to obtain single

cell suspension. Cells were counted, centrifuged at 300 x g for 5 minutes and resuspended at a density of 10^8 cells in 1 mL FACS buffer. Ter119 depletion was performed using the EasySep Mouse Streptavidin RapidSpheres Isolation Kit, according to manufacturer instructions. Ter119 negative fetal liver cells were resuspended in complete DMEM supplemented with 25 ng/mL Thpo and 25 ng/mL Scf.

3.2.2.4. Isolation of mBM-HSPCs

Murine adult HSPCs were isolated from bone marrow of adult mice. To obtain single cell suspension, bones of up to five mice were crushed with a pistil into a mortar containing 5-8ml of medium. Collected medium was passed through a 100µm filter in a 50ml Falcon tube. Bone marrow cells were centrifuged at 300 x g for 5 minutes and resuspended in Erythrocyte lysis buffer. Then, bone marrow cells were centrifuged at 300 x g for 5 minutes, resuspended in medium and passed through a 70µm filter in a 50ml Falcon tube. Before sorting, cells were centrifuged at 300 x g for 5 minutes, resuspended in medium at the concentration of $2x10^7$ cells in 100µl in FACS buffer. Next, cells were incubated at 4°C for 30 minutes in the dark adding 10, 1.25 and 1.25 µL respectively of the following antibodies: Lineage antibody cocktail (Pacific Blue anti-mouse Lineage Cocktail, BioLegend), cKit (CD117) – APC (clone 2B8) and Sca1 – PE (or PE-Cy7) (clone D7). Last, cells were centrifuged at 300 x g for 5 minutes, resuspended in medium at the concentration of $2x10^7$ cells in 100µl in FACS buffer supplemented with DAPI at 0.33 µM. mBM-HSPCs (LSK) cells were sorted gating based on the following gating strategy (x axis/y axis): Forward Scatter-Area/ Side Scatter-Area, Forward Scatter-Area/ Forward Scatter-High, Side Scatter-Area/DAPI-Area, APC-Area/Pe-Area or PE-Cy7-Area. Sorted LSK cells were resuspended in complete IMDM supplemented with 50 ng/mL Thpo and 50 ng/mL Scf.

3.2.2.5. Isolation of human HSPCs

Human fetal and adult HSPCs were isolated from fetal liver and adult donor peripheral blood, respectively. Fetal livers were mechanically destroyed using scalpels and sliced tissue was passed through a 22G needle to obtain single cell suspension. Then, cells were passed through a 70µm filter in a 50ml Falcon tube. The Ficoll gradient separation of blood was performed and white blood cell ring was isolated in a 50ml Falcon tube. After cell counting, appropriate volume of blocking reagent and CD34 MicroBeads was added to cell suspension. After 1h incubation on ice, MACS separation columns on magnet were used to separate the CD34+ HSPCs. Cells were cultured in pre-stimulation medium as described in 3.1.5.3

3.2.2.6. Transfection

To produce lentiviral particles, HEK293T cells were co-transfected with the vector of interest and the packaging constructs, psPAX2 and pMD2.G (Addgene #12260 and #12259, respectively), using the polyethyleneimine (PEI) transfection method. First, HEK293T cells were seeded at a concentration of $4x10^6$ cells per 10 cm^2 dish 24-hours before the transfection. Then, shortly before transfection, medium was changed. Meanwhile, the PEI-DNA mixture was prepared (Table 14) and added after 5 minutes of incubation. To optimize the viral harvest, medium supplemented with 2 mM caffeine was replaced after 6-hour post-

transfection. Viral supernatant was harvested 36-hours after transfection and concentrated before the usage or the storage.

Table 14: Mix used for transfection

	Amount per 10 cm^2 dish
psPAX2	12µg
pMD2.G	2µg
Vector of interest	6µg
Opti-MEM	To 220µL
polyethyleneimine (PEI)	220µL

3.2.2.7. Virus concentration

Lentiviral supernatant was collected as mentioned above, centrifuged at g for 5 minutes and passed through a filter with a diameter of 0.45 µm, followed by ultracentrifugation over night at 13 000 g. For supernatant containing lentiviral particles expressing cDNAs, a further concentration was performed using Lenti-X-Concentrator. According to the manufacture's instruction, supernatant was removed and lentiviral particles resuspended in cold IMDM. Then, 1 volume of Lenti-X-Concentrator was added to 3 volumes of collected virus, followed by incubation at 4°C for 30 minutes. The mixture was further centrifuged at 1500 x g for 45 minutes at 4°C. After the supernatant was removed, lentiviral pellet was resuspended in 100 µL and used to transduced cells or stored at –80°C.

3.2.2.8. Transduction

Human cell lines were counted and seeded in medium supplemented with 5 g/mL polybrene. Murine primary cells, mFL-HSPCs and mBM-HSPCs, and human primary cells, hFL-HSPCs and PB-HSPCs, were counted and seeded in their corresponding medium supplemented with 2 g/mL polybrene in Retronectin-coated plates according to manufacturer's instructions (Takara Bio). Concentrated viral particles were added to the cells, aiming a Multiplicity Of Infection (MOI) of 0.3-0.6. After 6-hours post- transduction, fresh medium was added. Transduction efficacy was assessed 48 hours post-transduction by flow cytometry based on the signal of the co-expressed fluorescence reporter protein.

3.2.2.9. sgRNA-negative selection screen

15 x 10^6 NUP98::KDM5A$^+$ mFL-HSPCs and NUP98::KDM5A$^+$ mBM-HSPCs, Bcor$^{-/-}$ and Runx1$^{-/-}$ and Gata1s RUNX1A$^+$ mFL-HSPCs were lentivirally transduced with the Fetal signature sgRNA library (MOI=0.3) to achieve sufficient representation (1000-fold coverage of X sgRNAs). Samples were harvested after 2 days post-transduction and 16 population doublings, corresponding to approximately 30 days of culture. Genomic DNA was isolated as describe in 3.2.1.2.

3.2.2.10. Proliferation and rescue assays

To evaluate the effect of NUP98::KDM5A transformation, mFL-HSPCs and mBM-HSPCs were co-transduced with lentiviral vectors overexpressing the human cDNA encoding NUP98::KDM5A, which was assigned to a green fluorescent protein thereby allowing direct clonal growth competition.
To assess growth advantages conferred by overexpression of sgRNA(s) or TRIP13 cDNA and for rescue experiments, transduced mFL-HSPCs were measured every 2/3 days starting 72 hours post-transduction and analyzed for reporter gene expression. For inducible expression of TRIP13, doxycycline was added at a concentration of 0,5 µg/mL 96 hours post transduction.

3.2.2.11. Drug assays

Cells were seeded in a 96-well plate in 100 µl of corresponding media treated using a serial dilution (1:2) of DCZ0415 (TRIP13 inhibitor), Idasanutlin (MDM2 inhibitor), Navitoclax and 5-Azacytidine. For viability assays, cells were treated for seven days with the respective drugs and cell viability was measured by CellTiter-Glo® Luminescent Cell Viability Assay (Promega, USA).

3.2.2.12. Flow cytometry and Sorting

To assess the expression of fluorescent reporter protein, cells were centrifuged at 300 x g for 5 minutes. Then, cells were washed with phosphate-buffered-saline (PBS) followed by centrifugation at 300 x g for 5 minutes and resuspended in PBS with 2% FBS. To assess the immunophenotype, cells were further stained for 30 min in the dark at 4°C with diluted (1:100) antibodies, listed in Table 7. The following panels were used: Myeloid (CD11b and Gr-1), Progenitor (CD34, CD16/32, C-kit/CD117, Sca-1), Megakaryocytic (CD41, CD42d) Erythroid (CD71 and CD235a for human cells or Ter119 for murine cells). Flow cytometry was performed on a CytoFLEX flow cytometer (Beckman Coulter) and the data analysis were done using Kaluza 1.5 (Beckman Coulter) software.
The same procedure was performed to sort the cell subpopulation of interest. Cells were sorted using BD FACSAria™ II Flow Cytometer (BD Biosciences).

3.2.2.13. Apoptosis and Cell cycle assays

Apoptotic cell death was assessed using the Annexin V apoptosis Detection Kit II with APC conjugated anti-Annexin-V antibody. Cell cycle analysis was performed with the BrdU Flow Kit using PE-Cy7 conjugated anti-BrdU antibody. Both assays were performed according to manufacturers' instruction.

3.2.2.14. Cytospins

Cells were cytocentrifuged onto glass slides and stained with May-Grunwald-Giemsa, before microscopic analysis.

3.2.3. Animal Studies

All experiments involving mice were performed in accordance with protocols approved by the local authorities (Land-esverwaltungsamt Sachsen-Anhalt). B6J.129 (Cg)-

Gt(ROSA)26Sortm1.1(CAG-cas9*,-EGFP)Fezh/J) (Jackson Laboratory, RRID: IMSR_JAX:026179), C57BL/6N (Charles River, RRID: IMSR_JAX:000664) mice were maintained in a specific pathogen-free environment in individual ventilated cages and fed with autoclaved food and water at the Martin-Luther-University Halle-Wittenberg.

3.2.3.1. Transplantations

One day before transplantation, C57BL/6N mice were irradiated inside Faxitron MultiRad160 with a dose of 7 Gy. Immediate treatment with ciprofloxacin was started and administrated up to three weeks to prevent infections. Transformed mFL-HSPCs and mBM-HSPCs were centrifuged at 300 x g for 5 minutes and resuspended in IMDM supplied with 2% FBS. 2 x 10^6 cells in 150 µL per mouse were injected into irradiated mice. Each group was composed of five to ten mice per condition. Transplanted mice were checked every day after transplantation for five days in a row and later every two days to assess the vitality score. Tail bleedings were performed every two weeks starting at four weeks post-transplantation. 100 µL of blood was drawn to assess the presence of leukemia. In presence of leukemia and/or impaired vitality, mice were euthanized and analyzed.

3.2.3.2. Analysis of leukemic mice

Bone marrow cells were isolated as described in Isolation of mBM-HSPCs . Liver and spleen were mashed through 70 µm filter and single cell suspension was obtained. Part of the spleen was taken and stored in 4% formaldehyde in PBS for possible histopathologic analysis. Flow cytometry analysis was performed using the panels described in Flow cytometry and Sorting . Part of cells isolated from bone marrow and spleen and liver were frozen alive. Part of cells isolated from bone marrow were used for DNA or RNA isolation. 10^5 bone marrow cells were used for preparation of cytospins as described in Cytospins.

3.2.4. Quantification and statistical analysis

3.2.4.1. sgRNA quantification: sgRNA negative selection screen

Model-based analysis of genome-wide CRISPR/Cas9 knockout (MAGeCK) (Li, Xu et al. 2014) was used to identify hits from the sgRNA screen (pipeline was performed by Konstantin Schuschel). Double barcoded reads were demultiplexed using custom R scripts; guides with fewer than 20 reads in ≥75% of all samples were excluded. Raw read counts were passed to the MAGeCK test command using default parameters. Samples collected at the endpoint were compared to day 2 to determine negative enrichment. Genes with a p-value <0.05 as determined by MAGeCK were deemed significant.

3.2.4.2. Gene Quantification: RNA-sequencing

Transduced mFL-HSPCs and mBM-HSPCs were FACS-sorted 3, 21 days after transduction; sgLuc- and sgTrip13- transduced mFL-HSPCs expressing NUP98::KDM5A translocation were FACS-sorted 4 days after transduction. RNA was extracted using the Quick-RNA Miniprep Kit (Zymo Research). Quantification of total RNA was performed using a QuBit (Applied Biosystems, Thermo Fisher Scientific). A minimum amount of 150ng RNA was used as input material for the RNA sample preparations. RNA-Sequencing was performed by Novogene

Company, Ltd. Sequencing libraries were generated using NEBNext® UltraTM RNA Library Prep Kit for Illumina® (New England Biolabs) and sequenced on an Illumina NovaSeq using a paired-end 150bp system. Raw FASTQ data (raw reads) were first pre-processed using fastp (Chen, Zhou et al. 2018) and then further processed as previously described (Spinozzi, Tini et al. 2018). Differential expression analysis was performed using the DESeq2 package in R (Love, Huber et al. 2014). The resulting P values were adjusted using the Benjamini and Hochberg's approach for controlling the False Discovery Rate (FDR) (Benjamini and Hochberg 1995). Genes with an adjusted P value <0.05 were considered differentially expressed.

3.2.4.3. Gene set enrichment analysis (GSEA)

GSEA was performed using the Broad GSEA software (Mootha, Lindgren et al. 2003, Subramanian, Tamayo et al. 2005) with the permutation type set to "Gene_set" (1000 permutations). Human gene symbols were mapped to murine gene symbols using orthologue annotations provided by Ensembl (Harrison, Amode et al. 2023), considering only one-to-one orthologue relationships.

3.2.4.4. Drug assays: Synergy effect

Synergy plots, summary Bliss score calculations were generated and performed with SynergyFinder (Ianevski, Giri et al. 2022). All conditions were normalized to DMSO treated control. Data represents the mean ± SD of biological triplicates.

3.2.4.5. Mass Spectrometry

Proteome Discoverer 2.4 (Thermo Fisher Scientific) was used to process raw data (performed in collaboration with Professor Andrea Sinz´ lab by Dr. Christian Ihling). MS/MS data were searched against the Uniprot database (version Nov. 2019, tax. Homo sapiens, 73801 entries) (Consortium, 2020) (Garcia, Bolleman et al. 2019) using Sequest-HT (Eng, McCormack et al. 1994). Label-free quantification of proteins was based on extracted peak areas of corresponding peptide precursor ions.

3.2.4.6. Statistical analysis

All statistical analyses were performed with GraphPad Prism 8 (San Diego, CA). Unless indicated otherwise, 2-tailed Student t tests was used to determine the P-value between 2 groups. Statistical analyses of experiments were performed with analysis of variance (ANOVA) with Bonferroni post hoc analysis for comparisons between ≥3 groups. Kaplan-Meier method was used to determine mice survival using log-rank (Mantel-Cox) tests for statistical analyses. *P , .05, **P , .01, ***P , .001, ****P , .0001. A value of P , .05 was considered statistically significant.
All statistical tests and sample numbers are disclosed in the respective figure legends and supplemental tables.

4. Results

4.1. Modeling NUP98::KDM5A^{+} AMKL

4.1.1. NUP98::KDM5A induces an aggressive leukemia in mFL-HSPCs

Aiming to decipher the contribution of fetal hematopoiesis in NUP98::KDM5A-driven AMKL transformation and potential vulnerabilities arising from it, we generated murine cell models by overexpressing the cDNA encoding for the human NUP98::KDM5A fusion protein. Murine HSPCs isolated from E13.5 fetal liver (mFL-HSPCs) and from bone marrow of adult mice (mBM-HSPCs) were utilized in the study to interrogate the impact of the ontogenic effects on NUP98::KDM5A^{+} AMKL *in vitro* and *in vivo* (Figure 11). The vector encoded GFP signal and cell counts were tracked over time to assess transformative capacity of NUP98::KDM5A fusion oncoprotein in these two ontogenic settings.

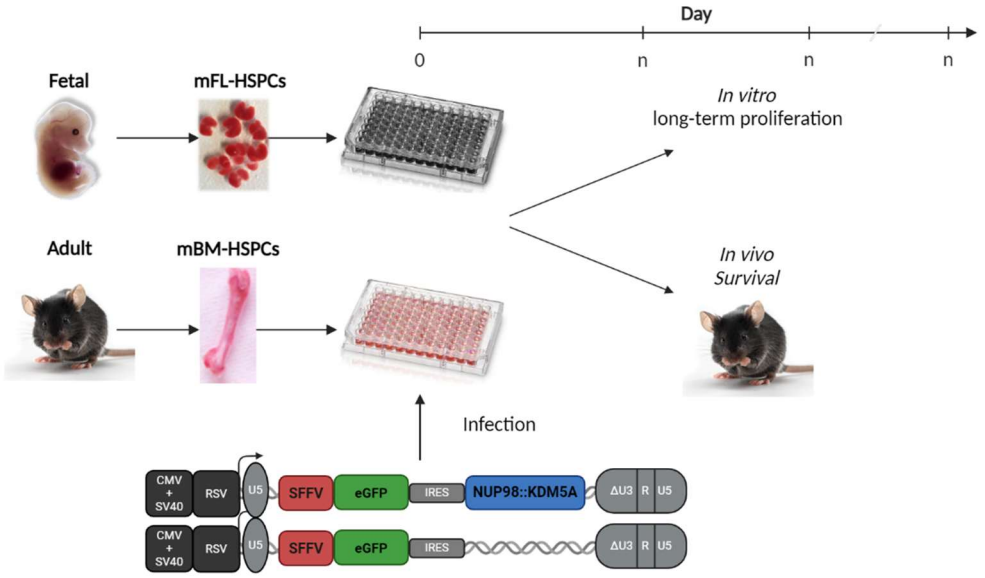

Figure 11 Modeling NUP98-KDM5A^{+} AMKL in murine system.
Schematic workflow for the generation of *in vitro* and *in vivo* murine models of constitutive overexpression of NUP98::KDM5A fusion oncoprotein in murine Hematopoietic Stem and Progenitor Cells (HSPCs) from fetal liver (mFL-HSPCs) and bone marrow (mBM-HSPCs). Created in Biorender.com

Based on GFP fluorescence, independent cell cultures were evaluated for GFP^{+} cell number, immunophenotype and cytology. Fetal and adult *in vitro* models showed a progressive enrichment of GFP^{+} transformed cells over the time, completely overcoming the normal culture after 3-4 weeks (Figure 12A). On the other hand, control cells (EV) stopped proliferating by day 14 to 21 of culture (Figure 12A). Interestingly, fetal transformed cells showed significantly accelerated growth compared to adult cells (n ≥ 3), despite highly comparable transduction rates (Figure 12A). Gene expression profiling further highlighted that fetal NUP98::KDM5A^{+} cells retained fetal signatures compared to adult NUP98::KDM5A^{+} cells (Figure 12F). In line with previous studies (Xu, Valerio et al. 2016, Schmoellerl, Barbosa et al. 2020), NUP98::KDM5A fusion exerted its oncogenic function in sustaining cell proliferation and blocking differentiation (Figure 12A-D). Transformed murine NUP98::KDM5A^{+} cells exhibited Lineage negativity, c-kit^{+} and Sca1^{+} immunophenotype and immature morphology as assessed by flow cytometric immunophenotyping and Cytospin slide preparation (Figure

12B-C-D). This observation was corroborated by gene expression analysis. GSEA confirmed negative enrichment of gene sets involved in cell differentiation and revealed positive enrichment of signatures related to *RB1* loss in both fetal and adult NUP98::KDM5A^{+} cells (Figure 12E). The latter findings aligns with the clinical observation of frequent *RB1* loss in pediatric NUP98::KDM5A^{+} AMKL patients (Figure 12E) (de Rooij, Branstetter et al. 2017).

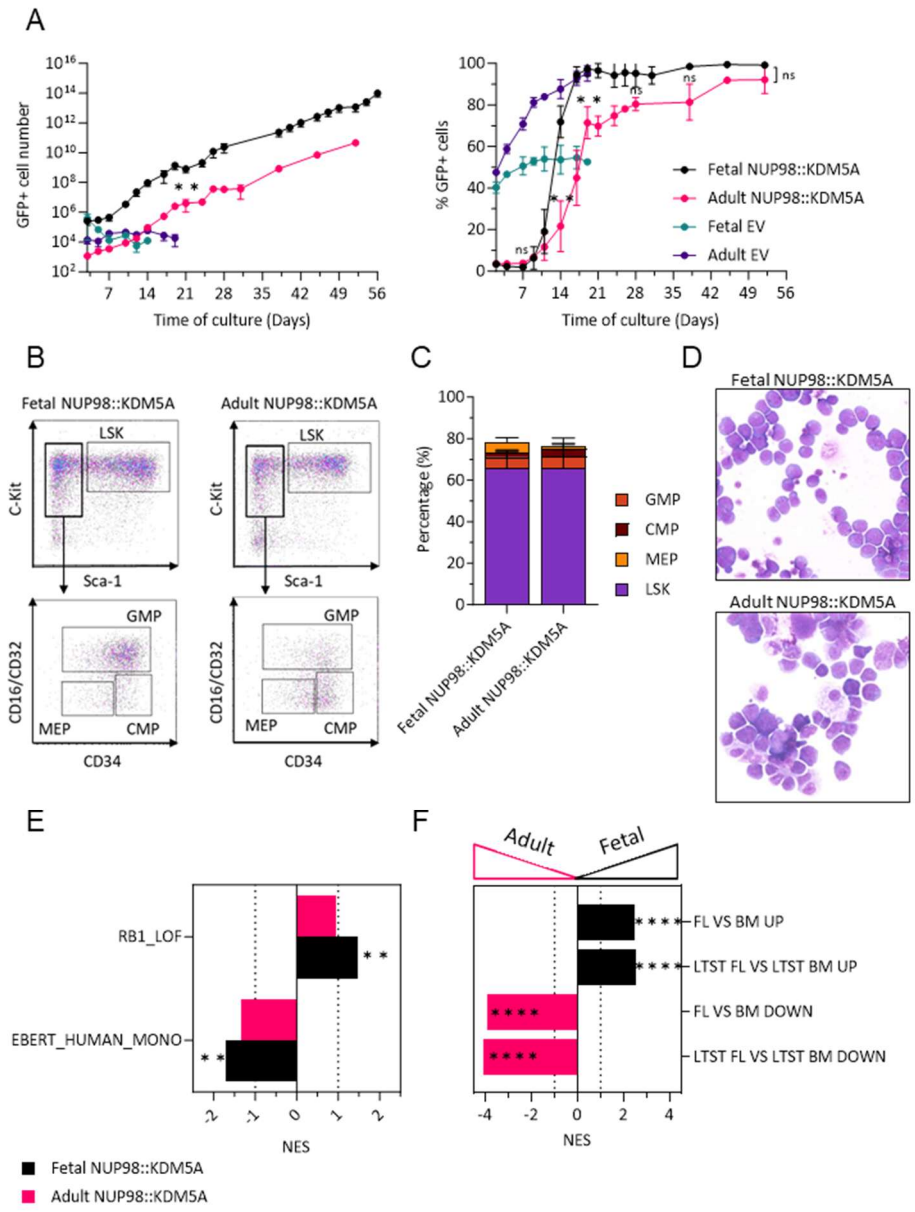

Figure 12 NUP98::KDM5A induces an aggressive leukemia in fetal HSPCs *in vitro*.

A) Dot plot showing GFP^{+} cell number (right) and percentage of GFP^{+} cells (left) of control (EV) or NUP98::KDM5A in mFL-HSPCs and mBM-HSPCs maintained in liquid culture. Data from 1 representative experiment performed in replicates are shown as mean s.d. (One-way ANOVA).

B) Representative flow cytometry analysis of fetal and adult NUP98::KDM5A^{+} cells after 4 weeks of culture.

C) Bar graph showing the percentage of LSK (Lineage negative, c-kit+ and Sca1+), Megakaryocytic-erythroid (MEP; Lineage negative, c-kit+, Sca1-, CD16/CD32- and CD34+) and common myeloid (CMP; Lineage negative, c-kit+, Sca1-, CD16/CD32- and CD34-) and granulocyte/monocyte (CMP; Lineage negative, c-kit+, Sca1-, CD16/CD32+ and CD34+) progenitors of fetal and adult NUP98::KDM5A^{+} cells after 4 weeks of culture. (mean ± s.d., n > 3)

D) Representative cytospin images (x40 original magnification) of fetal and adult NUP98::KDM5A^{+} cells from *in vitro* culture.

E) Bar graphs showing the normalized enrichment scores (NES) of significantly upregulated or downregulated gene sets in fetal and adult NUP98::KDM5A$^+$ cells compared to the respective control (EV). *False discovery rate (FDR) q <.25; ** q<.05, ns, not significant.

F) Bar graphs showing the normalized enrichment scores (NES) of significantly upregulated or downregulated gene sets in fetal NUP98::KDM5A$^+$ cells compared to adult NUP98::KDM5A$^+$ cells. *False discovery rate (FDR) q <.25; ** q<.05, ns, not significant.

ns, not significant * P < .05, ** P < .01, ***P < .001, ****P < .0001.

In our experimental design, we overexpressed the human cDNA encoding NUP98::KDM5A fusion oncoprotein and GFP separated by IRES sequence, which allows the translation of two independent proteins from one mRNA sequence (Figure 11). We produced lentiviral particles via HEK293T cell transfection, assessing transfection efficiency using a fluorescence microscope (see methods: Transfection). qRT-PCR detected 25 fold higher NUP98::KDM5A mRNA expression in fetal NUP98::KDM5A$^+$ cells compared to the control (Figure 13A). Western Blot analysis failed to detect the NUP98::KDM5A fusion oncoprotein in fetal NUP98::KDM5A$^+$ cells, although we confirmed antibody functionality using NUP98::KDM5A-transfected 293T cells as a positive control (Figure 13B). Of note, transfection resulted in 5.75-fold higher NUP98::KDM5A mRNA expression in NUP98::KDM5A-transfected 293T cells compared to fetal NUP98::KDM5A$^+$ cells (Figure 13A). To validate that the transformation is driven by NUP98::KDM5A oncoprotein, we thus performed a rescue experiment using a GFP-targeting shRNA. Knockdown of NUP98::KDM5A/GFP resulted in a strong depletion of shRNA$^+$ cells within two weeks of culture, validating the dependence on NUP98::KDM5A (Figure 13C).

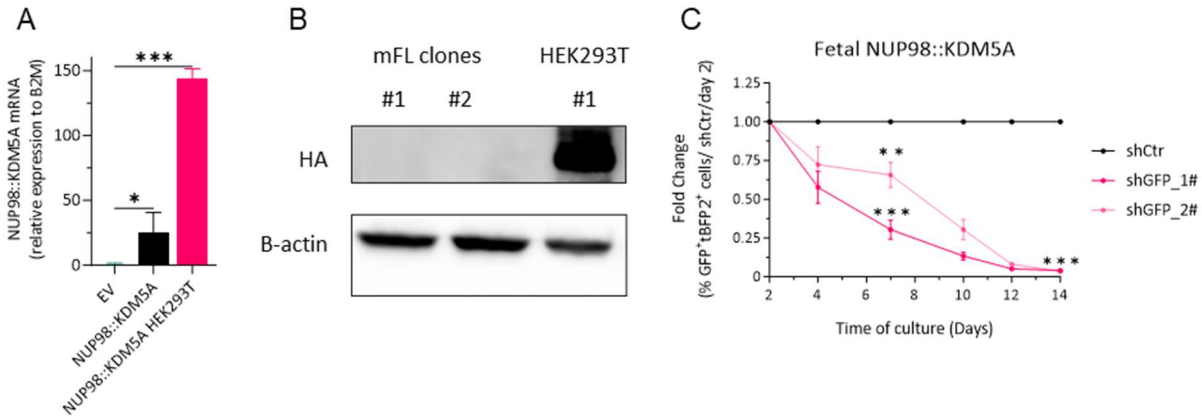

Figure 13 NUP98::KDM5A fusion protein is expressed at very low level in murine primary cells.

A) Bar graph showing NUP98::KDM5A mRNA expression relative to murine B2M Housekeeping gene in control (EV) or NUP98-KDM5A$^+$ fetal cells and NUP98-KDM5A transfected HEK293T cells.

B) Western Blot showing NUP98-KDM5A protein levels in fetal NUP98-KDM5A$^+$ cells and NUP98-KDM5A-transfected HEK293T cells. Endogenous B-actin was used as the loading control. NUP98-KDM5A-transfected HEK293T cells were used as positive protein control. Two representative independent clones of fetal NUP98-KDM5A$^+$ cells are shown as example.

C) Dot plot showing the fold change of percentage in shRNA-transduced (negative control sgRNA [sgCtrl], shGFP_1-2#) fetal NUP98-KDM5A$^+$ cells after 14 days of culture, normalized to day 2 (mean ± s.d., n > 3 per shRNA, 1-way ANOVA).

ns, not significant * P < .05, ** P < .01, ***P < .001, ****P < .0001.

To induce *de novo* leukemia *in vivo*, 2x10^6 fetal and adult NUP98::KDM5A$^+$ cells were injected into sub lethally irradiated (C57BL/6N) mice to induce de novo leukemia *in vivo* (Figure 11 and Figure 14A). Upon transplantation into syngeneic mice, fetal NUP98-KDM5A$^+$ cells induced leukemia development with a latency of 36 days, which was significantly faster than leukemia

development in mice injected with adult NUP98-KDM5A$^+$ cells (latency of 70 days) ($P_{Long\text{-}rank}$ < 0.001) (Figure 14A). Leukemic mice presented splenomegaly, with spleen weights exceeding 100 mg (Figure 14B). We observed significantly higher spleen weights when mice were transplanted with fetal NUP98-KDM5A$^+$ cells compared to adult NUP98-KDM5A$^+$ cells (Figure 14B). Flow cytometric analysis of leukemic cells in bone marrow revealed a mature myeloid surface phenotype (Gr-1 and Cd11b (Mac-1)), with 17 and 21% retaining an immature phenotype in fetal and adult NUP98-KDM5A$^+$ cells respectively, as observed *in vitro* (Figure 14C-D). No significant difference in immunophenotype was observed between fetal and adult NUP98-KDM5A$^+$ cells (Figure 14C-D).

Overall, our *in vitro* and *in vivo* experiments base on murine models demonstrate accelerated leukemogenesis in the fetal hematopoietic context.

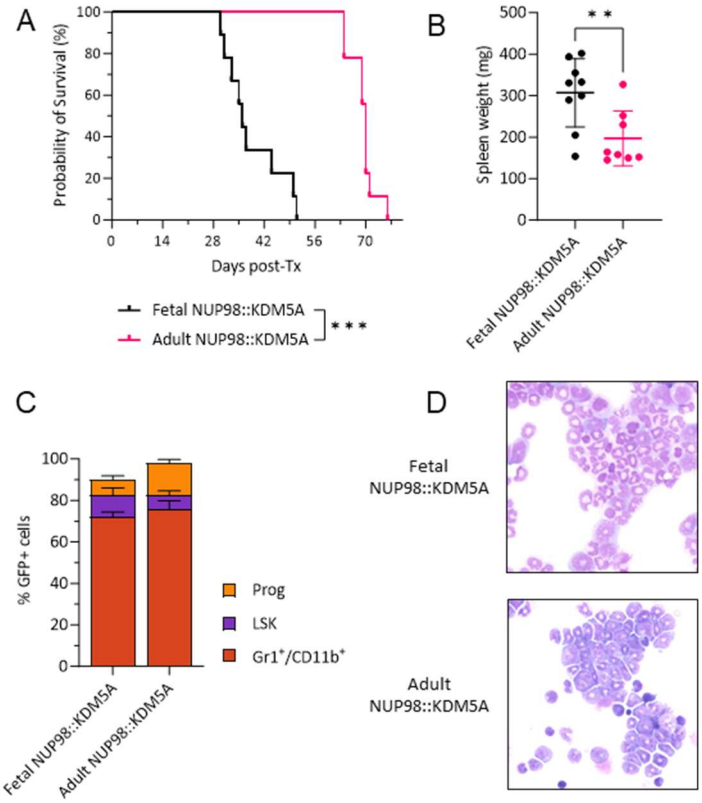

Figure 14 NUP98::KDM5A oncoprotein induces a more aggressive leukemia in mFL-HSPCs *in vivo*.

A) Kaplan-Meier survival curves of C57BL/6N mice transplanted with fetal and adult NUP98::KDM5A$^+$ cells (n ≥ 6).

B) Dot plot showing spleen weights of C57BL/6N mice injected with fetal and adult NUP98::KDM5A$^+$ cells (mean ± s.d., n > 3).

C) Bar graph showing the percentage of LSK (Lin$^-$, c-kit$^+$ and Sca1$^+$), Progenitor LSK (Lin$^-$, c-kit$^+$ and Sca1$^-$) and myeloid (Gr1$^+$ and CD11b$^+$) population in leukemic blasts isolated from bone marrow of mice transplanted with fetal and adult NUP98-KDM5A$^+$ cells.

D) Representative bone marrow cytospin images (x40 original magnification) of C57BL/6N mice transplanted with fetal and adult NUP98-KDM5A$^+$ cells.

** P < .01, ***P < .001.

4.1.2. NUP98::KDM5A transforms only human fetal HSPCs

Given the limited availability of patient materials and the absence of cell lines expressing NUP98::KDM5A fusion oncoprotein, we established a human NUP98::KDM5A model by

overexpressing NUP98::KDM5A oncoprotein in human HSPCs isolated from fetal liver (hFL-HSPCs) and adult donor peripheral blood (PB-HSPCs). Similar to our approach with murine HPSCs, we transduced human cells using a lentiviral vector encoding NUP98::KDM5A cDNA and GFP, enabling us to track cell counts over time to assess transformative capacity of NUP98::KDM5A in these two human hematopoietic ontogenies.

We evaluated two independent cell cultures based on GFP fluorescence, assessing GFP$^+$ cell number, immunophenotype and cytology. Long-term *in vitro* cell proliferation assay showed a progressive enrichment of GFP$^+$ human fetal (hFL) NUP98::KDM5A$^+$ cells over the time, which outcompeted normal cells in culture after 2-3 weeks, similar to our findings with murine fetal NUP98::KDM5A$^+$ cells (Figure 15A). In contrast, human adult NUP98::KDM5A$^+$ cells failed to overcome normal cells, despite similar initial transduction rates compared to fetal cells (Figure 15B). While control human fetal cells (EV) resulted in a mast cell phenotype (73% positive for CD15, surface marker for mast cells), hFL NUP98::KDM5A$^+$ cells displayed an immature megakaryoblastic surface phenotype (13% positive for CD41) and notably a significantly higher percentage of early myeloid phenotype (67.8% of CD33$^+$/CD15$^-$) and retained a fraction of 14% immature CD34$^+$ cells compared to the control, consistent with our murine *in vivo* models (Figure 15C-D).

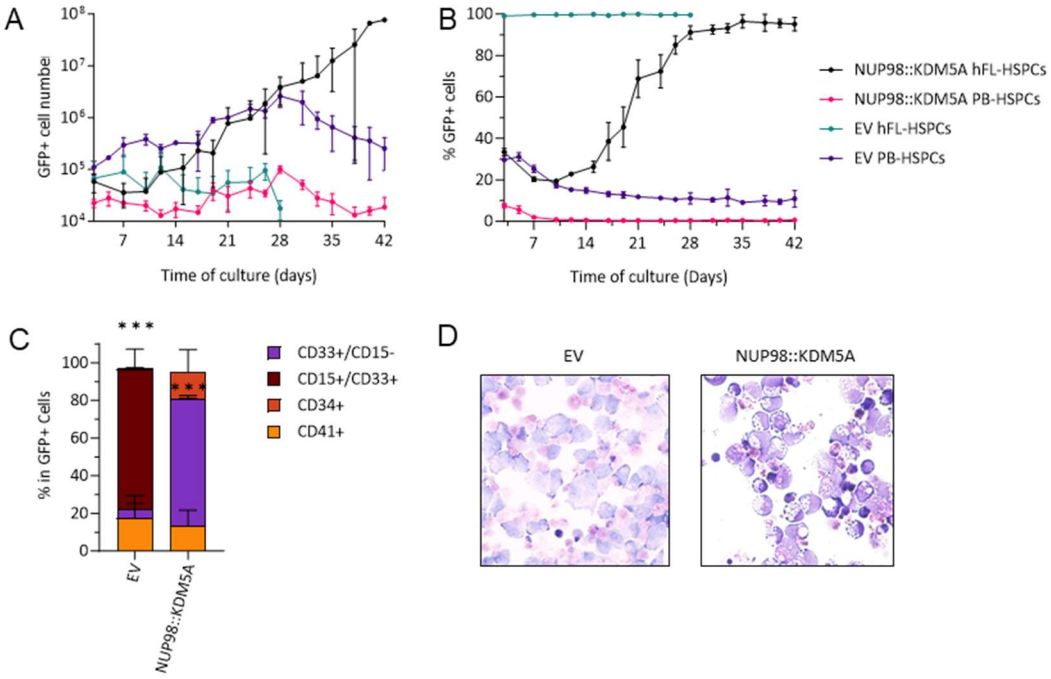

Figure 15 NUP98::KDM5A induces transformation only in human fetal HSPCs *in vitro*.

A) Dot plot showing GFP$^+$ cell number (right) and percentage (left) of control (EV) or NUP98-KDM5A in hFL-HSPCs and PB-HSPCs maintained in liquid culture. Data from 1 representative experiment performed in replicates, shown as mean s.d..

B) Representative flow cytometry analysis of human fetal control (EV) or NUP98-KDM5A$^+$ cells.

C) Bar graph showing the percentage of indicated cell subsets in human fetal control (EV) or NUP98-KDM5A$^+$ cells after 4 weeks of culture. (mean ± s.d., n > 3)

D) Representative bone marrow cytospin images (x400 original magnification) of human fetal control (EV) or NUP98-KDM5A$^+$ cells.

ns, not significant * P < .05, ** P < .01, ***P < .001, ****P < .0001.

Although we could not detect NUP98::KDM5A protein by Western blot(Figure 16A), as previously observed in murine fetal NUP98::KDM5A$^+$ cells before, we observed a strong

depletion of hFL NUP98::KDM5A$^+$ cells when transduced with shRNAs targeting NUP98::KDM5A/GFP, confirming their dependence on NUP98::KDM5A cDNA expression (Figure 16B).

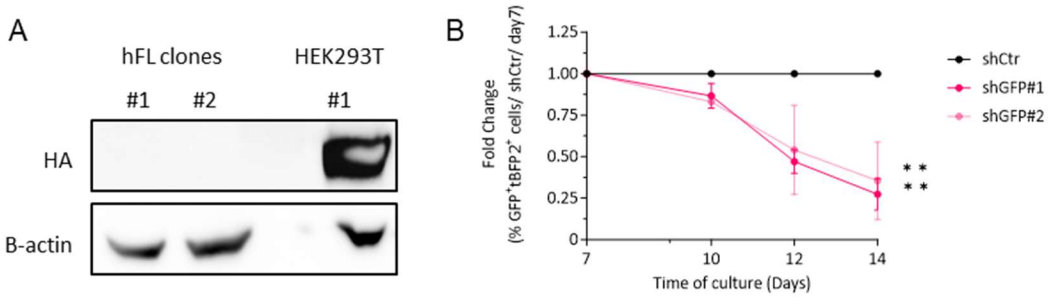

Figure 16 hFL NUP98::KDM5A cells are dependent on low expression of NUP98::KDM5A fusion protein.

A) Western Blot showing NUP98::KDM5A protein levels in hFL NUP98::KDM5A$^+$ cells and NUP98::KDM5A-transfected HEK293T cells. Endogenous B-actin was used as the loading control. NUP98::KDM5A-transfected HEK293T cells were used as positive protein control. Two representative independent clones of hFL NUP98::KDM5A$^+$ cells are shown as example.

B) Dot plot showing the fold change of percentage in shRNA-transduced (negative control sgRNA [sgCtrl], shGFP_1-2#) hFL NUP98::KDM5A$^+$ cells after 14 days of culture, normalized to day 2 (mean ± s.d., n > 3 per shRNA, 1-way ANOVA)

ns, not significant * P < .05, ** P < .01, ***P < .001, ****P < .0001.

It is important to note that hFL NUP98::KDM5A$^+$ cells demonstrated only partial transformation, as they were unable to proliferate beyond ~90 days. Due to limited availability of human fetal liver tissue and the partial transformation, large scale experiments performed along this study were not feasible with the human fetal NUP98::KDM5A model. Given that murine fetal and adult NUP98-KDM5A$^+$ cells shared an overlapping phenotype with hFL NUP98::KDM5A$^+$ cells, we leveraged these two murine models to further investigate the effect of fetal gene expression in NUP98::KDM5A-driven leukemogenesis for therapeutic proposes.
In summary and in accordance with other studies (Lopez, Noguera et al. 2019), fetal NUP98::KDM5A$^+$ cells developed a more aggressive phenotype than adult NUP98::KDM5A$^+$ cells, highlighting the crucial involvement of the fetal genes in NUP98::KDM5A-driven leukemogenesis.

4.2. CRISPR-Cas9 screen reveals TRIP13 dependency in fetal NUP98::KDM5A$^+$ leukemia

Beyond a stunning disease-specificity of chromosomal translocations in pediatric AMKL (i.e. NUP98::KDM5A, CBF2A3::GLIS2, RBM15::MKL1), the early onset -post birth- is another critical aspect of AMKL. Predominantly infants and children within 2 years of age are affected (Noort, Wander et al. 2021). Recent studies have shown the importance of fetal cellular context in modeling pediatric leukemias, suggesting that the different properties of fetal HSPCs compared to adults HSPCs might lead to leukemia initiation (Lopez, Noguera et al. 2019, Camiolo, Mullen et al. 2024). Since both murine and human NUP98::KDM5A model highlighted ontogenic differences in the NUP98::KDM5A-mediated transformation, we aimed to elucidate the involvement of the fetal transcriptional landscape in the development of the malignant transformation induced by NUP98::KDM5A oncoprotein and its implication for potential therapeutic strategies. We conducted an *in vitro* CRISPR-Cas9 loss of function screening in

fetal and adult NUP98::KDM5A models was performed to probe 880 genes found to be differently expressed between fetal and adult murine and human primary HSPCs (Figure 17A).

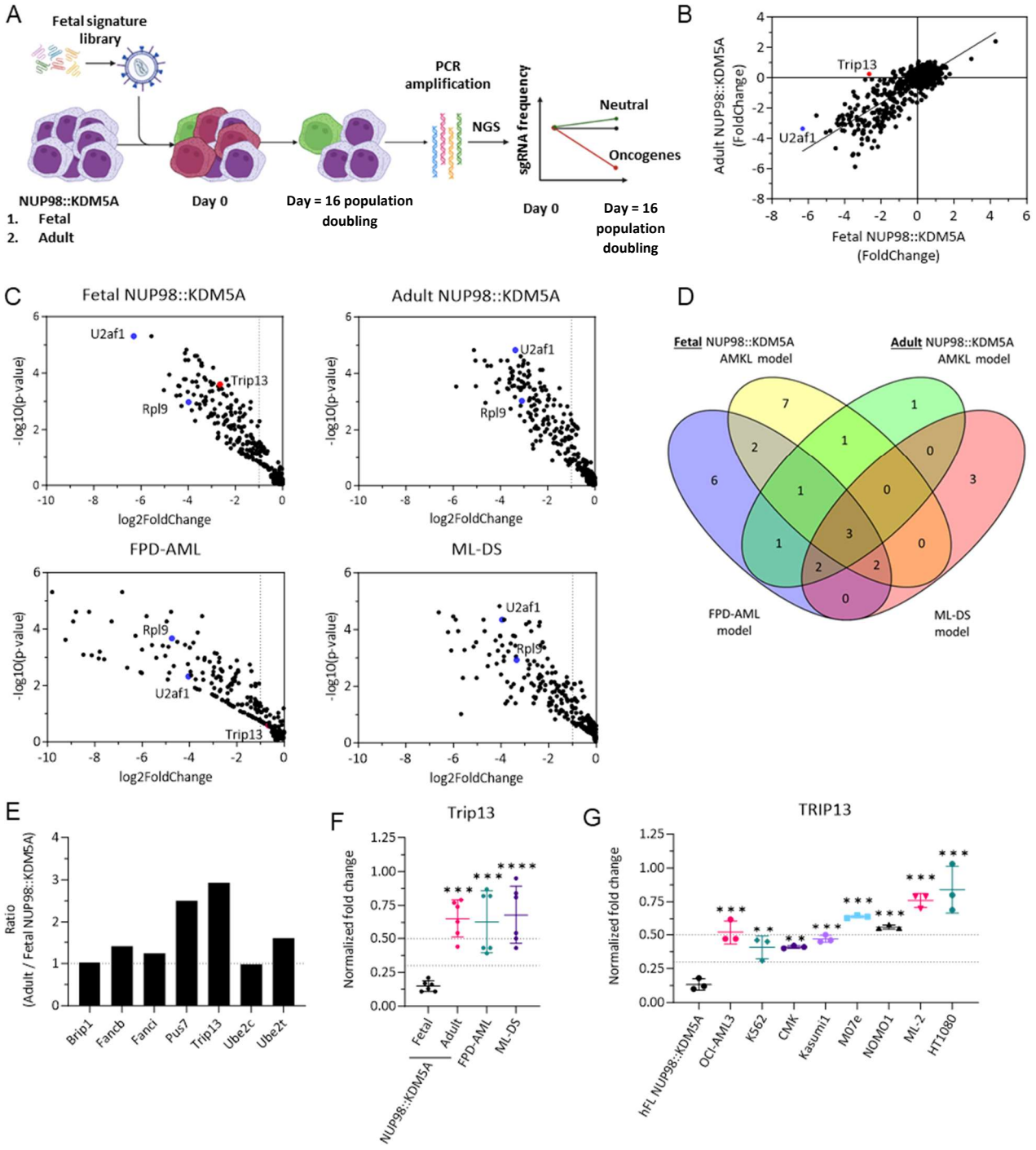

Figure 17 Identification of *Trip13* as selective candidate in fetal NUP98::KDM5A model.

A) Schematic workflow of the high-throughput fetal signatures based CRISPR-Cas9 *in vitro* screen.

B) Dot plots showing the log2 fold change of the fetal enriched gene targeted by sgRNAs in fetal (x-axis), adult (y-axis) NUP98::KDM5A models. Blue dots represent positive controls (*Rpl9*, *U2af1*). Red dots represent selected candidate gene *Trip13*. (n =2)

C) Dot plots showing the log2 fold change and –log10 (P- value) of the fetal enriched gene targeted by sgRNAs in fetal (top-left), adult (top-right) NUP98::KDM5A, FPD-AML (bottom-left) and ML-DS (bottom-right) models. Blue dots represent positive controls (*Rpl9*, *U2af1*). Red dots represent selected candidate gene *Trip13*. (n =2)

D) Venn diagram illustrating significantly (P < .05) depleted (depletion > 70%) sgRNAs in different murine leukemia models.

E) Bar plot showing the ratio between adult and fetal NUP98::KDM5A models in fold change of the seven selective candidates of fetal NUP98::KDM5A models.

F) Dot plot showing the fold change in percentage of sgRNA-transduced (negative control sgRNA [sgCtrl], sgTrip13_1-3 and positive control sgRNA [sgRpl9 and sgU2af1]) fetal, adult NUP98::KDM5A, FPD-AML and ML-DS models after 21 days of culture, normalized to (negative control sgRNA [sgCtrl]) and to day 2 (mean ± s.d., n > 3 per sgRNA, 1-way ANOVA).

G) Dot plot showing the fold change in percentage of sgRNA-transduced (negative control sgRNA [sgCtrl], sgTrip13_1-3 and positive control sgRNA [sgRPL9 and sgU2AF1]) hFL NUP98::KDM5A^{+} cells and leukemia cell lines (OCI-AML3; K562; CMK; Kasumi1; M07e; NOMO1; ML2)and non-leukemia cell line (HT1080) after 21 days of culture, normalized to (negative control sgRNA [sgCtrl]) and to day 2 (mean ± s.d., n > 3 per sgRNA, 1-way ANOVA).

ns, not significant * P < .05, ** P < .01, ***P < .001, ****P < .0001.

Next-generation sequencing-based sgRNA frequency at the beginning of the screening and after 16 population doublings, followed by MAGeCK analysis, revealed 16 and 6 candidate genes in fetal and adult NUP98::KDM5A models, respectively. Our selection criteria was based on significant depletion (> 70% with p-value < 0.05) and Chronos score, which defines gene essentiality (Figure 17B-D). To identify a selective dependence in fetal NUP98::KDM5A model, we compared our data with two additional murine leukemic models, previously generated: Bcor$^{-/-}$ Runx1$^{-/-}$ and Gata1s RUNX1A^{+} mFL-HSPCs, which recapitulate familial platelet disorder with predisposition to AML (FPD-AML) and myeloid leukemia associated to down syndrome (ML-DS), respectively. Among 7 candidates with higher depletion rates in fetal NUP98::KDM5A models, only 1 candidate, the AAA+ (ATPases Associated with diverse cellular Activities) ATPase *TRIP13*, showed significantly higher dependence in fetal NUP98::KDM5A cells based on the fetal vs adult ratio (Figure 17E-F).

To corroborate these findings in human hematopoiesis, we assessed the effect of *TRIP13* knockout using the CRISPR-cas9 system in a broad variety of human leukemic and non-leukemic (HT0180) cell lines, as well as in hFL NUP98::KDM5A^{+} cells. Upon *TRIP13* ablation, hFL NUP98::KDM5A^{+} cells showed an 87% reduction in viability, compared to a mild depletion (24-59%) in human leukemic cell lines and 16 % depletion in the HT1080 non-leukemia cell line (Figure 17G).

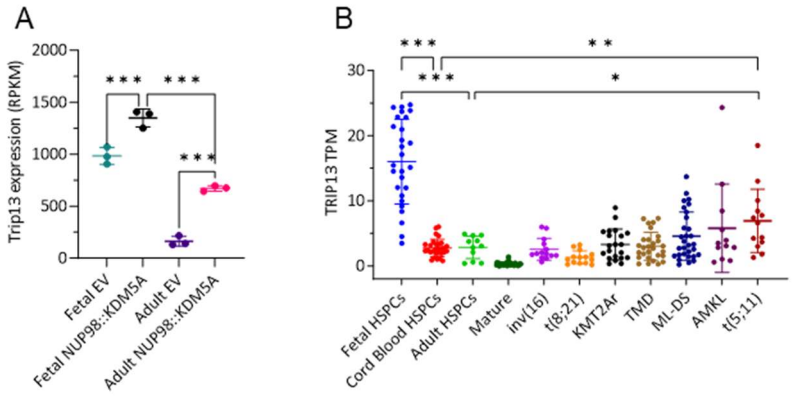

Figure 18 *TRIP13/Trip13* expression is upregulated by NUP98::KDM5A oncoprotein retaining the fetal-enrichment

A) Dot plot showing the expression of *Trip13* in control (EV) or NUP98::KDM5A^{+} murine fetal and adult cells after 2 weeks of culture (n = 3).

B) Dot plot showing the expression of *TRIP13* in subgroups of HSPCs and pediatric AML patients from the HemAtlas dataset.

ns, not significant * P < .05, ** P < .01, ***P < .001, ****P < .0001

Furthermore, gene expression profiling of murine fetal and adult cells showed that *Trip13* expression was elevated in cells overexpressing the NUP98::KDM5A fusion oncoprotein, with

a more pronounced effect in fetal cells (Figure 18A). This result was validated by gene expression analysis of stringently sorted human blood cells, highlighting upregulation of *TRIP13* in pediatric AMKL and NUP98-rearranged (t (5;11) = NUP98::NSD1) patients (Figure 18B). Collectively, the integration of these complementary screening approaches indicates a strong dependence on *TRIP13* in fetal NUP98::KDM5A$^+$ cells.

4.3. *TRIP13* is a molecular dependency in NUP98::KDM5A$^+$ AMKL

4.3.1. *Trip13* loss induces higher cell death in a fetal context in vitro

To elucidate the mechanisms underlying *TRIP13* dependence in fetal-derived NUP98::KDM5A$^+$ leukemia cells, we investigated the cellular effects of *TRIP13* loss. First, *Trip13* knockout was assessed at the protein level by Western Blot (Figure 20B). Upon *Trip13* genetic ablation, we observed a strong arrest of cell proliferation in fetal NUP98::KDM5A$^+$ cells within 14 days post-transduction, whereas adult NUP98::KDM5A$^+$ cells exhibited only mild proliferative defects (Figure 19A). The depletion of fetal NUP98::KDM5A$^+$ leukemia cells was associated with global increased apoptosis and cell cycle arrest, but no alterations in immunophenotype. Annexin-V apoptosis assay showed a 1.3-1.4-fold increase in late apoptotic cells following *Trip13* depletion (Figure 19B). Cell cycle analysis revealed a 1.39-1.45-fold increase in the proportion of *Trip13*-knockout cells arrested in G2/M phase, coupled with a decrease in G0/G1 phase (Figure 19C). Immunophenotype profiling did not reveal significant differences, indicating that TRIP13 is not involved in the regulation of cell differentiation but rather directly modulates cell cycle progression and viability (Figure 19D).

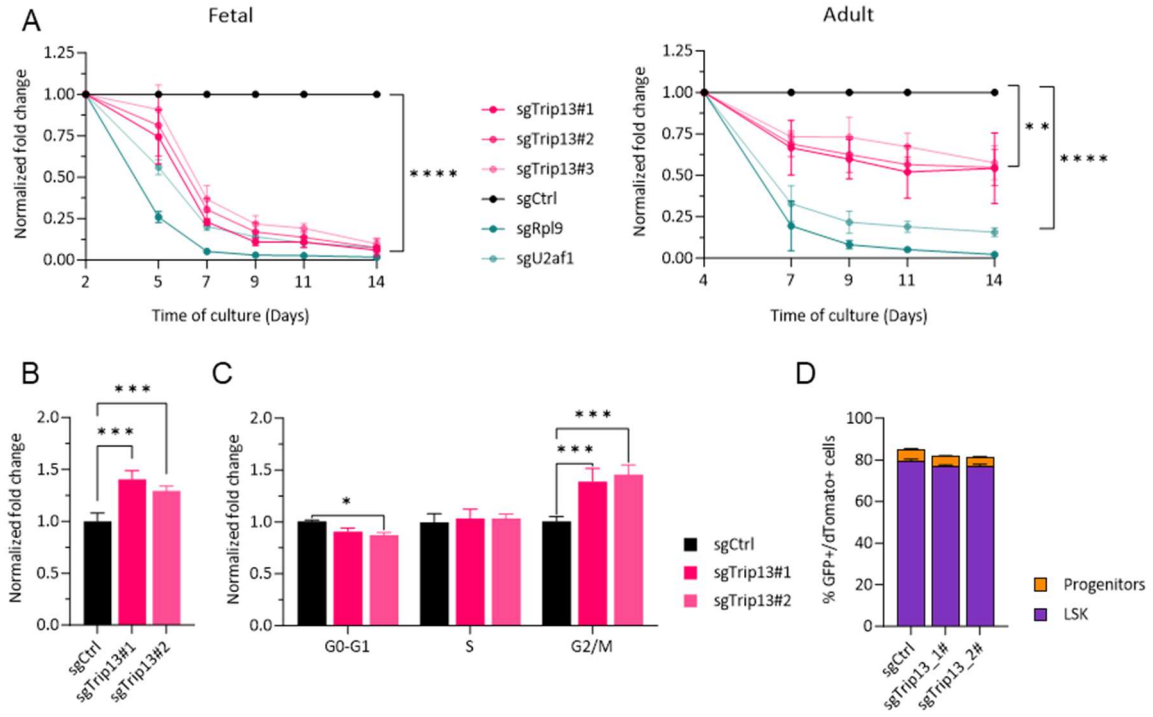

Figure 19 Loss of *Trip13* induces apoptosis and arrests cell cycle of fetal NUP98::KDM5A$^+$ cells *in vitro*.

A) Dot plot showing the fold change of percentage in sgRNA-transduced (negative control sgRNA [sgCtrl], sgTrip13_1-3 and positive control sgRNA [sgRpl9 and sgU2af1]) fetal (left) and adult (right) NUP98::KDM5A$^+$ cells after 14 days of culture, normalized to day 2 (mean ± s.d., n > 3 per sgRNA, 1-way ANOVA)

B) Bar graphs showing the fold change of the percentage of Annexin-V$^+$ sgRNA-transduced (negative control sgRNA [sgCtrl], sgTrip13_1-2) fetal NUP98::KDM5A$^+$ cells after 5 days of culture, normalized to control sgRNA (Ctr) (mean ± s.d., n > 3 per sgRNA, 2-way ANOVA).

C) Bar plot showing the percentage of sgRNA-transduced (negative control sgRNA [sgCtrl], sgTrip13_1-2) fetal NUP98::KDM5A$^+$ cells in subG1, G0-G1, S and G2/M phase after 5 days of culture (mean ± s.d., n > 3 per sgRNA, 2-way ANOVA).

D) Bar graph showing the percentage of LSK (Lineage negative, c-kit+ and Sca1+) and progenitors (Lineage negative, c-kit+, Sca1) in sgRNA-transduced (negative control sgRNA [sgCtrl], sgTrip13_1-2) fetal NUP98::KDM5A$^+$ cells after 5 days of culture (mean ± s.d., n > 3 per sgRNA, 2-way ANOVA).

ns, not significant * P < .05, ** P < .01, ***P < .001, ****P < .0001.

Several studies have shown that TRIP13 is involved in the regulation DNA damage repair (Banerjee, Russo et al. 2014, Hama, Nagesh et al. 2021, Jeong, Wie et al. 2022) and we therefore further tested DNA damage by yH2AX Western Blot. Noteworthy, no changes in yH2AX protein level were found in *Trip13* knockout fetal NUP98::KDM5A$^+$ cells compared to control (Figure 20A), thus arguing a mode of action involving DNA damage.

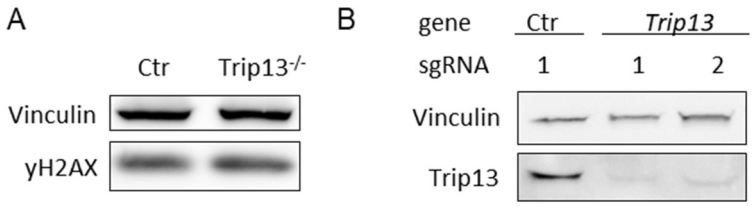

Figure 20 Loss of *Trip13* do not affect DNA damage response of fetal NUP98::KDM5A$^+$ cells.

A) Western Blot showing yH2AX protein levels in sorted sgRNA-transduced (negative control sgRNA [Luc], sgTrip13) fetal NUP98::KDM5A cells 4 days after transduction. Endogenous Vinculin was used as the loading control.

B) Western Blot showing Trip13 protein levels in sorted sgRNA-transduced (negative control sgRNA [Luc], sgTrip13_1-2) fetal NUP98::KDM5A$^+$ cells 4 days after transduction. Endogenous Vinculin was used as the loading control.

In summary, the loss of *Trip13* led to a block of cell proliferation and an arrest of cell cycle of fetal NUP98::KDM5A$^+$ cells without affecting cell differentiation and DNA damage.

4.3.2. *Trip13* knockout activates TP53 pathway in fetal NUP98::KDM5A$^+$ cells

To further frame the molecular mechanisms behind the dependence on *TRIP13*, gene expression profiling was performed in fetal NUP98::KDM5A$^+$ cells upon *Trip13* genetic ablation 4 days post-transduction (Figure 21A). GSEA revealed only perturbation of the TP53 signaling pathway, which was positively enriched in *Trip13* -depleted fetal NUP98::KDM5A$^+$ cells (mean NES = 2) (Figure 21B-C). These findings were consistent with analyses conducted at 2 days post-transduction (data not shown).

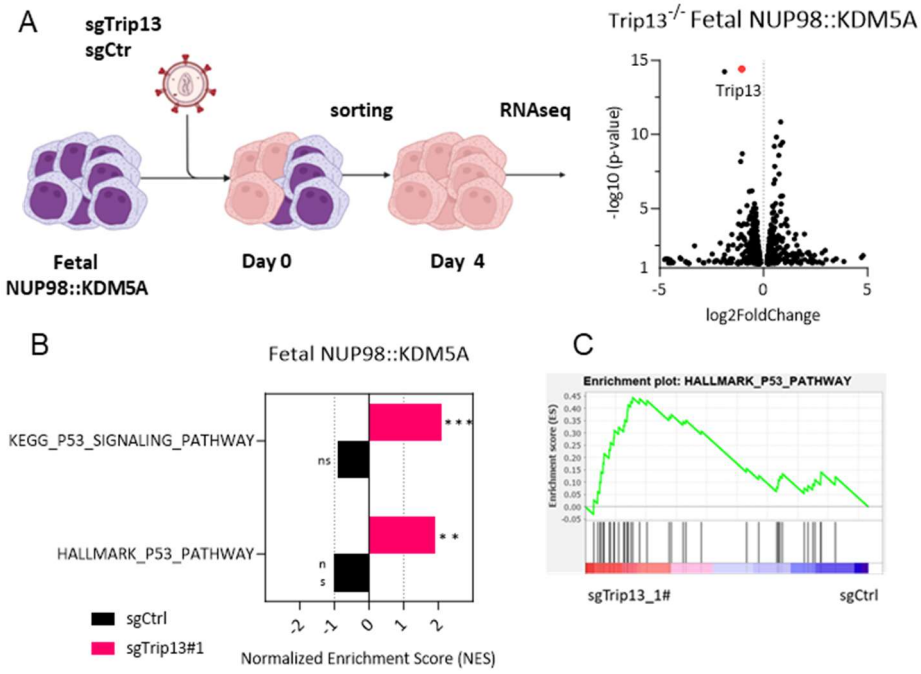

Figure 21 *Trip13* knockout activates TP53 signaling pathway in fetal NUP98::KDM5A⁺ cells.

A) Experimental workflow aiming at the molecular characterization of *Trip13* knocked-out in fetal NUP98::KDM5A⁺ cells. RNA-seq-based gene expression analysis of sgRNA-transduced (negative control sgRNA [sgCtrl], sgTrip13, sgTrp53) fetal NUP98::KDM5A⁺ cells was performed after 4 days of culture. Volcano plot showing the differential expressed genes upon *Trip13* knocked-out in fetal NUP98::KDM5A cells P-value < .05 (n = 2-3 per sgRNA)

B) Bar graphs showing the normalized enrichment scores (NES) of significantly upregulated or downregulated gene sets associated with TP53 pathway in *Trip13* knocked-out fetal NUP98::KDM5A⁺ cells compared to control. *False discovery rate (FDR) q <.25; ** q<.05, ns, not significant.

C) Gene Set Enrichment Analysis (GSEA) plot showing deregulated genes involved in TP53 pathway in *Trip13* knocked-out fetal NUP98::KDM5A⁺ cells compared to control.

To further corroborate these findings, we conducted a time-course Western blot analysis, which revealed increased TP53 protein levels in *Trip13*-knockout fetal NUP98::KDM5A⁺ cells (Figure 22).

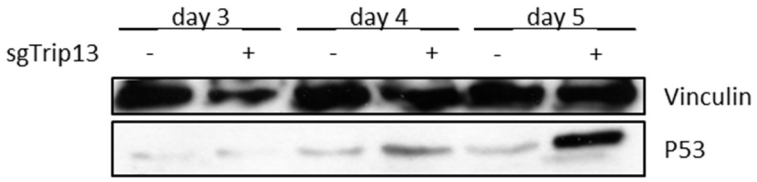

Figure 22 *Trip13* depletion leads to increased TP53 protein level

Timeline Western Blot showing TP53 protein levels in sorted sgRNA-transduced (negative control sgRNA [Luc], sgTrip13_1-2) fetal NUP98::KDM5A⁺ cells 4 days after transduction. Endogenous Vinculin was used as the loading control.

To assess the dependency on the activation of TP53 pathway, we performed a rescue experiment by combining *Trip13* and murine *TP53* (*Trp53*) knockout (Figure 23A). Our experimental setup showed that this combined knockout could reverse the depletion observed in Trip13-knockout cells (Figure 23B). To exclude potential off-target effects and confirm the specificity of the *Trip13* knockout phenotype, we performed a complementary rescue experiment. We co-transduced fetal NUP98::KDM5A⁺ cells with a lentiviral vector constitutively expressing TRIP13 cDNA alongside sgRNAs targeting *Trip13* (Figure 23A). Our

experimental setup underlined that the overexpression of *TRIP13* was able to completely rescue the depletion of fetal NUP98::KDM5A^{+} cell upon *Trip13* knockout (Figure 23C).

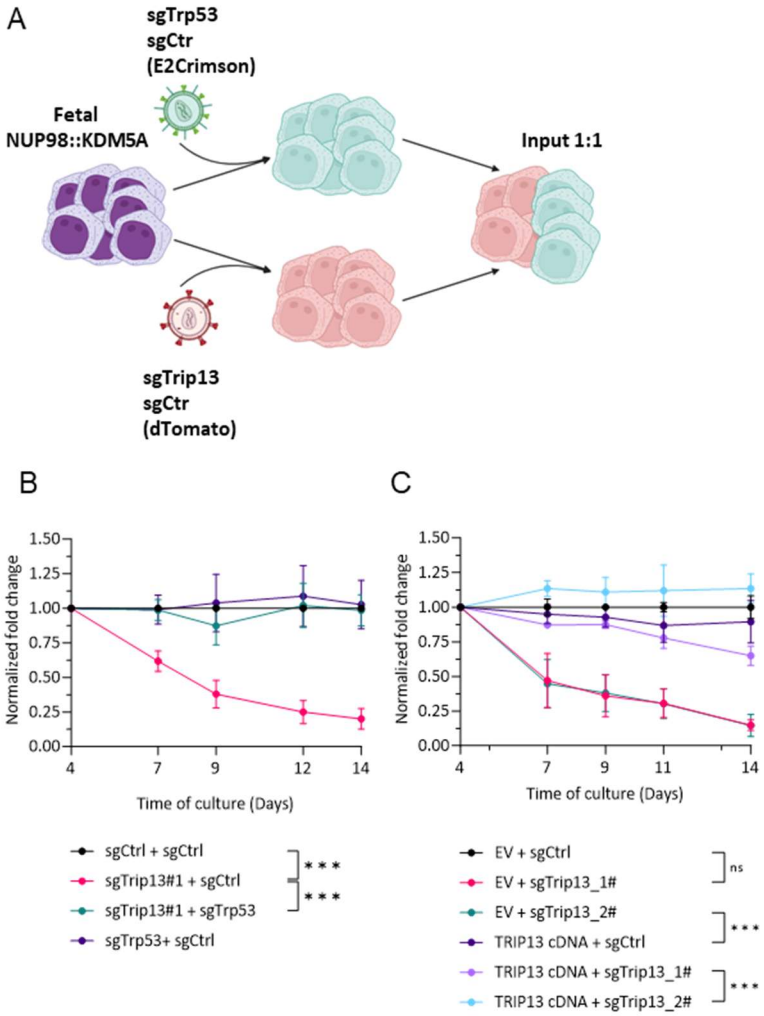

Figure 23 Rescue experiments confirm the mechanism acting through TRIP13/TP53 axis.

A) Experimental setup for evaluating the rescue effect of *Trp53* knockout and TRIP13 overexpression after genetic ablation of *Trip13*. Fetal NUP98::KDM5A^{+} cells were transduced with TRIP13 (dTomato^{+}) and EV (dTomato^{+}) or transduced with sgTrp53 (E2Crimson^{+}) and sgCtr (E2Crimson^{+}) and mixed 1:1 with sgCtr (FP^{+}) or with sgTrip13 (FP^{+}).

B) Dot plot showing the percentage of sgRNA-transduced (negative control sgRNA [sgCtrl], sgTrip13, sgTrp53) fetal NUP98::KDM5A^{+} cells after 14 days of culture, normalized to day 2 (mean±s.d., n > 3 per sgRNA, 1-way ANOVA)

C) Dot plot showing the percentage of fetal NUP98::KDM5A^{+} cells transduced after a combined transduction with sgRNA-transduced (negative control sgRNA [sgCtrl], sgTrip13_1-2) and empty vector or TRIP13 cDNA expression after 14 days of culture, normalized to day 2 (mean±s.d., n > 3 per sgRNA, 1-way ANOVA).

ns, not significant ***P < .001.

4.3.3. TRIP13 interacts with PPM1D/WIP1 to repress TP53 pathway

While no direct linkage between TRIP13 and TP53 has been described, our analysis did not indicate an indirect DNA-damage related connection between TRIP13 and TP53. To better understand the regulation of TP53 protein by TRIP13 and we investigated the TRIP13 protein interaction network. We performed coimmunoprecipitation of doxycycline-inducible hemagglutinin (HA)-tagged TRIP13 in a *TP53* wild-type human leukemia cell line (OCI-AML3) followed by mass spectrometry (LC-MS/MS) of the bound cofactors (Figure 24A). A total of 1942 proteins were significantly bound by TRIP13, including previously described TRIP13

interactors, such as MAD2L1BP and MAD2L2 (Figure 24B) (Vader 2015). Among these 1942 proteins identified as TRIP13 interactors, 33 proteins were known to regulate TP53 at the gene or protein level based on the public database GSEA and STRING (Figure 24C).

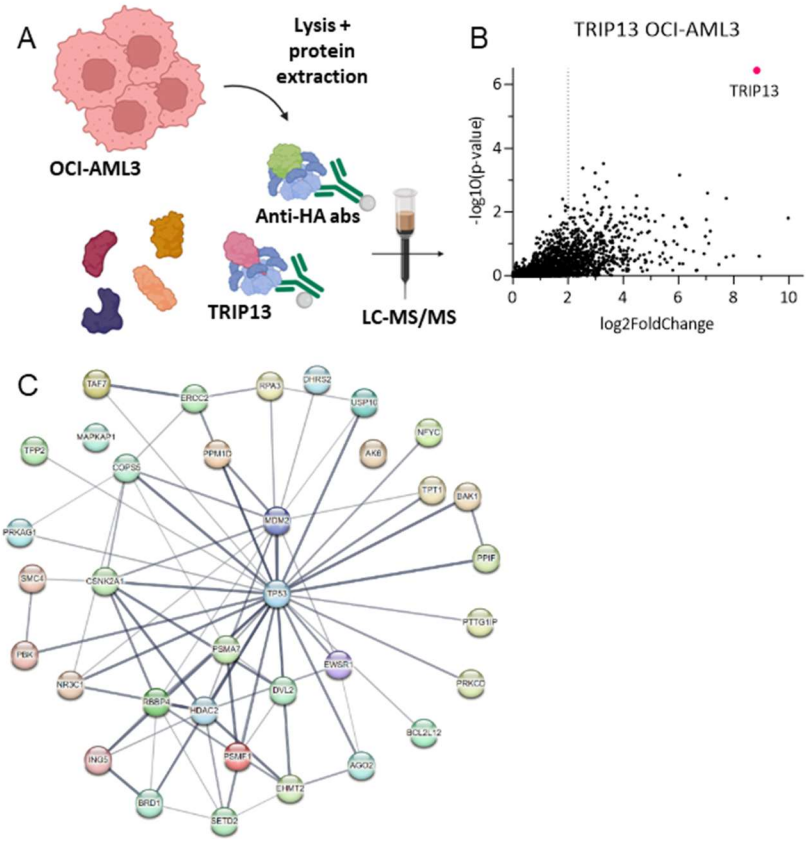

Figure 24 TRIP13 might interact with PPM1D/WIP1 and promote TP53 pathway activation.

A) Experimental workflow for isolating HA-tagged TRIP13 protein and its interactors from OCI-AML3 cells.

B) Volcano plot showing the differential enriched protein-interactors upon HA pulldown in TRIP13^{+} OCI-AML3 cells. (n = 3).

C) STRING Protein-Protein Interaction network of 33 TRIP13-interacting candidates. Network nodes (colored circles) represent proteins, lines between the nodes (edges) indicates the different types of interaction (functional and physical protein associations), line thickness indicates the confidence (0.4).

To assess the relevance of these 33 TRIP13-/TP53-interactors in the TRIP13-knockout phenotype, we tested whether their loss could either mimic or rescue the depletion observed in *Trip13*-knockout fetal NUP98::KDM5A^{+} cells. Among these 33 candidates, 16 interactors showed a similar depletion rate to *Trip13* (Figure 25A). We then combined *Trp53* knockout to these 16 depleting candidates to validate that the depletion observed upon knockout of these 16 candidates is caused by TP53 activation (as similarly done in Figure 23A). We found the protein phosphates PPM1D/WIP1, a well-known regulator of TP53 in a direct and indirect manner via MDM2 stabilization (Deng, Li et al. 2020), as a top TRIP13 interactor that mimicked the *Trip13* knockout phenotype (Figure 25B).

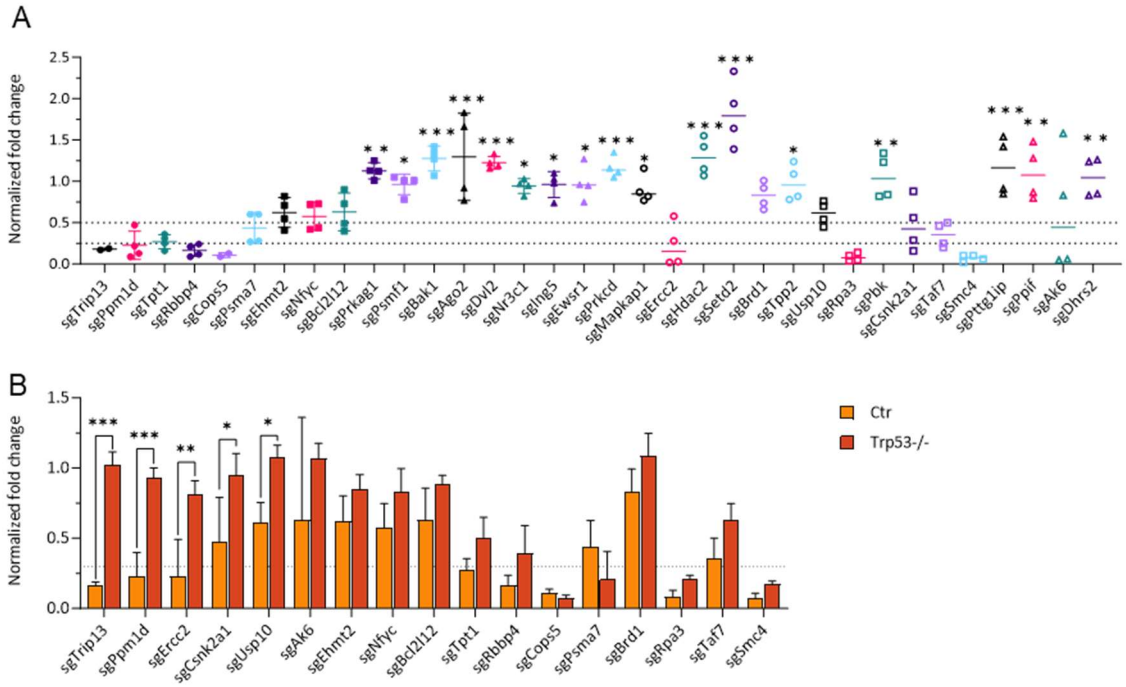

Figure 25 PPM1D/WIP1 mimics TRIP13

A) Dot plot showing the percentage of sgRNA-transduced fetal NUP98::KDM5A^{+} cells after 14 days of culture, normalized to day 2 (mean±s.d., n > 3 per sgRNA, 1-way ANOVA).

B) Dot plot showing the percentage of sgRNA-transduced fetal NUP98::KDM5A^{+} cells in combination with (negative control sgRNA [sgCtrl], sgTrp53) after 14 days of culture, normalized to day 2 (mean±s.d., n > 3 per sgRNA, 1-way ANOVA)

ns, not significant * P < .05, ** P < .01, ***P < .001, ****P < .0001.

Next, IP-MS results were validated by coimmunoprecipitation of TRIP13 and PPM1D in OCI-AML3 cell line (Figure 26A). In line with the known role of PPM1D and given that *PPM1D* phenocopies *TRIP13*, Western blot of *Trip13* knockout and *Ppm1d* knockout fetal NUP98::KDM5A^{+} cells confirmed higher murine TP53 protein level compared to the control (Figure 26B).

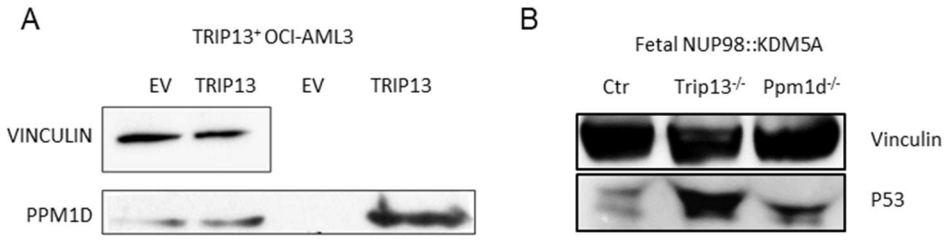

Figure 26 TRIP13 interacts with PPM1D/WIP1 to repress TP53

A) Western Blot showing coimmunoprecipitation of PPM1D with HA-tagged TRIP13 in OCI-AML3 cells. Endogenous Vinculin was used as the loading control.

B) Western Blot showing TP53 protein levels in sorted sgRNA-transduced (negative control sgRNA [Luc], sgTrip13 and sgPpm1d) fetal NUP98::KDM5A^{+} cells 4 days after transduction. Endogenous Vinculin was used as the loading control.

4.4. Targeting the TRIP13/TP53-axis as a novel treatment approach for NUP98:: KDM5A$^+$ AMKL

4.4.1. Loss of *Trip13* shows sensitivity in NUP98::KDM5A$^+$ AMKL *in vivo*

Next, we assessed *Trip13* knockout *in vivo* through fluorescence-based competitive transplantation assays using fetal NUP98::KDM5A$^+$ cells (Figure 27A). Trip13-depleted leukemic blasts were significantly diminished in the bone marrow of recipient mice at the experimental endpoint (Figure 27B). These results were in line with the cell depletion observed *in vitro*.

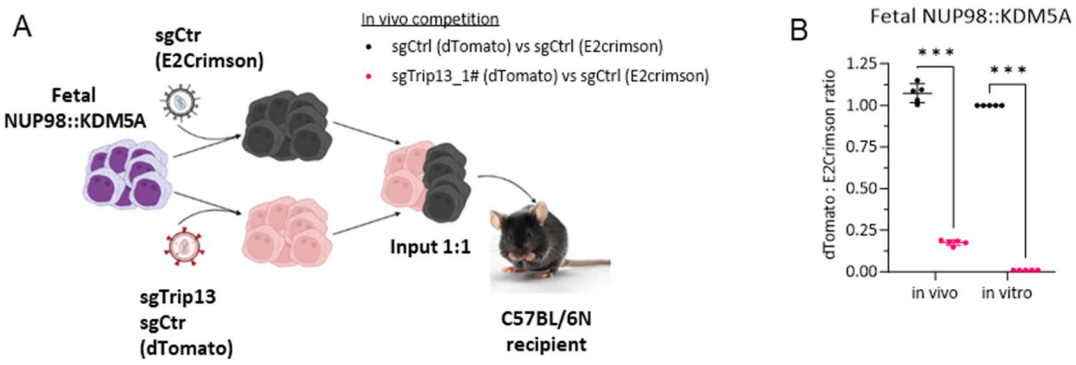

Figure 27 Loss of *Trip13* shows sensitivity in fetal NUP98::KDM5A$^+$ model *in vivo*.

A) Experimental setup for evaluating the genetic ablation of *Trip13* in fetal NUP98::KDM5A$^+$ cells *in vivo*. fetal NUP98::KDM5A$^+$ cells (with stable Cas9 expression) were transduced with sgTrip13 (dTomato$^+$) and sgCtr (dTomato$^+$) and mixed 1:1 with sgCtr (E2Crimson$^+$), before transplantation into sublethally irradiated recipient mice.

B) Dot plot showing the ratio of dTomato$^+$ to E2Crimson$^+$ cells in the bone marrow of mice euthanized 4 weeks after transplantation (middle; n = 5, 2-way ANOVA) and after 4 weeks of culture, normalized to day 0 (right; n = 3, 2-way ANOVA) ***P <.001

4.4.2. Pharmacological TRIP13 inhibition as treatment of NUP98::KDM5A$^+$ AMKL *in vitro*

Given the dependence on *TRIP13* in fetal NUP98::KDM5A$^+$ cells both *in vitro* and *in vivo*, we assessed the potential of pharmacological TRIP13 inhibition as a novel treatment option for pediatric NUP98::KDM5A$^+$ AMKL.

Pharmacological inhibition of TRIP13 using DCZ0415 induced apoptotic cell death after 5 days of treatment in both fetal and adult NUP98::KDM5A$^+$ cells, in a dose dependent manner (Figure 28A-C). Fetal and adult NUP98::KDM5A$^+$ cells treated with DCZ0415 showed mean lethal concentration (50% inhibitory concentration [IC_{50}]) of 22 µM and 26 µM, respectively. In line with the experiments targeting *Trip13* genetically. As controls, FPD-AML and ML-DS were also treated with DCZ0415 and had significantly higher mean IC_{50} values of 50 µM and 35 µM, respectively (Figure 28A). Notably, adult HSPCs isolated from healthy donor mice treated with DCZ0415 had a significantly higher mean IC_{50} value of 45 µM.

We then evaluated the efficacy of DCZ0415 on human cells and observed high sensitivity in hFL NUP98::KDM5A$^+$ cells with a mean lethal concentration of 19 µM. In comparison, OCI-AML3 cells showed mean IC_{50} values of 32µM while M07E and Kasumi1 cells did not show a response allowing IC_{50} calculation (Figure 28D). Consistent with murine NUP98::KDM5A$^+$ cells, Annexin-V and DAPI staining (flow cytometry) confirmed that DCZ0415 induced dose-

dependent apoptotic cell death after 5 days of treatment in hFL NUP98::KDM5A$^+$ cells (Figure 28E).

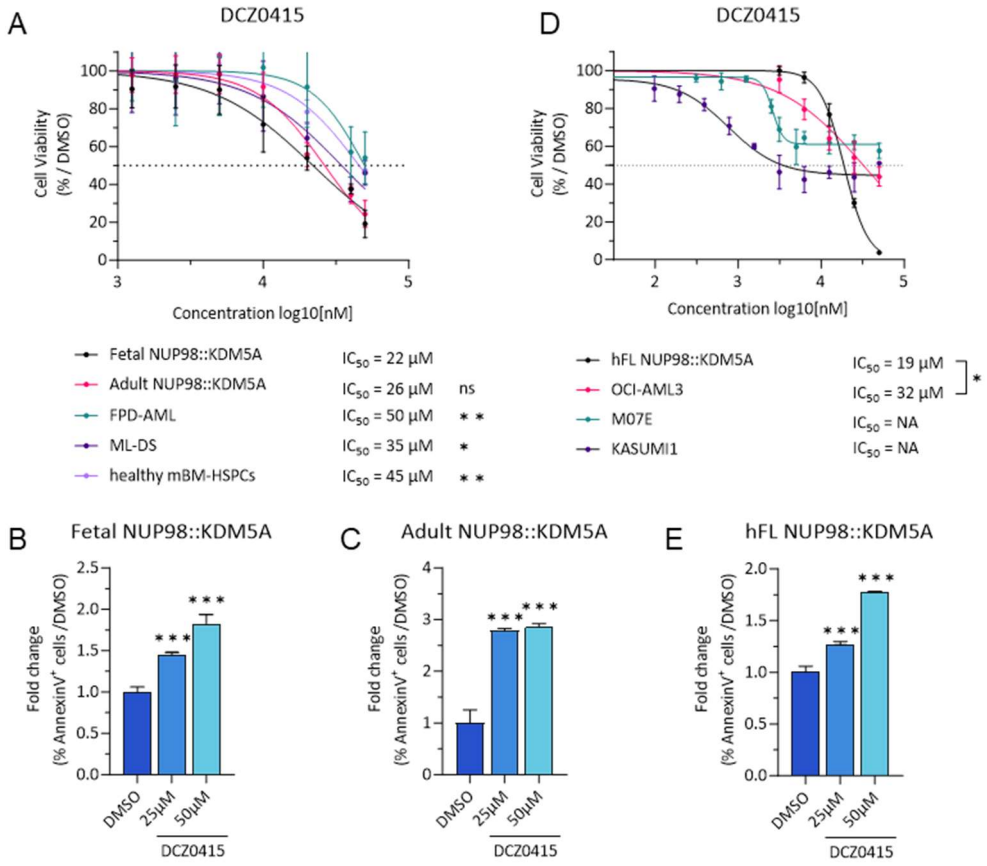

Figure 28 Pharmacological TRIP13 inhibition as treatment of NUP98::KDM5A$^+$ AMKL *in vitro*

A) Dose response curves for DCZ0415 (TRIP13 inhibitor) in fetal and adult NUP98::KDM5A$^+$, ML-DS and FPD-AML models and healthy mBM-HSPCs after 5 days of treatment *in vitro*. The corresponding IC_{50}-values are depicted below the graphs. (mean ± s.d. , n > 3, 1-way ANOVA)

B) Bar graphs showing the fold changes in percentage of Annexin-V$^+$ cells after treatment with the indicated doses of DCZ0415 compared to dimethyl sulfoxide control (DMSO) in fetal NUP98::KDM5A$^+$cells after 5 days of treatment *in vitro*. (mean±s.d., n > 3, 1-way ANOVA)

C) Bar graphs showing the fold changes in percentage of Annexin-V$^+$ cells after treatment with the indicated doses of DCZ0415 compared to dimethyl sulfoxide control (DMSO) in adult NUP98::KDM5A$^+$cells after 5 days of treatment *in vitro*. (mean±s.d., n > 3, 1-way ANOVA)

D) Dose response curves for DCZ0415 (TRIP13 inhibitor) in hFL NUP98::KDM5A$^+$ cells and OCI-AML3, M07E and Kasumi1 after 5 days of treatment *in vitro*. The corresponding IC_{50}-values are depicted below the graphs. (mean ± s.d. , n > 3, 1-way ANOVA).

E) Bar graphs showing the fold changes in percentage of Annexin-V$^+$ cells after treatment with the indicated doses of DCZ0415 compared to dimethyl sulfoxide (DMSO) control in hFL NUP98::KDM5A$^+$ cells after 5 days of treatment in vitro. (mean±s.d., n > 3, 1-way ANOVA)

ns, not significant * P < .05, ** P < .01, ***P < .001.

Recognizing that single-agent treatments are rarely successful in cancer therapy, we explored potential combination strategies to enhance the effect of TRIP13 inhibition. Based on our molecular data, we focused on leveraging the activation of the TP53 pathway. We therefore first tested the response of our murine models on the MDM2 inhibitor Idasanutlin, which is already clinically approved. After 5 days of treatment, fetal and adult NUP98::KDM5A$^+$ cells treated with Idasanutlin alone had mean IC_{50} values of 393 nM and 343 nM, respectively

(Figure 29A). FPD-AML, ML-DS cells and healthy donor adult HSPCs showed a non-significantly higher IC_{50} value of 395 nM, 553 nM and 550 nM, respectively (Figure 29A). hFL NUP98::KDM5A$^+$ cells were responsive to Idasanutlin treatment but exhibited a significantly higher mean IC_{50} value of 785 nM compared to the Idasanutlin-responsive OCI-AML3 cells (mean IC_{50} value of 234 nM) (Figure 29D). Pharmacological inhibition of MDM2 with Idasanutlin caused apoptotic cell death in both murine and human NUP98::KDM5A$^+$ cells in a dose-dependent manner, as assessed by Annexin-V and DAPI staining (Figure 29B-C-E).

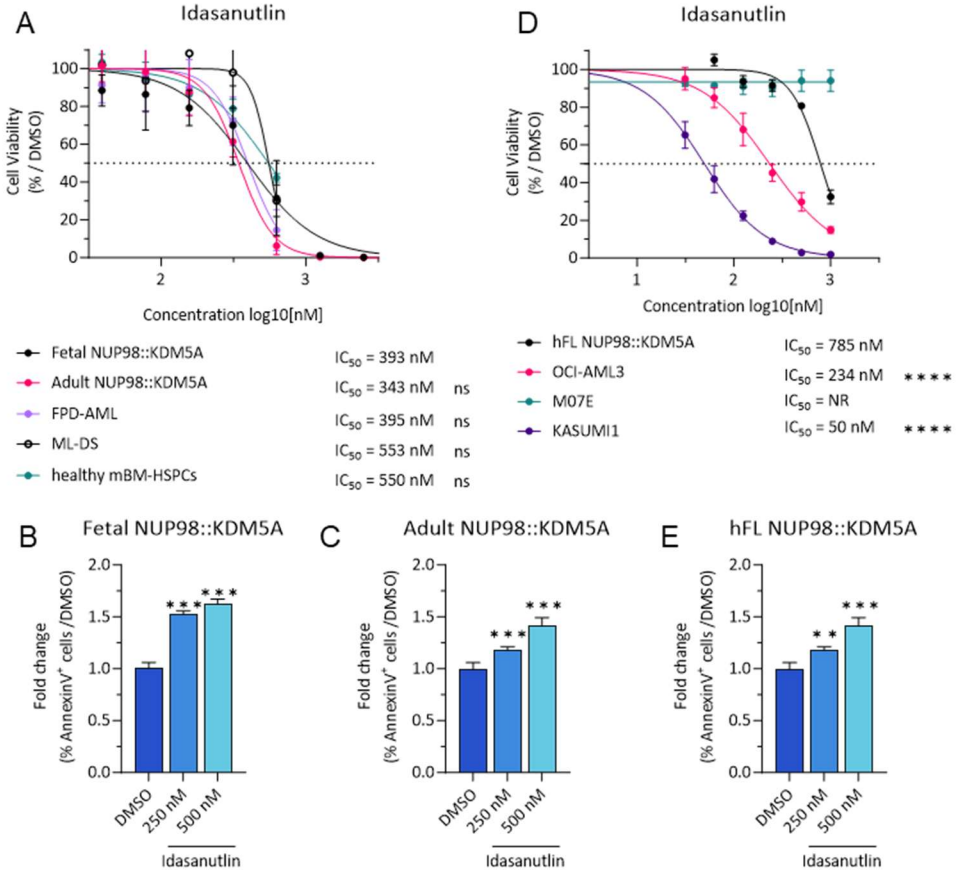

Figure 29 Targeting TRIP13 in combination with MDM2 inhibitor as therapeutic strategy for AMKL.

A) Dose response curves for Idasanutlin (MDM2 inhibitor) in fetal and adult NUP98::KDM5A, ML-DS and FPD-AML models and healthy mBM-HSPCs after 5 days of treatment *in vitro*. The corresponding IC_{50}-values are depicted below the graphs. (mean ± s.d. , n > 3, 1-way ANOVA)

B) Bar graphs showing the fold changes in percentage of Annexin-V$^+$ cells after treatment with the indicated doses of Idasanutlin compared to dimethyl sulfoxide control (DMSO) in fetal NUP98::KDM5A$^+$cells after 5 days of treatment *in vitro*. (mean±s.d., n > 3, 1-way ANOVA)

C) Bar graphs showing the fold changes in percentage of Annexin-V$^+$ cells after treatment with the indicated doses of Idasanutlin compared to dimethyl sulfoxide control (DMSO) in adult NUP98::KDM5A$^+$cells after 5 days of treatment *in vitro*. (mean±s.d., n > 3, 1-way ANOVA

D) Dose response curves for Idasanutlin in hFL NUP98::KDM5A$^+$ cells and OCI-AML3, M07E and Kasumi1 after 5 days of treatment *in vitro*. The corresponding IC_{50}-values are depicted below the graphs. (mean ± s.d. , n > 3, 1-way ANOVA).

E) Bar graphs showing the fold changes in percentage of Annexin-V$^+$ cells after treatment with the indicated doses of Idasanutlin compared to dimethyl sulfoxide (DMSO) control in hFL NUP98::KDM5A$^+$ cells after 5 days of treatment in vitro. (mean±s.d., n > 3, 1-way ANOVA)

ns, not significant * P < .05, ** P < .01, ***P < .001.

We then investigated the potential synergistic effects of combining DCZ0415 with Idasanutlin at various concentrations (Figure 30). Synergy maps highlighted that the combination of

DCZ0415 with Idasanutlin were indeed synergistic, with a summary Bliss synergy score of 9.7 and 21.5 in murine and human fetal NUP98::KDM5A^{+} cells, respectively (Figure 30D and F). In contrast, the combination had only a mild additive effect in adult NUP98::KDM5A^{+} cells (summary Bliss synergy score = 1.6) (Figure 30E).

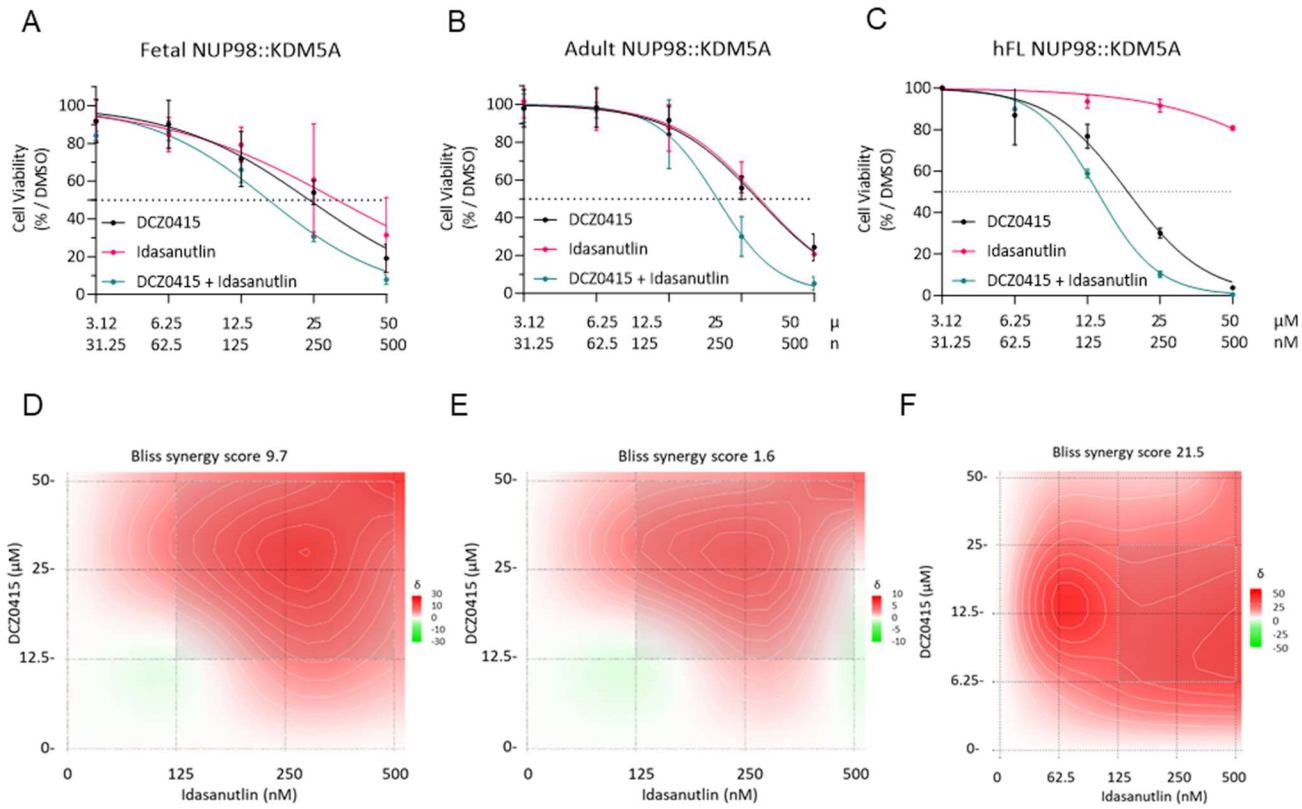

Figure 30 Targeting TRIP13 in combination with MDM2 inhibitor as therapeutic strategy for AMKL

A) Dose response curves for the combination of DCZ0415 (TRIP13 inhibitor) with Idasanutlin (MDM2 inhibitor) in fetal NUP98::KDM5A^{+} cells after 5 days of treatment *in vitro*. (mean ± s.d. , n > 3).

B) Dose response curves for the combination of DCZ0415 (TRIP13 inhibitor) with Idasanutlin (MDM2 inhibitor) in adult NUP98::KDM5A^{+} cells after 5 days of treatment *in vitro*. (mean ± s.d. , n > 3).

C) Dose response curves for the combination of DCZ0415 (TRIP13 inhibitor) with Idasanutlin (MDM2 inhibitor) in hFL NUP98::KDM5A^{+} cells after 5 days of treatment *in vitro*. (mean ± s.d. , n > 3).

D) Synergy map of fetal NUP98::KDM5A^{+} cells treated with DCZ0415 (TRIP13 inhibitor) in combination with Idasanutlin (MDM2 inhibitor) after 5 days of treatment *in vitro*. (mean ± s.d. , n > 3).

E) Synergy map of adult NUP98::KDM5A^{+} cells treated with DCZ0415 (TRIP13 inhibitor) in combination with Idasanutlin (MDM2 inhibitor) after 5 days of treatment *in vitro*. (mean ± s.d. , n > 3)

F) Synergy map of hFL NUP98::KDM5A^{+} cells treated with DCZ0415 (TRIP13 inhibitor) in combination with Idasanutlin (MDM2 inhibitor) after 5 days of treatment *in vitro*. (mean ± s.d. , n > 3).

ns, not significant * P < .05, ** P < .01, ***P < .001.

To validate that the pharmacological TP53 reactivation corroborates the observed depleting phenotype upon the genetic ablation of TRIP13/TP53 axis, we performed a rescue experiment combining DCZ0415 or Idasanutlin treatment with TRIP13 re-overexpression or *TP53* knockout (Figure 31A). This experimental setup demonstrated that cell death induced by either DCZ0415 or Idasanutlin could be rescued by re-overexpressing TRIP13 (Figure 31B-C). In

contrast, genetic ablation of TP53 restored cell proliferation in Idasanutlin-tread cells but in DCZ0415-tread cells (Figure 31B-C).

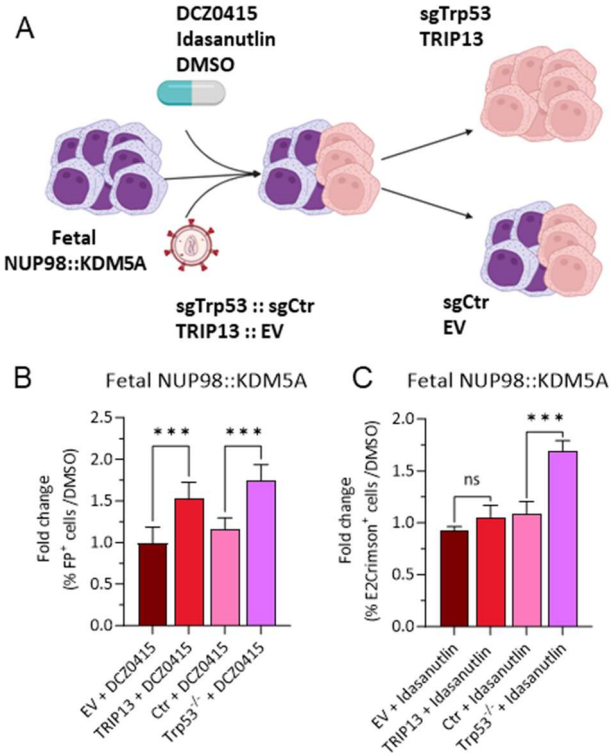

Figure 31 Rescue experiments confirm the mechanism acting through TRIP13/TP53 axis.

A) Experimental setup for evaluating the rescue effect of *Trp53* knockout and *TRIP13* overexpression after drug treatment *in vitro*. Fetal NUP98::KDM5A$^+$ cells were transduced with TRIP13 (dTomato$^+$) and EV (dTomato$^+$) or transduced sgTrp53 (E2Crimson$^+$) and sgCtr (E2Crimson$^+$) at low MOI (0.10-0.20), before treatment with DCZ0415 (25µM), Idasanutlin (250nM) and their combination and dimethyl sulfoxide control (DMSO).

B) Bar graphs showing the ratio fold change of percentage of dTomato$^+$ cells, transduced with *TRIP13* cDNA or control (EV), after treatment with the indicated doses of DCZ0415 (25µM), Idasanutlin (250nM) and their combination normalized to dimethyl sulfoxide control in fetal NUP98::KDM5A$^+$ cells after 7 days of treatment *in vitro*. (mean±s.d., n > 3, 1-way ANOVA)

C) Bar graphs showing the ratio fold change of percentage of E2crimson$^+$ cells, transduced with sgTrp53 or control (sgCtr), after treatment with the indicated doses of DCZ0415 (25µM), Idasanutlin (250nM) and their combination normalized to dimethyl sulfoxide control in fetal NUP98::KDM5A$^+$ cells after 7 days of treatment *in vitro*. (mean±s.d., n > 3, 1-way ANOVA)

ns, not significant * P < .05, ** P < .01, ***P < .001.

These findings indicate that TRIP13 acts upstream of TP53, with TP53 activation being a consequence of TRIP13 inhibition. This mechanistic insight provides a rationale for the observed synergy between TRIP13 and MDM2 inhibitors and suggests a promising therapeutic strategy for NUP98::KDM5A$^+$ AMKL.

4.5. Pharmacological TP53 activation as a therapeutic strategy for NUP98::KDM5A$^+$ AMKL

Combined therapies are often more effective in achieving cancer cell clearance and preventing resistance development. While we previously demonstrated synergy between DCZ0415 and Idasanutlin (Wang, Huang et al. 2020), DCZ0415 is an early-stage compound not readily applicable to patients (Li, Liu et al. 2021). In contrast, Idasanutlin, which also triggers TP53 activation, is clinically approved (Konopleva, Martinelli et al. 2020). To eliminate DCZ0415

from our treatment regimen while maintaining a multi-modal therapy approach, we sought to identify synthetic lethal dependencies with TP53 activation. We performed a CRISPR-Cas9 screening probing 704 TP53 pathway-related genes in fetal NUP98::KDM5A^{+} cells with and without *Trip13*-knockout (Figure 32A). We found 249 depleted genes in fetal NUP98::KDM5A^{+} cells and 232 depleted genes in *Trip13*-knockout fetal NUP98::KDM5A^{+} cells. Notably, *Bcl-xl/Bcl2l1* knockout showed enhanced depletion in combination with TP53 activation/*Trip13* ablation, suggesting potential combinatorial treatment options (Figure 32B). Inversely, murine *TP53* (*Trp53*) and *Bbc3/Puma* ablation were highly enriched in *Trip13*-knockout cells, highlighting potential resistance mechanisms (Figure 32B). Recent studies have demonstrated the molecular dependence in AMKL on *Bcl-xl* (Kuusanmäki, Dufva et al. 2023, Gress, Roussy et al. 2024), which our approach further validated. Additionally, we found elevated expression of *Bcl-xl* and *Bbc3* upon *Trip13* loss (Figure 32C-D).

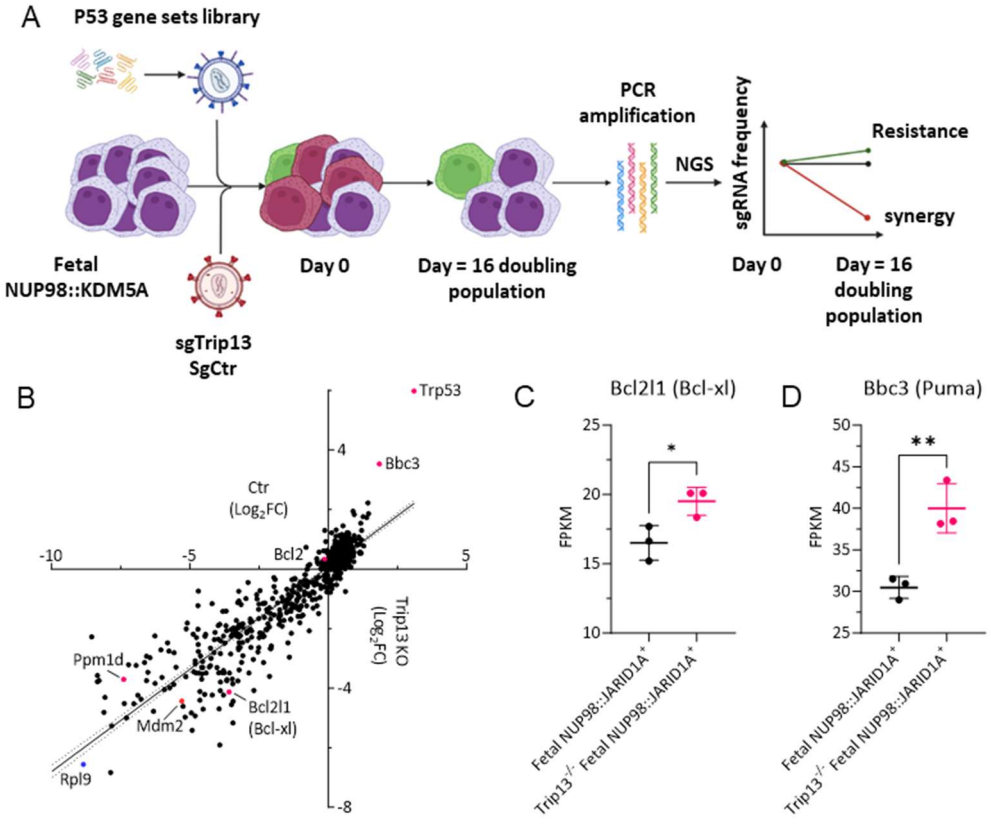

Figure 32 TP53 pathway based CRISPR-Cas9 *in vitro* screening combined with *Trip13* knockout identifies synthetic-lethal dependencies for combinatorial therapeutic approaches

A) Schematic workflow of the high-throughput TP53 pathway based CRISPR-Cas9 *in vitro* screening combined with *Trip13* loss to identify synthetic-lethal dependencies for combinatorial therapeutic approaches.

B) Dot plots showing the log2 fold change of the TP53 pathway related genes targeted by sgRNAs in control (x-axis), Trip13 depleted (y-axis) fetal NUP98::KDM5A^{+} cells. Blue dots represent positive controls (*Rpl9*). Red dots represent selected candidate genes (*Ppm1d*, *Mdm2*, *Bcl2l1*, *Bbc3*, *Trp53*). (n =2)

C) Dot plot showing the expression of *Bcl2l1* of control or *Trip13*-depleted fetal NUP98::KDM5A^{+} cells after 4 days of culture (n = 3).

D) Dot plot showing the expression of *Bbc3* of control or *Trip13*-depleted fetal NUP98::KDM5A^{+} cells after 4 days of culture (n = 3)

ns, not significant * P < .05, ** P < .01, ***P < .001.

Based on these findings, we treated our murine fetal and adult NUP98::KDM5A$^+$ leukemic models with Navitoclax, a BCL2 family inhibitor targeting BCL2 and BCL2L1 (BCL-X_L), and 5-Azacytidine, a chemotherapeutic agent frequently used in combination with BCL2 inhibitors (Stubbins, Francis et al. 2022). After 5 day of treatment with Navitoclax alone, only fetal NUP98::KDM5A$^+$ cells showed a significant response, with a mean IC_{50} value of 100 nM. Adult NUP98::KDM5A$^+$ AMKL, ML-DS and FPD-AML models showed minimal response, not reaching a mean IC_{50} value. 5-Azacytidine treatment resulted in significantly higher sensitivity in fetal NUP98::KDM5A$^+$ AMKL model (mean IC_{50} value of 1.7 µM) compared to adult NUP98::KDM5A$^+$ AMKL (mean IC_{50} value of 6.9 µM). FPD-AML and ML-DS models showed similar sensitivity to fetal NUP98::KDM5A$^+$ AMKL model, showing a mean IC_{50} value of 2.45 µM and 1.02 µM, respectively (Figure 33A-B). We next assessed the efficacy of Navitoclax and 5-Azacytidine in human cells. hFL NUP98::KDM5A$^+$ cells showed sensitivity to Navitoclax with a mean IC_{50} value of 158 nM, while OCI-AML3 and ML-2 cells exhibited higher mean IC_{50} values (463 nM and 660 nM, respectively). Kasumi1 cells displayed a superior sensitivity with a mean IC_{50} value of 35 nM (Figure 33C). When treated with 5-Azacytidine, hFL NUP98::KDM5A$^+$ cells were significantly more responsive (mean IC_{50} value of 2.8µM) compared to OCI-AML3, ML-2, Kasumi1 cells (mean IC_{50} value of 4.8 µM, 7.2 µM and 7 µM, respectively) (Figure 33D).

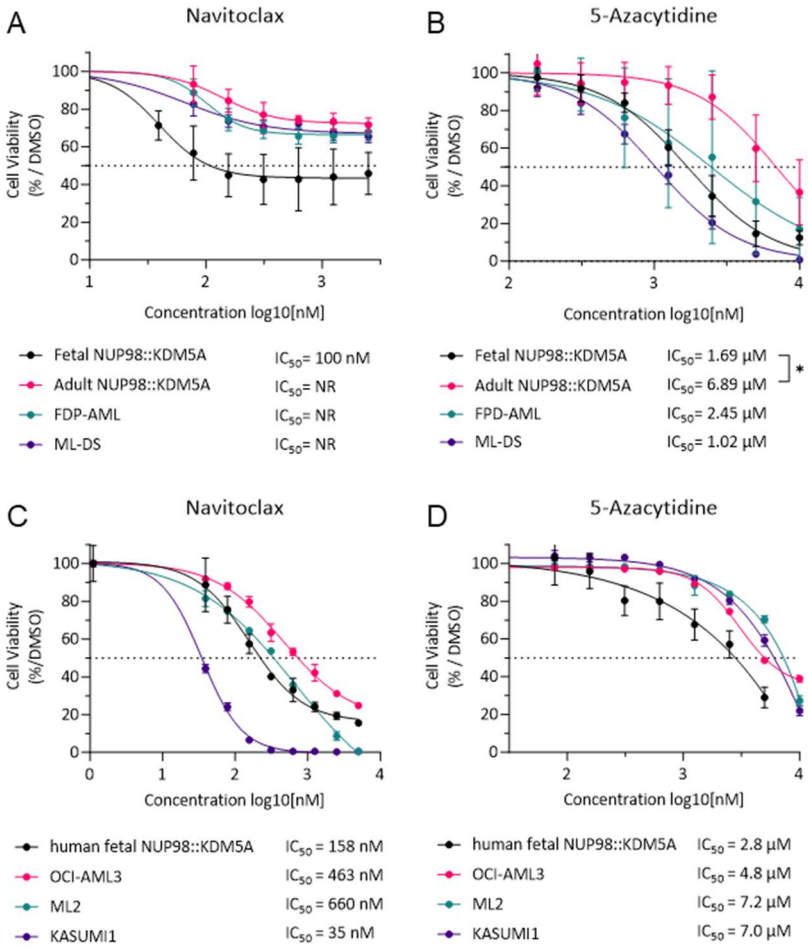

Figure 33 Fetal NUP98::KDM5A$^+$ cells are responsive to Navitoclax and 5-Azacytidine

A) Dose response curves for Navitoclax (BCL2 family inhibitor) in fetal and adult NUP98::KDM5A$^+$, ML-DS and FPD-AML models after 5 days of treatment *in vitro*. The corresponding IC_{50}-values are depicted below the graphs. (mean ± s.d. , n > 3, 1-way ANOVA)

B) Dose response curves for 5-Azacytidine (hypomethylating chemotherapeutic agents) in fetal and adult NUP98::KDM5A$^+$, ML-DS and FPD-AML models after 5 days of treatment *in vitro*. The corresponding IC_{50}-values are depicted below the graphs. (mean ± s.d. , n > 3, 1-way ANOVA)

C) Dose response curves for Navitoclax in hFL NUP98::KDM5A$^+$ cells and OCI-AML3, ML2 and Kasumi1 after 5 days of treatment *in vitro*. The corresponding IC_{50}-values are depicted below the graphs. (mean ± s.d. , n > 3, 1-way ANOVA).

D) Dose response curves for 5-Azacytidine in hFL NUP98::KDM5A$^+$ cells and OCI-AML3, ML2 and Kasumi1 after 5 days of treatment *in vitro*. The corresponding IC_{50}-values are depicted below the graphs. (mean ± s.d. , n > 3, 1-way ANOVA).

ns, not significant * P < .05, ** P < .01, ***P < .001.

We further combined these three FDA-approved drugs (Idasanutlin, Navitoclax and 5-Azacytidine) to reduce dosage, minimize toxicity, and exploit synergistic mechanisms while avoiding resistance. We first tested dual combinations. Idasanutlin and Navitoclax showed a mild additive effect in murine fetal and adult NUP98::KDM5A$^+$ cells, with a summary Bliss synergy score of -6 and -0.5, respectively (Figure 34A-B). Conversely, this combination exhibited a high synergistic effect in hFL NUP98::KDM5A$^+$ cells, with a summary Bliss synergy score of 20 (Figure 34C). Although the combination of Idasanutlin with 5-Azacytidine showed a synergistic effect in adult NUP98::KDM5A$^+$ cells (summary Bliss synergy score = 21), it exhibited an additive effect in murine and human fetal NUP98::KDM5A$^+$ cells (summary Bliss synergy score = 5 and 8, respectively) (Figure 34A-C).When 5-Azacytidine was combined with Navitoclax, we observed an additive effect in fetal NUP98::KDM5A$^+$ cells (summary Bliss synergy score = 5) and a synergistic effect in adult and hFL NUP98::KDM5A$^+$ cells (summary Bliss synergy score = 18 and 16, respectively) (Figure 34A-C). Most importantly, the triple combination of Idasanutlin, Navitoclax and 5-Azacytidine showed enhanced synergistic effects in murine fetal, adult and hFL NUP98::KDM5A$^+$ cells, with summary Bliss synergy score of 17, 42 and 26 respectively (Figure 34A-C).

In summary, the combination of Idasanutlin, Navitoclax and 5-Azacytidine, all FDA-approved drug, had a highly synergistic effect on NUP98::KDM5A$^+$ leukemia, offering a promising tailored therapeutic strategy for the treatment of high-risk pediatric leukemia subgroup.

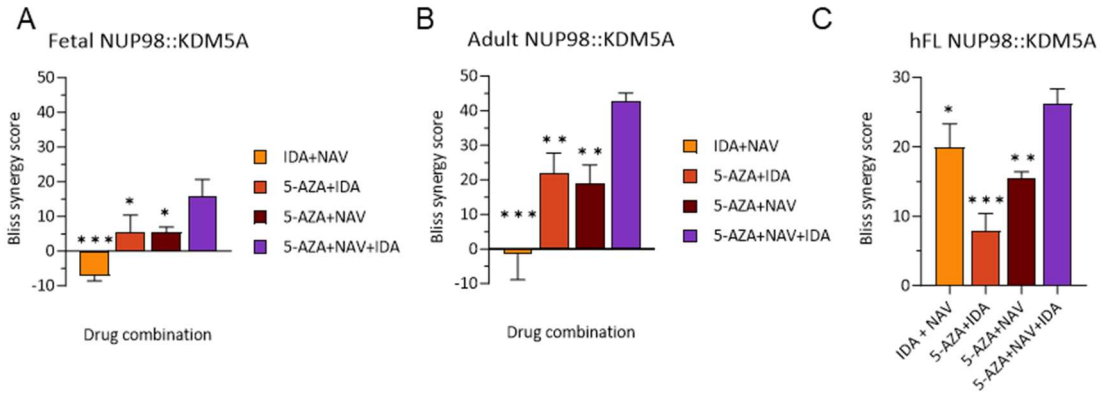

Figure 34 Triple combination of Idasanutlin, Navitoclax and 5-Azacytidine has high synergistic effect in NUP98::KDM5A models

A) Bar plot showing the summary Bliss synergy score of double or triple combinatorial treatment with FDA-approved drugs (IDA = Idasanutlin, NAV = Navitoclax, 5-AZA = 5-Azacytidine) of fetal NUP98::KDM5A$^+$ cells after 5 days. (mean ± s.d. , n = 3, 1-way ANOVA)

B) Bar plot showing the summary Bliss synergy score of double or triple combinatorial treatment with FDA-approved drugs (IDA = Idasanutlin, NAV = Navitoclax, 5-AZA = 5-Azacytidine) of adult NUP98::KDM5A^{+} cells after 5 days. (mean ± s.d. , n = 3, 1-way ANOVA)

C) Bar plot showing the summary Bliss synergy score of double or triple combinatorial treatment with FDA-approved drugs (IDA = Idasanutlin, NAV = Navitoclax, 5-AZA = 5-Azacytidine) of hFL NUP98::KDM5A^{+} cells after 5 days. (mean ± s.d. , n >=3, 1-way ANOVA)

ns, not significant * P < .05, ** P < .01, ***P < .001.

5. Discussion

NUP98 fusions, including the NUP98::KDM5A translocation, occur with high frequency in pediatric AML patients and NUP98::KDM5A is particularly frequent in young children (<2 years of age), suggesting that NUP98::KDM5A leukemia may originate from fetal hematopoiesis (de Smith and Spector 2024). However, the underlying pathomechanisms remain enigmatic. In this study, we established and leveraged a model system of NUP98::KDM5A with fetal and adult developmental origin to elucidate the implications of the ontogenic programs and changes on the malignant transformation driven by NUP98::KDM5A. Based on the difference between fetal and adult hematopoiesis, we identified vulnerabilities by functional genomics and highlighted how to exploit ontogenic programs for therapeutic purposes.

This thesis further demonstrates that NUP98::KDM5A fusion sustains the expression of the fetal gene programs, including the here identified targetable vulnerability TRIP13, which mechanistically represses the TP53 pathway through PPM1D. The inhibition of TRIP13 elevates TP53 activation resulting in arrest of leukemia proliferation and apoptosis. The thesis thereby highlights the central role of TP53 pathway in the NUP98::KDM5A-induced phenotype and establishes pharmacological interference by targeting the TRIP13/PPM1D/TP53 axis using the targeted agents Idasanutlin, Navitoclax and 5-Azacytidine. This proposed therapeutic strategy successfully and synergistically eliminates NUP98::KDM5A-induced malignant leukemia and offers a new therapeutic option for the high-risk group of NUP98::KDM5A^{+} AMKL with readily FDA-approved drugs.

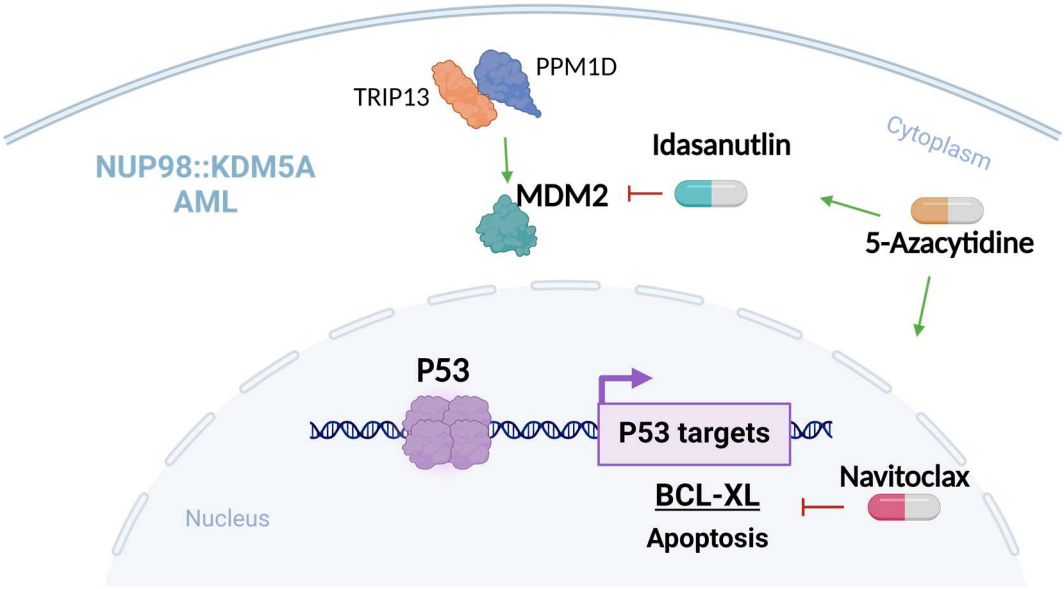

Figure 35 Proposed mechanism of TRIP13/PPM1D/TP53 vulnerability in NUP98-KDM5A-driven leukemia.
Created in Biorender.com

5.1. Modeling NUP98::KDM5A^{+} leukemia remains a challenge

Progress in the field of pediatric AMKL is often hampered by limited patient material available. This is true for the majority of genetic subtypes and includes NUP98::KDM5A. Furthermore, there is only a strongly restricted pool of representative cell lines and none of them includes NUP98:KDM5A. Results on humanized models are variable. Where others have shown

transformation of cord blood derived CD34$^+$ cells by NUP98::KDM5A (Cardin, Bilodeau et al. 2019), our own approaches to transform peripheral blood CD34$^+$ cells failed (not shown) and fetal liver derived CD34$^+$ cells showed a partially transformed phenotype. For this reason, modeling NUP98::KDM5A remains a challenge.

This study focused on cell ontogeny and the effect of NUP98::KDM5A-driven leukemia. We thus needed to generate and compare two NUP98::KDM5A models based on those two hematopoietic ontogenies (fetal and adult). This defined setting enabled us to highlight the more aggressive leukemia phenotype, when the fusion oncoprotein was expressed in fetal HSPCs compared to adult HSPCs.

Although previous studies have reported murine NUP98::KDM5A models using fetal or adult HSPCs (Xu, Valerio et al. 2016, Schmoellerl, Barbosa et al. 2020, Heikamp, Henrich et al. 2022), this thesis has, for the first time, directly compared NUP98::KDM5A-induced leukemia changes during ontogenetic stages. Notably, previously described fetal based NUP98::KDM5A models included additional expression of oncogenic NRAS, which may represent a confounder in downstream studies.

Overall, findings presented here are the first to demonstrate that ontogeny-specific differences play a role in the predisposition of NUP98::KDM5A$^+$ leukemia, which may explain the higher incidence in pediatric patients compared to adults (Noort, Wander et al. 2021, Bertrums, Smith et al. 2023). In line with this, a previous study based on CBFA2T3::GLIS2$^+$ and KMT2A::MLLT3$^+$ AMKL demonstrated that changes in the cellular architecture during hematopoietic ontogeny determine the aggressive features and the age- and phenotype-specific associations seen in pediatric AMKL patients (Lopez, Noguera et al. 2019).

Noteworthy, the NUP98::KDM5A oncogenic effect was more distinct in the human setting when comparing human fetal and adult HSPCs . After the initial depletion, the latter were not able to overcome the normal cell culture. A previous study demonstrated the NUP98::KDM5A transforming effect in another hematopoietic ontogeny by overexpressing the fusion oncoprotein in cord blood HSPCs (Cardin, Bilodeau et al. 2019). Although this model also demonstrated a strong propensity for NUP98::KDM5A to promote the development of multiple subtypes of leukemia, transformed cord blood HSPCs additionally recapitulated the AMKL phenotype. Thus, future studies should adopt cord blood HSPCs to overcome the limited source of human fetal HSPCs and patient material.

Overall, the findings of this thesis has shed light on the differences in the developmental transcriptional programs of the initiating cells (fetal vs adult hematopoietic stem cells), and/or the diversity of cells susceptible to NUP98::KDM5A-driven transformation.

5.2. The fetal-enriched *TRIP13* gene is a molecular vulnerability of NUP98::KDM5A$^+$ leukemia

This work first set out to interrogate the ontogenic effect on NUP98::KDM5A-induced transformation by comparative analysis in fetal and adult HSPCs. These NUP98::KDM5A models have shown a differential development of the disease with lower latency, when the fusion oncoprotein is expressed in fetal HPCs compared to adult HSPCs (Figure 14), which is in line with the high frequency of NUP98::KDM5A translocation in pediatric patients (Noort,

Wander et al. 2021, Bertrums, Smith et al. 2023). Gene expression analysis of fetal and adult NUP98::KDM5A transformed cells highlighted the maintained expression of fetal gene programs in transformed cells of fetal origin. Applying functional genomics, this work systematically profiled fetal-enriched coding genes and thereby contributed to deciphering the involvement of the fetal transcriptional landscape in pediatric NUP98::KDM5A$^+$ leukemogenesis.

Based on its expression profile and depletion characteristics in fetal NUP98::KDM5A cells, further analyses focused on the AAA ATPase TRIP13. Through detailed functional validation, it was determined that TRIP13 was more critical in the fetal NUP98::KDM5A model compared to adult NUP98::KDM5A, ML-DS and FDP-AML models. Notably, TRIP13 was found to be overexpressed not only in pediatric NUP98::KDM5A$^+$ AMKL but also in other NUP98-rearranged AML subgroups, and NUP98::KDM5A expression further elevated TRIP13 mRNA levels. A recent study has shown that all NUP98-fusions share common sets of target genes, which are critical for their oncogenicity (Schmoellerl, Barbosa et al. 2020). It is thus appealing to speculate that the NUP98-moiety is required for regulation of TRIP13 and may be a shared dependence in other NUP98-fusions, such as the NUP98::NSD1 rearrangement.

By dissecting the consequences of *Trip13* loss in fetal NUP98::KDM5A cells, this work demonstrated that its inhibition activates the TP53 pathway, which was rescued upon the genetic deletion of murine *TP53* or upon the overexpression of TRIP13 cDNA. Hence, the maintenance of high TRIP13 levels in fetal cells and the additional overexpression of TRIP13 induced by NUP98::KDM5A is crucial for leukemia cell survival, as it represses the TP53 pathway. TRIP13 has recently attracted attention from researchers due to its overexpression in several solid tumors and hematological malignancies (Banerjee, Russo et al. 2014, Lu, Qian et al. 2019). Consistent with our phenotypic characterization of TRIP13-depleted fetal NUP98::KDM5A$^+$ cells (Figure 19), several studies have shown that TRIP13 governs the cell cycle and inhibits apoptosis in solid cancer (Hama, Nagesh et al. 2021, Yu, Chen et al. 2022). Some studies have indicated an indirect connection between TRIP13 and TP53 (Yu, Xiao et al. 2019, Li, Xia et al. 2021). However, the precise regulatory mechanism remains elusive. Thus, the oncogenic mechanism of the TRIP13/TP53 axis remains not completely understood. A potential indirect activation through DNA damage was ruled out.

The second top candidate identified by CRISPRCas9 knockout screening is the pseudouridine synthase 7, *PUS7*. This gene is involved in RNA modification, which can impact on gene expression and cellular functions (Rosselló-Tortella, Ferrer et al. 2020). Recent studies have indicated a significant role for the PUS7 gene in AML (Guzzi, Cieśla et al. 2018). These studies have highlighted that the depletion of mTOG, a downstream target of PUS7, predicts poor disease outcomes independent of other genetic alterations, underscoring the complex role of PUS7 in AML pathogenesis (Guzzi, Muthukumar et al. 2022).

Moreover, our CRISPR-Cas9 knockout screening has also revealed five additional candidates, which deplete fetal NUP98::KDM5A$^+$ cells over adult ones. *FANCI*, *FANCB*, *FANCJ/BRIP1*, *FANCT/UBE2T* and *UBE2C* are all members of the Fanconi Anemia (FA) complementation group. A recent work has already elucidated the molecular implication of FA proteins in AML demonstrating that the FA genes are synthetic lethal with aldehyde dehydrogenase 2 (ALDH2)

(Yang, Wu et al. 2021). The authors showed that upon inactivation of FA genes in ALDH2-deficient AML the level of aldehyde-induced DNA damage reaches a threshold that triggers TP53-mediated cell-cycle arrest and cell death (Yang, Wu et al. 2021). Thus, the FA proteins represent molecular vulnerabilities also in pediatric NUP98-rearranged leukemia and can be therapeutically exploited.

Noteworthy, our main candidate TRIP13 was found to act through TP53 suppression, linking >85% of the identified top targets to this pathway. Thus, our CRISPRCas9 knockout screening in fetal NUP98::KDM5A^{+} leukemia point towards a major role of TP53 control in this pediatric subgroup of AML, which is of major interest since this hallmark of cancer has been insufficiently investigated in pediatric leukemias (Hainaut 2013).

5.3. TRIP13 and PPM1D repress the TP53 pathway in NUP98::KDM5A^{+} leukemia

To identify the mechanism of TRIP13 mediated TP53 regulation, we performed IP-MS for TRIP13. This proteomics analysis identified 33 candidate genes bound by TRIP13 with a known involvement in TP53 regulation (detailed in the next section). To identify the major regulator of TP53 bound by TRIP13, we genetically tested which gene phenocopies the TRIP13 (depletion) phenotype in NUP98::KDM5A cells. These combined analyses pointed towards the protein phosphatase PPM1D/WIP1, as top TRIP13-partner for the repression of TP53. Co-immunoprecipitation assays confirmed the physical interaction between TRIP13 and PPM1D/WIP1, highlighting their cooperative role in regulating TP53 activity. Mechanistically, this study has shown that TRIP13 together with PPM1D maintain TP53 pathway repressed and sustain NUP98::KDM5A cell proliferation. Upon *TRIP13* knockout, PPM1D fails to interact with TRIP13 and TP53 is de-repressed leading to the expression of TP53-target genes. These findings, although not formally shown, suggest TRIP13 as a co-activator of PPM1D, since the loss of TRIP13 did not affect PPM1D protein levels. However, additional assays on PPM1D activity and conformational activation may shed more light on the price mechanism guided by TRIP13/PPM1D.

The protein phosphatase PPM1D, also known as WIP1, is transcriptionally activated by *TP53* and negatively regulates TP53 signaling via dephosphorylation of numerous substrates upstream of TP53, downstream of TP53, and TP53 itself (Deng, Li et al. 2020, Husby, Hjermind Justesen et al. 2021). The well-established role of PPM1D is to regulate cell cycle and stress response pathways (Miller, Sperling et al. 2023). Recent study found that PPM1D governs the competitive fitness and self-renewal of HSCs (Miller, Sperling et al. 2023). The authors investigated the reliance of PPM1D activity on TP53 by conducting a CRISPR/Cas9 resistance screening in a human AML cell line and demonstrated that the inhibition of PPM1D led to a strong selection of sgRNAs targeting *TP53* (Miller, Sperling et al. 2023). This, in line with the presented findings here, suggests that the effects of PPM1D inhibition on cellular proliferation necessitate the presence of TP53. Similar to *TRIP13*, *PPM1D* has also been found to be amplified and mutated in various tumors and is currently considered to be an oncogene (Deng, Li et al. 2020, Husby, Hjermind Justesen et al. 2021). For this reason, the selective inhibition of PPM1D has emerged as a promising drug target in cancer (Pecháčková, Burdová et al. 2017, Nahta and Castellino 2021, Marcellino 2023). Several studies have indicated that PPM1D

inhibition acts synergistically with specific chemotherapeutics and the MDM2-antagonist nutlin in different cancer cell lines (Andrysik, Sullivan et al. 2022, Zanjirband, Rahgozar et al. 2023). Several small-molecules targeting PPM1D have been developed (Ogasawara, Kiyota et al. 2015). However, they have encountered challenges concerning low selectivity or inadequate bioavailability, which have prevented their prospective clinical application so far.
Nevertheless, the precise mechanism through which TRIP13/PPM1D regulates the TP53 protein and pathway remains unresolved. Since PPM1D protein structure has still not been determined, one hypothesis based on our protein-protein interaction analysis suggests that TRIP13 interacts with PPM1D, inducing a conformational change from an inactive to an active state. Alternatively, TRIP13 ATPase activity might sustain PPM1D function as activating factor. Future investigations should investigate the conformational changes of PPM1D upon interaction with TRIP13 with orthogonal biophysical, biochemical, and structural assays as similarly done with the PPM1D inhibitor GSK2830371 (Miller, Sathappa et al. 2022).

5.4. TRIP13 protein interactome reveals several TP53 regulators

Since our proteomic data has shown that TRIP13 interacts with more than 33 TP53 regulators, diverse mechanisms may be accountable for the repression of the TP53 pathway in NUP98::KDM5A^{+} AMKL.
The second top candidate identified by IP/MS ERCC is an ATP-dependent DNA helicase Excision Repair 2 gene (ERCC2/XPD), subunit of the transcription factor II Human (TFIIH) complex. Previous study showed that ERCC2 interacts both physically and functionally with TP53, which inhibits the TFIIH complex and its multiple functions in transcription, DNA repair and possibly the cell cycle (Léveillard, Andera et al. 1996). Since ERCC2 relies on ATP, the AAA ATPase TRIP13 may act as cofactor sustaining ERCC2 functions. ERCC2 has been identified to play a role in cancer, especially the association between its polymorphisms and the response to platinum-based chemotherapy (Geredeli, Artac et al. 2015, Zhang, Guan et al. 2017). Notably, ERCC2/XPD Lys751Gln (rs13181) polymorphism causes apoptosis and cell cycle arrest through TP53 pathway altering DNA repair efficiency of platinum-induced DNA damage (Zhang, Guan et al. 2017). This may suggest that alteration in ERCC2 may impair the binding with TP53 as well as the overall TFIIH complex. Inversely, it has also been shown that ERCC2/PXD acts as tumor suppressor in Cutaneous Squamous Cell Carcinoma inducing cell cycle arrest and apoptosis and improving the level of TP53 and HIPK2 (Liu, Xiong et al. 2018). However, the mechanism behind ERCC2 deregulation remains not fully elucidated.
Another candidate among the 33 selected TRIP13-interactors is Casein kinase II subunit alpha (CSNK2α1/CK2 α1), a serine/threonine protein kinase involved in several cellular processes (Hussain, Guo et al. 2024). The CSNK2α1 kinase exists as a tetramer and the alpha subunits contain the catalytic activity while the beta subunits undergo autophosphorylation (Hussain, Guo et al. 2024). The interaction between TRIP13 and CSNK2α1 found by IP/MS suggests that TRIP13 may favor the autophosphorylation of the beta subunits. Protein Kinase CK2 has been found to be highly expressed in many malignant tumor tissues and may contribute to the development of malignant lymphoma and leukemia (Jiang, Zhang et al. 2018). A recent study showed that CK2 activates and mediates CCDC106 phosphorylation for TP53 degradation in

cervical and breast cancer (Ning, Wang et al. 2019). A previous work showed that CSNK2α1 knockdown induces a TP53-dependent apoptosis in AML. Furthermore, the authors have shown that it can be a promising therapeutic target, since the combination of a small inhibitor with daunorubicin shows synergistic effects (Quotti Tubi, Gurrieri et al. 2013). Interestingly, a recent study found that CK2 inhibition shows a synthetic lethal dependency with loss of *RB1* in high-grade serous ovarian carcinoma and triple-negative breast cancer and thus being a promising approach for the treatment of *RB1*-deficient tumors (Bulanova, Akimov et al. 2024), as in the case of NUP98::KDM5A leukemia (de Rooij, Branstetter et al. 2017).

A recent work found that the overexpression of TRIP13 in multiple myeloma and B cell lymphoma resulted in excess cellular deubiquitination (Li, Xia et al. 2021). The authors proposed a model where TRIP13 interacts with the Ubiquitin Specific Peptidase 7 (USP7), which is regulates deubiquitination of critical oncogenic (NEK2, MDM2) and tumor suppressor (PTEN, TP53) proteins (Li, Xia et al. 2021). However, USP7 was not found in the proteomic data of this study.

Inversely, our IP/MS data revealed another protein belonging to the deubiquitinase (DUBs) family, the Ubiquitin Specific Peptidase 10 (USP10), whose genetic depletion was able to mimic *Trip13* loss as shown by our experimental setup (Figure 25). USP10 is a DUB and a known regulator of TP53 stability and localization (Jochemsen and Shiloh 2010, Reece and Figg 2010, Lei, Wang et al. 2021). A previous study showed that *USP10* acts as a tumor suppressor and is responsible for the nuclear-cytoplasmic localization of TP53, counteracting MDM2 function (Yuan, Luo et al. 2010). Inversely, another work showed that USP10 interacts with and deubiquitinates GTPase-activating protein-binding protein 2 (G3BP2) and together inhibit TP53 signaling contributing to a poor outcome of patients with prostate cancer (Takayama, Suzuki et al. 2018). A more recent study confirmed that USP10 destabilizes TP53 and regulates autophagy and survival in neonatal mice (Li, Li et al. 2022). In line with the USP10 findings of this thesis, the authors also observed that combined deletion of murine *TP53* and *Usp10* rescued the death phenotype. This suggests that USP10 might also be directly involved in the repression of TP53 pathway in NUP98::KDM5A leukemia. Future studies should elucidate the mechanism behind the interaction of USP10 with TRIP13. However, other mechanisms may rely on USP10-dependent TP53 regulation. A previous work has shown that IGF2BP3 (Insulin-like growth factor 2 mRNA binding protein 3) physically interacts with USP10 and attenuates USP10 mediated deubiquitination of TP53 promoting lung tumorigenesis (Zhao, Lu et al. 2017). *IGF2BP3* is a known fetal oncogene (Lederer, Bley et al. 2014). Gene expression analysis of *in vitro* murine NUP98::KDM5A models showed that *IGF2BP3* is overexpressed by the fusion oncoprotein and is a molecular dependency, as found after the CRISPRcas9 screening. Based on these works and the high depletion upon *Usp10* knockout, the proposed mechanism in lung cancer may be applied to our NUP98::KDM5A leukemia context. Recently, new USP10 inhibitors have been developed holding promise as novel therapeutic approaches for solid cancer as well as for hematological malignancies (Zhang, Sartori et al. 2017, Lu, Gao et al. 2024).

Noteworthy, among the 1942 proteins found by IP-MS there are other TRIP13 interactors, which might be involved in vulnerable pathways and were not further investigated in this

study, such as the Exportin 1 (XPO1/CRM1). A previous study has shown that NUP98::HOXA9 binds XPO1 through the FG to regulate the HOX cluster expression (Takeda, Sarma et al. 2010, Oka, Mura et al. 2016). Based on these works, we hypothesize that TRIP13 might be essential for the interaction of NUP98-fusions and XPO1 and the expression of essential cluster genes.
Overall, this thesis has elucidated the intricated molecular mechanism of NUP98::KDM5A-driven leukemogenesis and identified vulnerabilities of fetal-enriched genes, which pointed toward a more global dependence on TP53 in pediatric NUP98::KDM5A$^+$ AMKL.

5.5. TP53 re-activation is a vulnerability in NUP98::KDM5A$^+$ leukemia

Our systematic investigation of fetal hematopoiesis contribution in NUP98::KDM5A-driven leukemogenesis has revealed a critical dependence on TP53 suppression in pediatric NUP98::KDM5A$^+$ AMKL. Through high-throughput genomic and proteomic approaches, we have uncovered a complex and global regulation of the TP53 protein. While we focused on TRIP13, the abundance of TP53-linked hits in our screening as well as the number of TP53 regulators bound to TRIP13, indicates a complex regulation that extends beyond simple linear pathways. As outlined, our CRISPR-Cas9 screen identified several candidates, including TRIP13 and FA proteins, while our IP/MS analysis revealed 33 TRIP13/TP53-regulators. These findings collectively indicate an overall repression of TP53 protein and suggested that NUP98::KDM5A$^+$ AMKL relies on low levels of TP53 for survival and proliferation, which we verified in our experiments.
One major role of TP53 is sensing and response to DNA-damage (Anbarasan and Bourdon 2019). Indeed, previous studies have demonstrated that TRIP13 primarily regulates the DNA damage response (Banerjee, Russo et al. 2014). However, our experiments did not show a significant increase in the protein level of γH2AX in TRIP13-depleted fetal NUP98::KDM5A$^+$ cells. While this observation initially suggests that the DNA damage response pathway might not be directly involved in TP53 regulation in NUP98::KDM5A$^+$ leukemia, we also detected a dependence of NUP98::KDM5A$^+$ AMKL on five members of the FA group, which are known to play crucial roles in both DNA damage response and TP53 activation (Yang, Wu et al. 2021). Furthermore, we identified ERCC2 as both a TRIP13- and TP53-interactor. ERCC2 is a well-established regulator of DNA repair processes and interacts with TP53, further implicating the DNA damage pathway in our model (Léveillard, Andera et al. 1996). The apparent discrepancy between the involvement of DNA damage response proteins and the lack of detectable changes in γH2AX levels may be attributed to the limitations of our assay or multiple parallel modes of action. Future studies may thus employ more sensitive techniques to assess DNA damage in this system and challenge cells with DNA damage or DNA-damage suppression while performing knockout of our candidate genes.
Indeed, recent research has shown that NUP98::KDM5A promotes the accumulation of DNA damage and aberrant mitosis by directly interfering with RAE1 activity, thereby inducing genomic instability (Domingo-Reinés, Montes et al. 2023). This observation aligns with another study that identified CDK6 (Cyclin Dependent Kinase 6), a known regulator of the cell cycle, as a molecular dependency in NUP98 fusion oncoproteins (Schmoellerl, Barbosa et al. 2020). Together, these studies suggest that the expression of NUP98 fusion proteins may

cause oncogene-induced replication stress, a well-described source of genomic instability in cancer (Kotsantis, Petermann et al. 2018, Bowry, Kelly et al. 2021). This replication stress could potentially activate TP53 through various mechanisms, including the DNA damage response pathway. To note, the majority of NUP98::KDM5A$^+$ AMKL patients harbor mutations in *RB1*, which has been linked to DNA damage response, genomic stability and oncogene induced stress in general (Vélez-Cruz, Manickavinayaham et al. 2016, Zamalloa, Pruitt et al. 2023).
While our study indicates a complex network of TP53 regulation in NUP98::KDM5A$^+$ AMKL, involving multiple proteins and pathways, the exact mechanisms by which some of these factors contribute to TP53 regulation and leukemogenesis remain to be fully elucidated. Future experiments should focus on: employing more sensitive techniques to detect subtle changes in DNA damage markers in NUP98::KDM5A cells, investigating the specific roles of identified TP53 regulators in maintaining low TP53 levels in NUP98::KDM5A$^+$ AMKL, exploring the potential link between NUP98-KDM5A-induced genomic instability and TP53 activation and examining the interplay between DNA damage response, cell cycle regulation, and TP53 activation in the context of NUP98::KDM5A-driven leukemogenesis. By addressing these questions, we can gain a more comprehensive understanding of the molecular TP53-dependency of NUP98::KDM5A$^+$ AMKL and potentially identify novel therapeutic targets for this aggressive form of pediatric leukemia.

5.6. TP53 re-activation is a therapeutic approach for NUP98::KDM5A$^+$ leukemia

This study has demonstrated that the dependency of fetal NUP98::KDM5A$^+$ leukemia on the TP53 pathway and *TRIP13* is one candidate, which we mechanistically dissected. We next aimed to globally exploit our gain of knowledge on low TP53 levels pharmacologically and first tested it based on our primary candidate *TRIP13*. The TRIP13 inhibitor DCZ0415 achieved strong antiproliferative response *in vitro*. To enhance the activation of TP53 pathway, we leverage the global repression of TRIP13 on TP53 using a combinatorial treatment with Idasanutlin, which showed a high synergistic response.
The treatment with DCZ0415 as single agent in NUP98::KDM5A cells revealed high IC_{50} values (20 µM), highlighting limitations for the use *in vivo* and for clinical translation. The IC50 detected here is in line with former studies utilizing this compound (Agarwal, Afaq et al. 2022, Dong, Hu et al. 2024).
For this reason and to avoid escape mechanisms of cancer cells, which lead to relapse, we next aimed to establish a combinatorial treatment with clinically accessible drugs. In this direction several studies have demonstrated that DCZ0415 can be used in combination with other drugs, such as PARP1 Inhibitors, the multiple myeloma chemotherapeutic melphalan or the HDAC inhibitor panobinostat, showing synergistic effect and enhancing the DNA-damage response (Wang, Huang et al. 2020). A recent study proposed that the balance between TRIP13 and MAD2L1 facilitates mitotic exit and survival in HPV-positive cancers, since the absence of *RB1*, and that this balance can be disrupted by combining Aurora kinase inhibitors with TRIP13 inhibitors. This combinatorial treatment may offer one therapeutic strategy and a wide therapeutic window, potentially enabling effective treatment of Rb-deficient cancers, which is true for NUP98:KDM5A$^+$ AMKL. However, it is important to note that Aurora kinase

inhibitors are highly toxic (Machado, EL et al. 2021). In line with these studies, this thesis has demonstrated the benefit of the combinatorial treatment of DCZ0415 with Idasanutlin, encouraging the improvement of the TRIP13 inhibitors. A recent study found a new molecule DCZ5418, which showed less toxicity in vivo and with a lower dose administration (15 mg/kg vs 25 mg/kg) than DCZ0415 for the treatment of multiple myeloma, offering in this direction promising results (Dong, Hu et al. 2024). Thus, the dose-limitation and the encouraging combinatorial approaches underscore the need for the development of novel and improved DCZ0415 analogs for clinical translation.

To extend our range of targetable proteins and combine this with our gained knowledge on TP53 dependence, we performed a CRISPR/Cas9-based dropout screening in *Trip13*-knockout fetal NUP98::KDM5A^{+} cells to deeply investigate the TP53 network and to identify synthetic lethality with TP53 activation for combinatorial treatments. This approach has revealed potential combinatory genetic vulnerabilities, as well as resistant mechanisms. We found that the anti-apoptotic protein B-cell lymphoma (BCL-X_L) is a synthetic lethality with TP53 activation. Inversely, the loss of the pro-apoptotic member BBC3/PUMA and TP53 counteracted this mechanism.

In contrast to BCL2, which is important for the myeloid lineage, it has been known that *BCL-X_L* is essential for the erythroid/megakaryocytic lineage and maintaining platelet survival (Afreen, Bohler et al. 2020). In accordance with this thesis, two recent studies have demonstrated the highly dependence on *BCL-X_L* in AMKL, rather than *BCL2* (Kuusanmäki, Dufva et al. 2023, Gress, Roussy et al. 2024). Kuusanmäki and colleagues showed that AEL and AMKL subgroups can be therapeutically treated with Navitoclax, while are resistant to the specific-BCL2 inhibitor Venetoclax (Kuusanmäki, Dufva et al. 2023). Similarly, Gress and colleagues demonstrated that CBFA2T3::GLIS2^{+} AMKL models was sensitive navitoclax and DT2216, a selective BCL-XL proteolysis-targeting chimera degrader, and resistant to BCL2 inhibition and that NUP98r AMKL were also sensitive to BCL-X_L inhibition but not the NUP98r monocytic leukemia, pointing to a lineage-specific dependency (Gress, Roussy et al. 2024). In line with this studies, our NUP98::KDM5A^{+} cells were responsive to the single agents Navitoclax and 5-Azacytidine but not responsive to Venetoclax (data not shown). This is an important finding since Venetoclax, a potent BCL2 specific-inhibitor, is rapidly emerging as a prominent treatment of leukemia including pediatric leukemia (Vogler, Walter et al. 2017, Place, Goldsmith et al. 2018, Pullarkat, Lacayo et al. 2021). However, Navitoclax-treated patients show adverse effects such as thrombocytopenia, highlighting a limitation (Roberts, Seymour et al. 2012). Interestingly, the presented approach has also revealed a high dependency on *Mcl1*, which was not found in these reports and was more linked to monocytic leukemia. Thus, to circumvent the adverse effects on normal thrombopoiesis, other strategies could include a BCL-X_L proteolysis-targeting chimera (PROTAC) or a MCL1 inhibitors, allowing the treatment of NUP98-rearranged leukemia with myeloid or with megakaryocytic phenotype (Khan, Zhang et al. 2019). In line with this studies, our NUP98::KDM5A^{+} cells were responsive to the single agents Navitoclax and 5-Azacytidine but not responsive to Venetoclax (data not shown). Combinatorial strategies with cytotoxic or targeted chemotherapy, which induces apoptosis, in addition to BCL-X_L inhibition, ultimately trigger apoptosis in

NUP98::KDM5A cells that express BCL-X_L, as recently suggested by the implementation with the hypomethylating agent 5-Azacytidine (Pullarkat, Lacayo et al. 2021).
This thesis has shown that the low level of TP53 in pediatric NUP98::KDM5A$^+$ AMKL is a consequence of TRIP13 molecular dependency in fetal HSPCs and can be therapeutically treated using the triple combination of Idasanutlin, Navitoclax and 5-Azacytidine. Since the high synergy score observed (Bliss synergy score >10), these data support the use of this triple combination as a therapeutic strategy in *TP53* wild-type leukemias and indicate that *TP53* mutations might emerge as a mechanism of resistance to this approach.

6. Conclusion

The association of young age and occurrence of NUP98::KDM5A$^+$ AMKL is incompletely understood. By comparative analysis of NUP98::KDM5A$^+$ leukemia models initiated at different ontogenic stages, we highlight fetal origin as an accelerator of disease aggressiveness. Moreover, which we comprehensively probed the transcriptional programs associated with fetal origin for susceptibilities converting this malignant driver into a leukemia weakness. As illustrated here exemplified through the TRIP13/PPM1D/TP53 pathway regulation and the therapeutic reactivation of TP53 activity, this knowledge not only offers immediate therapeutic implications for pediatric NUP98::KDM5A$^+$ AMKL patients but may also be applicable to other pediatric hematological malignancies.
This thesis thus significantly adds to the foundational framework for understanding the contribution of the fetal hematopoiesis in pediatric leukemogenesis. In the current state of cancer research, where a comprehensive map of the cytogenetic, mutational, and epigenetic landscape of cancer is available, the insights from this thesis will be crucial for deciphering the complex interplay between common fusion oncogenes and the ontogenic transcriptional landscape during leukemia onset and progression. The overall discussion of the cell of origin thus has to be revised for pediatric leukemia by not only including the cellular hierarchy but also developmental stage.
In conclusion, this thesis not only advances our understanding of the developmental origin of certain leukemias but also opens new avenues for targeted therapies in pediatric hematological cancers.

7. Outlook and future implications

Oncofetal genes, typically absent in normal postnatal tissues but re-expressed in some adult tumors, offer a promising avenue for cancer treatment (Zaidi, Frietze et al. 2017). In contrast to their reactivation in adult tumors, oncofetal genes may be natively expressed in tumors of fetal origin, such as infant AML. This thesis has explored the role of oncofetal genes in pediatric NUP98::KDM5A$^+$ leukemia, focusing on their potential as therapeutic targets. It has demonstrated that fetal signatures are maintained in transformed cells and how fetal signatures can be leveraged for developing novel and more precise approaches to cancer treatment.

The identification of the oncofetal gene TRIP13-mediating TP53 regulation as a molecular vulnerability in NUP98::KDM5A$^+$ leukemia opens new avenues for tailored therapies. Future research should focus on developing specific TRIP13 inhibitors, which could potentially be effective not only in NUP98::KDM5A$^+$ AMKL but more broadly also in other NUP98-rearranged leukemias and solid tumors, which rely on high *TRIP13* expression level. While the thesis has shed light on the TRIP13/PPM1D/TP53 axis, the precise mechanism of TP53 regulation remains to be fully elucidated. Advanced biophysical and biochemical techniques, such as FRET-based assays, should be employed to investigate conformational changes in PPM1D upon TRIP13 interaction. Additionally, exploring the roles of other identified TP53 regulators, such as USP10 and CSNK2α1, could reveal additional therapeutic targets.

The findings from this thesis may have implications beyond NUP98::KDM5A$^+$ leukemia. Unlike adult cancers, where TP53 mutations are common, pediatric cancers rarely harbor TP53 mutations (Cheng, Yung et al. 2023). This striking difference foremost suggests that TP53 inactivation may not confer major advantages for tumor growth in children. However, this work underlines that alternative mechanisms of TP53 inactivation are at play in childhood malignancies. Non-mutational suppression of TP53 potentially allows cells to dynamically change TP53 activity, raising questions about how different TP53 levels might be favored at various stages of transformation. Future studies should investigate the timing and mechanisms of TP53 up- or downregulation in pediatric AML and the molecular consequences of this dynamic regulation on tumor development. One potential mechanism to explore is self-renewal capacity, which has been associated with TP53 in adult HSCs and should be addressed through serial replating and transplantation (Liu, Elf et al. 2009, Asai, Liu et al. 2011).

The importance of fetal-enriched genes and the TP53 pathway in NUP98::KDM5A-driven leukemogenesis suggests that similar mechanisms might be widespread in other pediatric leukemias. Our patient dataset revealed TRIP13 overexpression not only in NUP98::KDM5A$^+$ leukemia but also in other AML subgroups with NUP98 rearrangements. In line with our results, a recent study demonstrated that all NUP98 fusion proteins share common target genes crucial for their oncogenic potential (Schmoellerl, Barbosa et al. 2020). This finding and our data suggest that the NUP98 moiety may be responsible for regulating *TRIP13* expression. Consequently, that TRIP13-dependent low level of TP53 could be a shared characteristic among various NUP98 fusion proteins, including NUP98::NSD1.

Future studies should thus explore how TP53 is maintained repressed in pediatric cancers, exploring epigenetic regulation through CUT&RUN, CUT&Tag, and ATACseq for histone modifications and chromatin accessibility analysis at the TP53 locus and its target genes. These epigenetic profiles should be compared with those in normal tissue and adult cancers. CRISPR-Cas9 screens targeting TP53 regulators (library in this thesis) using TP53 knock-in reporters should be conducted to identify putative fetal TP53 regulators enabling fine-tuned regulation in pediatric AML subgroups.

Furthermore, the synergistic combination of Idasanutlin, Navitoclax, and 5-Azacytidine observed in this study warrants further investigation in preclinical models and potentially clinical trials. Given the known side effects of Navitoclax, the use of selective BCL-xL PROTAC may represent an attractive alternative. Additionally, the role of 5-Azacytidine in affecting fetal gene signatures and/or TP53 regulation through its inhibitory function on DNMTs should be explored, potentially expanding its application in infant AML. Since Menin inhibitors have recently attracted attention for treating NUP98-rearrange leukemia (Heikamp, Henrich et al. 2022), it would be valuable to assess combinatorial treatments using these inhibitors alongside the targeted therapies presented in this thesis (Idasanutlin, Navitoclax, and 5-Azacytidine) and to explore how TP53 pathway is affected by this epigenetic drug.

Novel treatments, such as ADCs and immunotherapy, are currently under investigation for pediatric AML (Chen and Glasser 2020, Conneely and Stevens 2021). Oncofetal signatures may present a promising avenue for broad tumor targeting. A notable example is oncofetal chondroitin sulfate (ofCS), which has been the focus of recent studies exploring anti-ofCS antibody drug conjugates and bispecific immune cell engagers (Skeltved, Nordmaj et al. 2023, Vidal-Calvo, Martin-Salazar et al. 2024). Thus, leveraging oncofetal genes expressed on the surface of leukemic blasts could help identify potential targets for precision therapy with ADCs or immunotherapy (Tan, Yong et al. 2018, Skeltved, Nordmaj et al. 2023, Vidal-Calvo, Martin-Salazar et al. 2024). Additionally, it would be appealing to assess whether the TP53 re-activation or the deregulation of fetal oncogenes may influence the expression of specific surface-cell markers, potentially enhancing the treatment response. To advance this approach, preclinical studies will be essential to evaluate the safety and efficacy of these antibody fragments formulated as ADCs and bispecific immune engagers.

These studies will pave the way for more targeted and effective treatments in pediatric AML.

8. References

Afreen, S., S. Bohler, A. Müller, E. M. Demmerath, J. M. Weiss, J. S. Jutzi, K. Schachtrup, M. Kunze and M. Erlacher (2020). "BCL-XL expression is essential for human erythropoiesis and engraftment of hematopoietic stem cells." Cell Death Dis **11**(1): 8.

Agarwal, S., F. Afaq, P. Bajpai, H. G. Kim, A. Elkholy, M. Behring, D. S. Chandrashekar, S. A. Diffalha, M. Khushman, S. P. Sugandha, S. Varambally and U. Manne (2022). "DCZ0415, a small-molecule inhibitor targeting TRIP13, inhibits EMT and metastasis via inactivation of the FGFR4/STAT3 axis and the Wnt/β-catenin pathway in colorectal cancer." Mol Oncol **16**(8): 1728-1745.

Ahn, J. H., E. S. Davis, T. A. Daugird, S. Zhao, I. Y. Quiroga, H. Uryu, J. Li, A. J. Storey, Y. H. Tsai, D. P. Keeley, S. G. Mackintosh, R. D. Edmondson, S. D. Byrum, L. Cai, A. J. Tackett, D. Zheng, W. R. Legant, D. H. Phanstiel and G. G. Wang (2021). "Phase separation drives aberrant chromatin looping and cancer development." Nature **595**(7868): 591-595.

Akashi, K., D. Traver, T. Miyamoto and I. L. Weissman (2000). "A clonogenic common myeloid progenitor that gives rise to all myeloid lineages." Nature **404**(6774): 193-197.

Anbarasan, T. and J. C. Bourdon (2019). "The Emerging Landscape of p53 Isoforms in Physiology, Cancer and Degenerative Diseases." Int J Mol Sci **20**(24).

Andrysik, Z., K. D. Sullivan, J. S. Kieft and J. M. Espinosa (2022). "PPM1D suppresses p53-dependent transactivation and cell death by inhibiting the Integrated Stress Response." Nat Commun **13**(1): 7400.

Asai, T., Y. Liu, N. Bae and S. D. Nimer (2011). "The p53 tumor suppressor protein regulates hematopoietic stem cell fate." J Cell Physiol **226**(9): 2215-2221.

Athale, U. H., B. I. Razzouk, S. C. Raimondi, X. Tong, F. G. Behm, D. R. Head, D. K. Srivastava, J. E. Rubnitz, L. Bowman, C. H. Pui and R. C. Ribeiro (2001). "Biology and outcome of childhood acute megakaryoblastic leukemia: a single institution's experience." Blood **97**(12): 3727-3732.

Aung, M. M. K., M. L. Mills, J. Bittencourt-Silvestre and K. Keeshan (2021). "Insights into the molecular profiles of adult and paediatric acute myeloid leukaemia." Mol Oncol **15**(9): 2253-2272.

Awada, H., M. K. Mustafa Ali, B. Thapa, H. Awada, L. Seymour, L. Liu, C. Gurnari, A. Kishtagari, E. Wang and M. R. Baer (2022). "A Focus on Intermediate-Risk Acute Myeloid Leukemia: Sub-Classification Updates and Therapeutic Challenges." Cancers (Basel) **14**(17).

Banerjee, R., N. Russo, M. Liu, V. Basrur, E. Bellile, N. Palanisamy, C. S. Scanlon, E. van Tubergen, R. C. Inglehart, T. Metwally, R. S. Mani, A. Yocum, M. K. Nyati, R. M. Castilho, S. Varambally, A. M. Chinnaiyan and N. J. D'Silva (2014). "TRIP13 promotes error-prone nonhomologous end joining and induces chemoresistance in head and neck cancer." Nat Commun **5**: 4527.

Becker, A. J., C. E. Mc and J. E. Till (1963). "Cytological demonstration of the clonal nature of spleen colonies derived from transplanted mouse marrow cells." Nature **197**: 452-454.

Benjamini, Y. and Y. Hochberg (1995). "Controlling the False Discovery Rate: A Practical and Powerful Approach to Multiple Testing." Journal of the Royal Statistical Society: Series B (Methodological) **57**(1): 289-300.

Benveniste, P., C. Frelin, S. Janmohamed, M. Barbara, R. Herrington, D. Hyam and N. N. Iscove (2010). "Intermediate-term hematopoietic stem cells with extended but time-limited reconstitution potential." Cell Stem Cell **6**(1): 48-58.

Bertrums, E. J. M., J. L. Smith, L. Harmon, R. E. Ries, Y. J. Wang, T. A. Alonzo, A. J. Menssen, K. M. Chisholm, A. R. Leonti, K. Tarlock, F. Ostronoff, E. L. Pogosova-Agadjanyan, G. J. L. Kaspers, H. Hasle, M. Dworzak, C. Walter, N. Muhlegger, C. Morerio, L. Pardo, B. Hirsch, S. Raimondi, T. M. Cooper, R. Aplenc, A. S. Gamis, E. A. Kolb, J. E. Farrar, D. Stirewalt, X. Ma, T. I. Shaw, S. N. Furlan, L. E. Brodersen, M. R. Loken, M. M. Van den Heuvel-Eibrink, C. M. Zwaan, T. J. Triche, B. F. Goemans and S. Meshinchi (2023). "Comprehensive molecular and clinical characterization of NUP98 fusions in pediatric acute myeloid leukemia." Haematologica.

Bhansali, R. S., K. W. Pratz and C. Lai (2023). "Recent advances in targeted therapies in acute myeloid leukemia." J Hematol Oncol **16**(1): 29.

Bigas, A., L. Galán Palma, G. M. Kartha and A. Giorgetti (2022). "Using Pluripotent Stem Cells to Understand Normal and Leukemic Hematopoietic Development." Stem Cells Transl Med **11**(11): 1123-1134.

Bolouri, H., J. E. Farrar, T. Triche, Jr., R. E. Ries, E. L. Lim, T. A. Alonzo, Y. Ma, R. Moore, A. J. Mungall, M. A. Marra, J. Zhang, X. Ma, Y. Liu, Y. Liu, J. M. G. Auvil, T. M. Davidsen, P. Gesuwan, L. C. Hermida, B. Salhia, S. Capone, G. Ramsingh, C. M. Zwaan, S. Noort, S. R. Piccolo, E. A. Kolb, A. S. Gamis, M. A. Smith, D. S. Gerhard and S. Meshinchi (2018). "The molecular landscape of pediatric acute myeloid leukemia reveals recurrent structural alterations and age-specific mutational interactions." Nat Med **24**(1): 103-112.

Bonnet, D. and J. E. Dick (1997). "Human acute myeloid leukemia is organized as a hierarchy that originates from a primitive hematopoietic cell." Nat Med **3**(7): 730-737.

Börner, G. V., A. Barot and N. Kleckner (2008). "Yeast Pch2 promotes domainal axis organization, timely recombination progression, and arrest of defective recombinosomes during meiosis." Proc Natl Acad Sci U S A **105**(9): 3327-3332.

Bowie, M. B., D. G. Kent, B. Dykstra, K. D. McKnight, L. McCaffrey, P. A. Hoodless and C. J. Eaves (2007). "Identification of a new intrinsically timed developmental checkpoint that reprograms key hematopoietic stem cell properties." Proc Natl Acad Sci U S A **104**(14): 5878-5882.

Bowman, R. L., L. Busque and R. L. Levine (2018). "Clonal Hematopoiesis and Evolution to Hematopoietic Malignancies." Cell Stem Cell **22**(2): 157-170.

Bowry, A., R. D. W. Kelly and E. Petermann (2021). "Hypertranscription and replication stress in cancer." Trends Cancer **7**(9): 863-877.

Buenrostro, J. D., M. R. Corces, C. A. Lareau, B. Wu, A. N. Schep, M. J. Aryee, R. Majeti, H. Y. Chang and W. J. Greenleaf (2018). "Integrated Single-Cell Analysis Maps the Continuous Regulatory Landscape of Human Hematopoietic Differentiation." Cell **173**(6): 1535-1548.e1516.

Bulanova, D., Y. Akimov, W. Senkowski, J. Oikkonen, L. Gall-Mas, S. Timonen, M. Elmadani, J. Hynninen, S. Hautaniemi, T. Aittokallio and K. Wennerberg (2024). "A synthetic lethal dependency on casein kinase 2 in response to replication-perturbing therapeutics in RB1-deficient cancer cells." Sci Adv **10**(21): eadj1564.

Calvanese, V. and H. K. A. Mikkola (2023). "The genesis of human hematopoietic stem cells." Blood **142**(6): 519-532.

Calvi, L. M. and D. C. Link (2015). "The hematopoietic stem cell niche in homeostasis and disease." Blood **126**(22): 2443-2451.

Camiolo, G., C. G. Mullen and K. Ottersbach (2024). "Mechanistic insights into the developmental origin of pediatric hematologic disorders." Exp Hematol: 104583.

Capelson, M., Y. Liang, R. Schulte, W. Mair, U. Wagner and M. W. Hetzer (2010). "Chromatin-bound nuclear pore components regulate gene expression in higher eukaryotes." Cell **140**(3): 372-383.

Capitanio, J. S., B. Montpetit and R. W. Wozniak (2017). "Human Nup98 regulates the localization and activity of DExH/D-box helicase DHX9." Elife **6**.

Cardin, S., M. Bilodeau, M. Roussy, L. Aubert, T. Milan, L. Jouan, A. Rouette, L. Laramée, P. Gendron, J. Duchaine, H. Decaluwe, J. F. Spinella, S. Mourad, F. Couture, D. Sinnett, É. Haddad, J. R. Landry, J. Ma, R. K. Humphries, P. P. Roux, J. Hébert, T. A. Gruber, B. T. Wilhelm and S. Cellot (2019). "Human models of NUP98-KDM5A megakaryocytic leukemia in mice contribute to uncovering new biomarkers and therapeutic vulnerabilities." Blood Adv **3**(21): 3307-3321.

Cardoso da Silva, R. and G. Vader (2021). "Getting there: understanding the chromosomal recruitment of the AAA+ ATPase Pch2/TRIP13 during meiosis." Curr Genet **67**(4): 553-565.

Chen, C., A. Jomaa, J. Ortega and E. E. Alani (2014). "Pch2 is a hexameric ring ATPase that remodels the chromosome axis protein Hop1." Proc Natl Acad Sci U S A **111**(1): E44-53.

Chen, J. and C. L. Glasser (2020). "New and Emerging Targeted Therapies for Pediatric Acute Myeloid Leukemia (AML)." Children **7**(2): 12.

Chen, S., Y. Zhou, Y. Chen and J. Gu (2018). "fastp: an ultra-fast all-in-one FASTQ preprocessor." Bioinformatics **34**(17): i884-i890.

Chen, S. H., H. H. Lin, Y. F. Li, W. C. Tsai and D. Y. Hueng (2021). "Clinical Significance and Systematic Expression Analysis of the Thyroid Receptor Interacting Protein 13 (TRIP13) as Human Gliomas Biomarker." Cancers (Basel) **13**(10).

Cheng, C.-K., Y.-L. Yung, H.-Y. Chan, K.-T. Leung, K. Y. Y. Chan, A. W. K. Leung, F. W. T. Cheng, C.-K. Li, T. S. K. Wan, X. Luo, H.-A. Pitts, J. S. Cheung, N. P. H. Chan and M. H. L. Ng (2023). "Deep genomic characterization highlights complexities and prognostic markers of pediatric acute myeloid leukemia." Communications Biology **6**(1): 356.
Cheng, H., Z. Zheng and T. Cheng (2019). "New paradigms on hematopoietic stem cell differentiation." Protein & Cell **11**(1): 34-44.
Conneely, S. E. and A. M. Stevens (2021). "Acute Myeloid Leukemia in Children: Emerging Paradigms in Genetics and New Approaches to Therapy." Curr Oncol Rep **23**(2): 16.
Cooper, T. M., M. J. Absalon, T. A. Alonzo, R. B. Gerbing, K. J. Leger, B. A. Hirsch, J. Pollard, B. I. Razzouk, R. Aplenc and E. A. Kolb (2020). "Phase I/II Study of CPX-351 Followed by Fludarabine, Cytarabine, and Granulocyte-Colony Stimulating Factor for Children With Relapsed Acute Myeloid Leukemia: A Report From the Children's Oncology Group." Journal of Clinical Oncology **38**(19): 2170-2177.
Creutzig, U., M. M. van den Heuvel-Eibrink, B. Gibson, M. N. Dworzak, S. Adachi, E. de Bont, J. Harbott, H. Hasle, D. Johnston, A. Kinoshita, T. Lehrnbecher, G. Leverger, E. Mejstrikova, S. Meshinchi, A. Pession, S. C. Raimondi, L. Sung, J. Stary, C. M. Zwaan, G. J. Kaspers and D. Reinhardt (2012). "Diagnosis and management of acute myeloid leukemia in children and adolescents: recommendations from an international expert panel." Blood **120**(16): 3187-3205.
Daver, N., A. H. Wei, D. A. Pollyea, A. T. Fathi, P. Vyas and C. D. DiNardo (2020). "New directions for emerging therapies in acute myeloid leukemia: the next chapter." Blood Cancer Journal **10**(10): 107.
de Rooij, J. D., C. Branstetter, J. Ma, Y. Li, M. P. Walsh, J. Cheng, A. Obulkasim, J. Dang, J. Easton, L. J. Verboon, H. L. Mulder, M. Zimmermann, C. Koss, P. Gupta, M. Edmonson, M. Rusch, J. Y. Lim, K. Reinhardt, M. Pigazzi, G. Song, A. E. Yeoh, L. Y. Shih, D. C. Liang, S. Halene, D. S. Krause, J. Zhang, J. R. Downing, F. Locatelli, D. Reinhardt, M. M. van den Heuvel-Eibrink, C. M. Zwaan, M. Fornerod and T. A. Gruber (2017). "Pediatric non-Down syndrome acute megakaryoblastic leukemia is characterized by distinct genomic subsets with varying outcomes." Nat Genet **49**(3): 451-456.
de Rooij, J. D., I. H. Hollink, S. T. Arentsen-Peters, J. F. van Galen, H. Berna Beverloo, A. Baruchel, J. Trka, D. Reinhardt, E. Sonneveld, M. Zimmermann, T. A. Alonzo, R. Pieters, S. Meshinchi, M. M. van den Heuvel-Eibrink and C. M. Zwaan (2013). "NUP98/JARID1A is a novel recurrent abnormality in pediatric acute megakaryoblastic leukemia with a distinct HOX gene expression pattern." Leukemia **27**(12): 2280-2288.
de Rooij, J. D., R. Masetti, M. M. van den Heuvel-Eibrink, J. M. Cayuela, J. Trka, D. Reinhardt, M. Rasche, E. Sonneveld, T. A. Alonzo, M. Fornerod, M. Zimmermann, M. Pigazzi, R. Pieters, S. Meshinchi, C. M. Zwaan and F. Locatelli (2016). "Recurrent abnormalities can be used for risk group stratification in pediatric AMKL: a retrospective intergroup study." Blood **127**(26): 3424-3430.
de Smith, A. J. and L. G. Spector (2024). "In Utero Origins of Acute Leukemia in Children." Biomedicines **12**(1).
Deng, W., J. Li, K. Dorrah, D. Jimenez-Tapia, B. Arriaga, Q. Hao, W. Cao, Z. Gao, J. Vadgama and Y. Wu (2020). "The role of PPM1D in cancer and advances in studies of its inhibitors." Biomed Pharmacother **125**: 109956.
Dignum, T., B. Varnum-Finney, S. R. Srivatsan, S. Dozono, O. Waltner, A. M. Heck, T. Ishida, C. Nourigat-McKay, D. L. Jackson, S. Rafii, C. Trapnell, I. D. Bernstein and B. Hadland (2021). "Multipotent progenitors and hematopoietic stem cells arise independently from hemogenic endothelium in the mouse embryo." Cell Rep **36**(11): 109675.
DiNardo, C. D. and J. E. Cortes (2016). "Mutations in AML: prognostic and therapeutic implications." Hematology Am Soc Hematol Educ Program **2016**(1): 348-355.
Döhner, H., E. Estey, D. Grimwade, S. Amadori, F. R. Appelbaum, T. Büchner, H. Dombret, B. L. Ebert, P. Fenaux, R. A. Larson, R. L. Levine, F. Lo-Coco, T. Naoe, D. Niederwieser, G. J. Ossenkoppele, M. Sanz, J. Sierra, M. S. Tallman, H. F. Tien, A. H. Wei, B. Löwenberg and C. D. Bloomfield (2017). "Diagnosis and management of AML in adults: 2017 ELN recommendations from an international expert panel." Blood **129**(4): 424-447.
Domingo-Reinés, J., R. Montes, A. Garcia-Moreno, A. Gallardo, J. M. Sanchez-Manas, I. Ellson, M. Lamolda, C. Calabro, J. A. López-Escamez, P. Catalina, P. Carmona-Sáez, P. J. Real, D. Landeira and V.

Ramos-Mejia (2023). "The pediatric leukemia oncoprotein NUP98-KDM5A induces genomic instability that may facilitate malignant transformation." Cell Death Dis **14**(6): 357.
Dong, S., K. Hu, Y. Shi, G. Wang, D. Yu, Y. Zhao, H. Zhang, Y. Wang, H. Sun, Z. Xu, Q. Jia, Y. Li, Y. Li, B. Li, J. Shi and W. Zhu (2024). "Design and synthesis of cantharidin derivative DCZ5418 as a TRIP13 inhibitor with anti-multiple myeloma activity in vitro and in vivo." Bioorg Med Chem Lett **98**: 129590.
Dzierzak, E. and A. Bigas (2018). "Blood Development: Hematopoietic Stem Cell Dependence and Independence." Cell Stem Cell **22**(5): 639-651.
Elgarten, C. W. and R. Aplenc (2020). "Pediatric acute myeloid leukemia: updates on biology, risk stratification, and therapy." Current Opinion in Pediatrics **32**(1): 57-66.
Eng, J. K., A. L. McCormack and J. R. Yates (1994). "An approach to correlate tandem mass spectral data of peptides with amino acid sequences in a protein database." J Am Soc Mass Spectrom **5**(11): 976-989.
Estey, E. H. (2018). "Acute myeloid leukemia: 2019 update on risk-stratification and management." Am J Hematol **93**(10): 1267-1291.
Franks, T. M., A. McCloskey, M. N. Shokirev, C. Benner, A. Rathore and M. W. Hetzer (2017). "Nup98 recruits the Wdr82-Set1A/COMPASS complex to promoters to regulate H3K4 trimethylation in hematopoietic progenitor cells." Genes Dev **31**(22): 2222-2234.
Garcia-Alegria, E., S. Menegatti, M. Z. H. Fadlullah, P. Menendez, G. Lacaud and V. Kouskoff (2018). "Early Human Hemogenic Endothelium Generates Primitive and Definitive Hematopoiesis In Vitro." Stem Cell Reports **11**(5): 1061-1074.
Garcia, L., J. Bolleman, S. Gehant, N. Redaschi, M. Martin and C. UniProt (2019) "FAIR adoption, assessment and challenges at UniProt." Scientific data **6**, 175 DOI: 10.1038/s41597-019-0180-9.
Geredeli, C., M. Artac, S. Yildirim, A. Inal, I. Dede, T. Guler, M. C. Boruban, L. Koral, M. Karaagac, A. G. Zamani, T. Altinok, O. Aribas, H. Bozcuk and A. Demirkazik (2015). "Prognostic value of ERCC1, ERCC2, XRCC1, and TP53 single nucleotide polymorphisms in patients with early-stage non-small cell lung cancer." Tumour Biol **36**(6): 4279-4285.
Getz, K. D., J. E. Szymczak, Y. Li, R. Madding, Y.-S. V. Huang, C. Aftandilian, S. D. Arnold, K. O. Bona, E. Caywood, A. B. Collier, M. M. Gramatges, M. Henry, C. Lotterman, K. Maloney, A. Mian, R. Mody, E. Morgan, E. A. Raetz, J. Rubnitz, A. Verma, N. Winick, J. J. Wilkes, J. C. Yu, B. T. Fisher and R. Aplenc (2021). "Medical Outcomes, Quality of Life, and Family Perceptions for Outpatient vs Inpatient Neutropenia Management After Chemotherapy for Pediatric Acute Myeloid Leukemia." JAMA Network Open **4**(10): e2128385-e2128385.
Gialesaki, S., D. Bräuer-Hartmann, H. Issa, R. Bhayadia, O. Alejo-Valle, L. Verboon, A.-L. Schmell, S. Laszig, E. Regényi, K. Schuschel, M. Labuhn, M. Ng, R. Winkler, C. Ihling, A. Sinz, M. Glaß, S. Hüttelmaier, S. Matzk, L. Schmid, F. J. Strüwe, S.-K. Kadel, D. Reinhardt, M.-L. Yaspo, D. Heckl and J.-H. Klusmann (2023). "RUNX1 isoform disequilibrium promotes the development of trisomy 21–associated myeloid leukemia." Blood **141**(10): 1105-1118.
Gough, S. M., F. Lee, F. Yang, R. L. Walker, Y. J. Zhu, M. Pineda, M. Onozawa, Y. J. Chung, S. Bilke, E. K. Wagner, J. M. Denu, Y. Ning, B. Xu, G. G. Wang, P. S. Meltzer and P. D. Aplan (2014). "NUP98-PHF23 is a chromatin-modifying oncoprotein that causes a wide array of leukemias sensitive to inhibition of PHD histone reader function." Cancer Discov **4**(5): 564-577.
Gough, S. M., C. I. Slape and P. D. Aplan (2011). "NUP98 gene fusions and hematopoietic malignancies: common themes and new biologic insights." Blood **118**(24): 6247-6257.
Gress, V., M. Roussy, L. Boulianne, M. Bilodeau, S. Cardin, N. El-Hachem, V. Lisi, B. Khakipoor, A. Rouette, A. Farah, L. Théret, L. Aubert, F. Fatima, É. Audemard, P. Thibault, É. Bonneil, J. Chagraoui, L. Laramée, P. Gendron, L. Jouan, S. Jammali, B. Paré, S. M. Simpson, T. H. Tran, M. Duval, P. Teira, H. Bittencourt, R. Santiago, F. Barabé, G. Sauvageau, M. A. Smith, J. Hébert, P. P. Roux, T. A. Gruber, V. P. Lavallée, B. T. Wilhelm and S. Cellot (2024). "CBFA2T3::GLIS2 pediatric acute megakaryoblastic leukemia is sensitive to BCL-XL inhibition by navitoclax and DT2216." Blood Adv **8**(1): 112-129.
Gruber, T. A. and J. R. Downing (2015). "The biology of pediatric acute megakaryoblastic leukemia." Blood **126**(8): 943-949.

Gruber, T. A., A. Larson Gedman, J. Zhang, C. S. Koss, S. Marada, H. Q. Ta, S. C. Chen, X. Su, S. K. Ogden, J. Dang, G. Wu, V. Gupta, A. K. Andersson, S. Pounds, L. Shi, J. Easton, M. I. Barbato, H. L. Mulder, J. Manne, J. Wang, M. Rusch, S. Ranade, R. Ganti, M. Parker, J. Ma, I. Radtke, L. Ding, G. Cazzaniga, A. Biondi, S. M. Kornblau, F. Ravandi, H. Kantarjian, S. D. Nimer, K. Döhner, H. Döhner, T. J. Ley, P. Ballerini, S. Shurtleff, D. Tomizawa, S. Adachi, Y. Hayashi, A. Tawa, L. Y. Shih, D. C. Liang, J. E. Rubnitz, C. H. Pui, E. R. Mardis, R. K. Wilson and J. R. Downing (2012). "An Inv(16)(p13.3q24.3)-encoded CBFA2T3-GLIS2 fusion protein defines an aggressive subtype of pediatric acute megakaryoblastic leukemia." Cancer Cell **22**(5): 683-697.

Guzzi, N., M. Cieśla, P. C. T. Ngoc, S. Lang, S. Arora, M. Dimitriou, K. Pimková, M. N. E. Sommarin, R. Munita, M. Lubas, Y. Lim, K. Okuyama, S. Soneji, G. Karlsson, J. Hansson, G. Jönsson, A. H. Lund, M. Sigvardsson, E. Hellström-Lindberg, A. C. Hsieh and C. Bellodi (2018). "Pseudouridylation of tRNA-Derived Fragments Steers Translational Control in Stem Cells." Cell **173**(5): 1204-1216.e1226.

Guzzi, N., S. Muthukumar, M. Cieśla, G. Todisco, P. C. T. Ngoc, M. Madej, R. Munita, S. Fazio, S. Ekström, T. Mortera-Blanco, M. Jansson, Y. Nannya, M. Cazzola, S. Ogawa, L. Malcovati, E. Hellström-Lindberg, M. Dimitriou and C. Bellodi (2022). "Pseudouridine-modified tRNA fragments repress aberrant protein synthesis and predict leukaemic progression in myelodysplastic syndrome." Nature Cell Biology **24**(3): 299-306.

Hainaut, P. (2013). TP53: Coordinator of the Processes That Underlie the Hallmarks of Cancer. p53 in the Clinics. P. Hainaut, M. Olivier and K. G. Wiman. New York, NY, Springer New York**:** 1-23.

Hama, T., P. K. Nagesh, P. Chowdhury, B. M. Moore, 2nd, M. M. Yallapu, K. R. Regner and F. Park (2021). "DNA damage is overcome by TRIP13 overexpression during cisplatin nephrotoxicity." JCI Insight **6**(22).

Harrison, P. W., M. R. Amode, O. Austine-Orimoloye, Andrey G. Azov, M. Barba, I. Barnes, A. Becker, R. Bennett, A. Berry, J. Bhai, S. K. Bhurji, S. Boddu, P. R. Branco Lins, L. Brooks, Shashank B. Ramaraju, Lahcen I. Campbell, M. C. Martinez, M. Charkhchi, K. Chougule, A. Cockburn, C. Davidson, Nishadi H. De Silva, K. Dodiya, S. Donaldson, B. El Houdaigui, Tamara E. Naboulsi, R. Fatima, C. G. Giron, T. Genez, D. Grigoriadis, Gurpreet S. Ghattaoraya, J. G. Martinez, Tatiana A. Gurbich, M. Hardy, Z. Hollis, T. Hourlier, T. Hunt, M. Kay, V. Kaykala, T. Le, D. Lemos, D. Lodha, D. Marques-Coelho, G. Maslen, Gabriela A. Merino, Louisse P. Mirabueno, A. Mushtaq, Syed N. Hossain, Denye N. Ogeh, M. P. Sakthivel, A. Parker, M. Perry, I. Piližota, D. Poppleton, I. Prosovetskaia, S. Raj, José G. Pérez-Silva, Ahamed Imran A. Salam, S. Saraf, N. Saraiva-Agostinho, D. Sheppard, S. Sinha, B. Sipos, V. Sitnik, W. Stark, E. Steed, M.-M. Suner, L. Surapaneni, K. Sutinen, F. F. Tricomi, D. Urbina-Gómez, A. Veidenberg, T. A. Walsh, D. Ware, E. Wass, Natalie L. Willhoft, J. Allen, J. Alvarez-Jarreta, M. Chakiachvili, B. Flint, S. Giorgetti, L. Haggerty, Garth R. Ilsley, J. Keatley, Jane E. Loveland, B. Moore, Jonathan M. Mudge, G. Naamati, J. Tate, Stephen J. Trevanion, A. Winterbottom, A. Frankish, S. E. Hunt, F. Cunningham, S. Dyer, Robert D. Finn, Fergal J. Martin and Andrew D. Yates (2023). "Ensembl 2024." Nucleic Acids Research **52**(D1): D891-D899.

Heikamp, E. B., J. A. Henrich, F. Perner, E. M. Wong, C. Hatton, Y. Wen, S. P. Barwe, A. Gopalakrishnapillai, H. Xu, H. J. Uckelmann, S. Takao, Y. Kazansky, Y. Pikman, G. M. McGeehan, E. A. Kolb, A. Kentsis and S. A. Armstrong (2022). "The menin-MLL1 interaction is a molecular dependency in NUP98-rearranged AML." Blood **139**(6): 894-906.

Ho, H.-C. and S. M. Burgess (2011). "Pch2 Acts through Xrs2 and Tel1/ATM to Modulate Interhomolog Bias and Checkpoint Function during Meiosis." PLOS Genetics **7**(11): e1002351.

Hsiao, H. H., M. Y. Yang, Y. C. Liu, H. P. Hsiao, S. B. Tseng, M. C. Chao, T. C. Liu and S. F. Lin (2005). "RBM15-MKL1 (OTT-MAL) fusion transcript in an adult acute myeloid leukemia patient." Am J Hematol **79**(1): 43-45.

Husby, S., E. Hjermind Justesen and K. Grønbæk (2021). "Protein phosphatase, Mg(2+)/Mn(2+)-dependent 1D (PPM1D) mutations in haematological cancer." Br J Haematol **192**(4): 697-705.

Hussain, S., Y. Guo, Y. Huo, J. Shi and Y. Hou (2024). "Regulation of cancer progression by CK2: an emerging therapeutic target." Medical Oncology **41**(5): 94.

Ianevski, A., A. K. Giri and T. Aittokallio (2022). "SynergyFinder 3.0: an interactive analysis and consensus interpretation of multi-drug synergies across multiple samples." Nucleic Acids Research **50**(W1): W739-W743.

Inlay, M. A., D. Bhattacharya, D. Sahoo, T. Serwold, J. Seita, H. Karsunky, S. K. Plevritis, D. L. Dill and I. L. Weissman (2009). "Ly6d marks the earliest stage of B-cell specification and identifies the branchpoint between B-cell and T-cell development." Genes Dev **23**(20): 2376-2381.
Iturri, L., L. Freyer, A. Biton, P. Dardenne, Y. Lallemand and E. Gomez Perdiguero (2021). "Megakaryocyte production is sustained by direct differentiation from erythromyeloid progenitors in the yolk sac until midgestation." Immunity **54**(7): 1433-1446.e1435.
Ivanovs, A., S. Rybtsov, E. S. Ng, E. G. Stanley, A. G. Elefanty and A. Medvinsky (2017). "Human haematopoietic stem cell development: from the embryo to the dish." Development **144**(13): 2323-2337.
Jagannathan-Bogdan, M. and L. I. Zon (2013). "Hematopoiesis." Development **140**(12): 2463-2467.
Jeganathan, K. B., L. Malureanu and J. M. van Deursen (2005). "The Rae1–Nup98 complex prevents aneuploidy by inhibiting securin degradation." Nature **438**(7070): 1036-1039.
Jeong, H., M. Wie, I. J. Baek, G. Sohn, S. H. Um, S. G. Lee, Y. Seo, J. Ra, E. A. Lee, S. Kim, B. G. Kim, R. A. Deshpande, T. T. Paull, J. S. Han, T. Kwon and K. Myung (2022). "TRIP13 Participates in Immediate-Early Sensing of DNA Strand Breaks and ATM Signaling Amplification through MRE11." Cells **11**(24).
Jiang, L., J. Zhang, N. Hu, A. Liu, H. Zhu, L. Li, Y. Tian, X. Chen and L. Quan (2018). "Lentivirus-mediated down-regulation of CK2α inhibits proliferation and induces apoptosis of malignant lymphoma and leukemia cells." Biochem Cell Biol **96**(6): 786-796.
Jochemsen, A. G. and Y. Shiloh (2010). "USP10: friend and foe." Cell **140**(3): 308-310.
Khan, S., X. Zhang, D. Lv, Q. Zhang, Y. He, P. Zhang, X. Liu, D. Thummuri, Y. Yuan, J. S. Wiegand, J. Pei, W. Zhang, A. Sharma, C. R. McCurdy, V. M. Kuruvilla, N. Baran, A. A. Ferrando, Y. M. Kim, A. Rogojina, P. J. Houghton, G. Huang, R. Hromas, M. Konopleva, G. Zheng and D. Zhou (2019). "A selective BCL-X(L) PROTAC degrader achieves safe and potent antitumor activity." Nat Med **25**(12): 1938-1947.
Khoury, J. D., E. Solary, O. Abla, Y. Akkari, R. Alaggio, J. F. Apperley, R. Bejar, E. Berti, L. Busque, J. K. C. Chan, W. Chen, X. Chen, W.-J. Chng, J. K. Choi, I. Colmenero, S. E. Coupland, N. C. P. Cross, D. De Jong, M. T. Elghetany, E. Takahashi, J.-F. Emile, J. Ferry, L. Fogelstrand, M. Fontenay, U. Germing, S. Gujral, T. Haferlach, C. Harrison, J. C. Hodge, S. Hu, J. H. Jansen, R. Kanagal-Shamanna, H. M. Kantarjian, C. P. Kratz, X.-Q. Li, M. S. Lim, K. Loeb, S. Loghavi, A. Marcogliese, S. Meshinchi, P. Michaels, K. N. Naresh, Y. Natkunam, R. Nejati, G. Ott, E. Padron, K. P. Patel, N. Patkar, J. Picarsic, U. Platzbecker, I. Roberts, A. Schuh, W. Sewell, R. Siebert, P. Tembhare, J. Tyner, S. Verstovsek, W. Wang, B. Wood, W. Xiao, C. Yeung and A. Hochhaus (2022). "The 5th edition of the World Health Organization Classification of Haematolymphoid Tumours: Myeloid and Histiocytic/Dendritic Neoplasms." Leukemia **36**(7): 1703-1719.
Kiel, M. J., T. Iwashita, O. H. Yilmaz and S. J. Morrison (2005). "Spatial differences in hematopoiesis but not in stem cells indicate a lack of regional patterning in definitive hematopoietic stem cells." Dev Biol **283**(1): 29-39.
Kondo, M., I. L. Weissman and K. Akashi (1997). "Identification of clonogenic common lymphoid progenitors in mouse bone marrow." Cell **91**(5): 661-672.
Konopleva, M., G. Martinelli, N. Daver, C. Papayannidis, A. Wei, B. Higgins, M. Ott, J. Mascarenhas and M. Andreeff (2020). "MDM2 inhibition: an important step forward in cancer therapy." Leukemia **34**(11): 2858-2874.
Kotsantis, P., E. Petermann and S. J. Boulton (2018). "Mechanisms of Oncogene-Induced Replication Stress: Jigsaw Falling into Place." Cancer Discov **8**(5): 537-555.
Kuusanmäki, H., O. Dufva, M. Vähä-Koskela, A. M. Leppä, J. Huuhtanen, I. Vänttinen, P. Nygren, J. Klievink, J. Bouhlal, P. Pölönen, Q. Zhang, S. Adnan-Awad, C. Mancebo-Pérez, J. Saad, J. Miettinen, K. K. Javarappa, S. Aakko, T. Ruokoranta, S. Eldfors, M. Heinäniemi, K. Theilgaard-Mönch, U. Wartiovaara-Kautto, M. Keränen, K. Porkka, M. Konopleva, K. Wennerberg, M. Kontro, C. A. Heckman and S. Mustjoki (2023). "Erythroid/megakaryocytic differentiation confers BCL-XL dependency and venetoclax resistance in acute myeloid leukemia." Blood **141**(13): 1610-1625.
Labuhn, M., F. F. Adams, M. Ng, S. Knoess, A. Schambach, E. M. Charpentier, A. Schwarzer, J. L. Mateo, J. H. Klusmann and D. Heckl (2018). "Refined sgRNA efficacy prediction improves large- and small-scale CRISPR-Cas9 applications." Nucleic Acids Res **46**(3): 1375-1385.

Lederer, M., N. Bley, C. Schleifer and S. Hüttelmaier (2014). "The role of the oncofetal IGF2 mRNA-binding protein 3 (IGF2BP3) in cancer." Semin Cancer Biol **29**: 3-12.
Lei, H., J. Wang, J. Hu, Q. Zhu and Y. Wu (2021). "Deubiquitinases in hematological malignancies." Biomarker Research **9**(1): 66.
Léveillard, T., L. Andera, N. Bissonnette, L. Schaeffer, L. Bracco, J. M. Egly and B. Wasylyk (1996). "Functional interactions between p53 and the TFIIH complex are affected by tumour-associated mutations." Embo j **15**(7): 1615-1624.
Levine, M. S. and A. J. Holland (2018). "The impact of mitotic errors on cell proliferation and tumorigenesis." Genes Dev **32**(9-10): 620-638.
Ley, T. J., C. Miller, L. Ding, B. J. Raphael, A. J. Mungall, A. Robertson, K. Hoadley, T. J. Triche, Jr., P. W. Laird, J. D. Baty, L. L. Fulton, R. Fulton, S. E. Heath, J. Kalicki-Veizer, C. Kandoth, J. M. Klco, D. C. Koboldt, K. L. Kanchi, S. Kulkarni, T. L. Lamprecht, D. E. Larson, L. Lin, C. Lu, M. D. McLellan, J. F. McMichael, J. Payton, H. Schmidt, D. H. Spencer, M. H. Tomasson, J. W. Wallis, L. D. Wartman, M. A. Watson, J. Welch, M. C. Wendl, A. Ally, M. Balasundaram, I. Birol, Y. Butterfield, R. Chiu, A. Chu, E. Chuah, H. J. Chun, R. Corbett, N. Dhalla, R. Guin, A. He, C. Hirst, M. Hirst, R. A. Holt, S. Jones, A. Karsan, D. Lee, H. I. Li, M. A. Marra, M. Mayo, R. A. Moore, K. Mungall, J. Parker, E. Pleasance, P. Plettner, J. Schein, D. Stoll, L. Swanson, A. Tam, N. Thiessen, R. Varhol, N. Wye, Y. Zhao, S. Gabriel, G. Getz, C. Sougnez, L. Zou, M. D. Leiserson, F. Vandin, H. T. Wu, F. Applebaum, S. B. Baylin, R. Akbani, B. M. Broom, K. Chen, T. C. Motter, K. Nguyen, J. N. Weinstein, N. Zhang, M. L. Ferguson, C. Adams, A. Black, J. Bowen, J. Gastier-Foster, T. Grossman, T. Lichtenberg, L. Wise, T. Davidsen, J. A. Demchok, K. R. Shaw, M. Sheth, H. J. Sofia, L. Yang, J. R. Downing and G. Eley (2013). "Genomic and epigenomic landscapes of adult de novo acute myeloid leukemia." N Engl J Med **368**(22): 2059-2074.
Li, C., J. Xia, R. Franqui-Machin, F. Chen, Y. He, T. C. Ashby, F. Teng, H. Xu, D. Liu, D. Gai, S. K. Johnson, F. van Rhee, S. Janz, J. D. Shaughnessy, Jr., G. Tricot, I. Frech and F. Zhan (2021). "TRIP13 modulates protein deubiquitination and accelerates tumor development and progression of B cell malignancies." J Clin Invest **131**(14).
Li, F., P. Sarangi, D. R. Iyer, H. Feng, L. Moreau, H. Nguyen, C. Clairmont and A. D. D'Andrea (2022). "CHAMP1 binds to REV7/FANCV and promotes homologous recombination repair." Cell Rep **40**(9): 111297.
Li, H., C. Li, W. Zhai, X. Zhang, L. Li, B. Wu, B. Yu, P. Zhang, J. Li, C. P. Cui and L. Zhang (2022). "Destabilization of TP53 by USP10 is essential for neonatal autophagy and survival." Cell Rep **41**(1): 111435.
Li, W., H. Xu, T. Xiao, L. Cong, M. I. Love, F. Zhang, R. A. Irizarry, J. S. Liu, M. Brown and X. S. Liu (2014). "MAGeCK enables robust identification of essential genes from genome-scale CRISPR/Cas9 knockout screens." Genome Biol **15**(12): 554.
Li, Y., W. Kong, W. Yang, R. M. Patel, E. B. Casey, T. Okeyo-Owuor, J. M. White, S. N. Porter, S. A. Morris and J. A. Magee (2020). "Single-Cell Analysis of Neonatal HSC Ontogeny Reveals Gradual and Uncoordinated Transcriptional Reprogramming that Begins before Birth." Cell Stem Cell **27**(5): 732-747.e737.
Li, Z., J. Liu, T. Chen, R. Sun, Z. Liu, B. Qiu, Y. Xu and Z. Zhang (2021). "HMGA1-TRIP13 axis promotes stemness and epithelial mesenchymal transition of perihilar cholangiocarcinoma in a positive feedback loop dependent on c-Myc." J Exp Clin Cancer Res **40**(1): 86.
Lichtman, M. A. (2013). "A historical perspective on the development of the cytarabine (7days) and daunorubicin (3days) treatment regimen for acute myelogenous leukemia: 2013 the 40th anniversary of 7+3." Blood Cells Mol Dis **50**(2): 119-130.
Liu, L., Z. Zhang, X. Xia and J. Lei (2022). "KIF18B promotes breast cancer cell proliferation, migration and invasion by targeting TRIP13 and activating the Wnt/β-catenin signaling pathway." Oncol Lett **23**(4): 112.
Liu, O. G., X. Y. Xiong, C. M. Li, X. S. Zhou and S. S. Li (2018). "Role of Xeroderma Pigmentosum Group D in Cell Cycle and Apoptosis in Cutaneous Squamous Cell Carcinoma A431 Cells." Med Sci Monit **24**: 453-460.

Liu, Y., S. E. Elf, Y. Miyata, G. Sashida, Y. Liu, G. Huang, S. Di Giandomenico, J. M. Lee, A. Deblasio, S. Menendez, J. Antipin, B. Reva, A. Koff and S. D. Nimer (2009). "p53 regulates hematopoietic stem cell quiescence." Cell Stem Cell **4**(1): 37-48.
Lo, Y.-H., C.-N. Chuang and T.-F. Wang (2014). "Pch2 Prevents Mec1/Tel1-Mediated Hop1 Phosphorylation Occurring Independently of Red1 in Budding Yeast Meiosis." PLOS ONE **9**(1): e85687.
Lopez, C. K., E. Noguera, V. Stavropoulou, E. Robert, Z. Aid, P. Ballerini, C. Bilhou-Nabera, H. Lapillonne, F. Boudia, C. Thirant, A. Fagnan, M. L. Arcangeli, S. J. Kinston, M. Diop, B. Job, Y. Lecluse, E. Brunet, L. Babin, J. L. Villeval, E. Delabesse, A. Peters, W. Vainchenker, M. Gaudry, R. Masetti, F. Locatelli, S. Malinge, C. Nerlov, N. Droin, C. Lobry, I. Godin, O. A. Bernard, B. Göttgens, A. Petit, F. Pflumio, J. Schwaller and T. Mercher (2019). "Ontogenic Changes in Hematopoietic Hierarchy Determine Pediatric Specificity and Disease Phenotype in Fusion Oncogene-Driven Myeloid Leukemia." Cancer Discov **9**(12): 1736-1753.
Love, M. I., W. Huber and S. Anders (2014). "Moderated estimation of fold change and dispersion for RNA-seq data with DESeq2." Genome Biol **15**(12): 550.
Lu, S., J. Qian, M. Guo, C. Gu and Y. Yang (2019). "Insights into a Crucial Role of TRIP13 in Human Cancer." Computational and Structural Biotechnology Journal **17**: 854-861.
Lu, W., Z. Mengxuan, R. Ming, G. Zixu, Z. Yong, Z. Simin, Y. Yang, Q. Leqi, S. Kangjie, L. Yanlin, F. Jia, D. Yiteng, W. Chuanyuan and G. Jianying (2022). "TRIP13/FLNA Complex Promotes Tumor Progression and Is Associated with Unfavorable Outcomes in Melanoma." J Oncol **2022**: 1419179.
Lu, Y., J. Gao, P. Wang, H. Chen, X. He, M. Luo, Y. Guo, L. Li, W. Zhuang, B. Zhang, N. Lin, J. Li, Y. Zhou, X. Dong and J. Che (2024). "Discovery of potent small molecule ubiquitin-specific protease 10 inhibitors with anti-hepatocellular carcinoma activity through regulating YAP expression." Eur J Med Chem **272**: 116468.
Machado, C. B., D. A. S. EL, B. M. Dias Nogueira, D. A. S. JBS, D. E. M. F. MO, R. C. Montenegro, D. E. M. MEA and C. A. Moreira-Nunes (2021). "The Relevance of Aurora Kinase Inhibition in Hematological Malignancies." Cancer Diagn Progn **1**(3): 111-126.
Mack, R., L. Zhang, P. Breslin Sj and J. Zhang (2021). "The Fetal-to-Adult Hematopoietic Stem Cell Transition and its Role in Childhood Hematopoietic Malignancies." Stem Cell Rev Rep **17**(6): 2059-2080.
Mapelli, M. and A. Musacchio (2007). "MAD contortions: conformational dimerization boosts spindle checkpoint signaling." Curr Opin Struct Biol **17**(6): 716-725.
Marceau-Renaut, A., N. Duployez, B. Ducourneau, M. Labopin, A. Petit, A. Rousseau, S. Geffroy, M. Bucci, W. Cuccuini, O. Fenneteau, P. Ruminy, B. Nelken, S. Ducassou, V. Gandemer, T. Leblanc, G. Michel, Y. Bertrand, A. Baruchel, G. Leverger, C. Preudhomme and H. Lapillonne (2018). "Molecular Profiling Defines Distinct Prognostic Subgroups in Childhood AML: A Report From the French ELAM02 Study Group." Hemasphere **2**(1): e31.
Marcellino, B. K. (2023). "PPM1D inhibition may allow us to WIP leukemia." Blood **142**(24): 2040-2042.
Masetti, R., V. Guidi, L. Ronchini, N. S. Bertuccio, F. Locatelli and A. Pession (2019). "The changing scenario of non-Down syndrome acute megakaryoblastic leukemia in children." Crit Rev Oncol Hematol **138**: 132-138.
Michmerhuizen, N. L., J. M. Klco and C. G. Mullighan (2020). "Mechanistic insights and potential therapeutic approaches for NUP98-rearranged hematologic malignancies." Blood **136**(20): 2275-2289.
Mikkola, H. K. and S. H. Orkin (2006). "The journey of developing hematopoietic stem cells." Development **133**(19): 3733-3744.
Miller, P. G., M. Sathappa, J. A. Moroco, W. Jiang, Y. Qian, S. Iqbal, Q. Guo, A. O. Giacomelli, S. Shaw, C. Vernier, B. Bajrami, X. Yang, C. Raffier, A. S. Sperling, C. J. Gibson, J. Kahn, C. Jin, M. Ranaghan, A. Caliman, M. Brousseau, E. S. Fischer, R. Lintner, F. Piccioni, A. J. Campbell, D. E. Root, C. W. Garvie and B. L. Ebert (2022). "Allosteric inhibition of PPM1D serine/threonine phosphatase via an altered conformational state." Nature Communications **13**(1): 3778.
Miller, P. G., A. S. Sperling, C. Mayerhofer, M. E. McConkey, J. M. Ellegast, C. Da Silva, D. N. Cohen, C. Wang, A. Sharda, N. Yan, S. Saha, C. Schluter, I. Schechter, M. Słabicki, B. Sandoval, J. Kahn, S. Boettcher, C. J. Gibson, D. T. Scadden, K. Stegmaier, S. Bhatt, R. C. Lindsley and B. L. Ebert (2023).

"PPM1D modulates hematopoietic cell fitness and response to DNA damage and is a therapeutic target in myeloid malignancy." Blood **142**(24): 2079-2091.
Mootha, V. K., C. M. Lindgren, K.-F. Eriksson, A. Subramanian, S. Sihag, J. Lehar, P. Puigserver, E. Carlsson, M. Ridderstråle, E. Laurila, N. Houstis, M. J. Daly, N. Patterson, J. P. Mesirov, T. R. Golub, P. Tamayo, B. Spiegelman, E. S. Lander, J. N. Hirschhorn, D. Altshuler and L. C. Groop (2003). "PGC-1α-responsive genes involved in oxidative phosphorylation are coordinately downregulated in human diabetes." Nature Genetics **34**(3): 267-273.
Morrison, S. J., A. M. Wandycz, H. D. Hemmati, D. E. Wright and I. L. Weissman (1997). "Identification of a lineage of multipotent hematopoietic progenitors." Development **124**(10): 1929-1939.
Morrison, S. J. and I. L. Weissman (1994). "The long-term repopulating subset of hematopoietic stem cells is deterministic and isolatable by phenotype." Immunity **1**(8): 661-673.
Musacchio, A. (2015). "The Molecular Biology of Spindle Assembly Checkpoint Signaling Dynamics." Curr Biol **25**(20): R1002-1018.
Musacchio, A. and E. D. Salmon (2007). "The spindle-assembly checkpoint in space and time." Nat Rev Mol Cell Biol **8**(5): 379-393.
Nahta, R. and R. C. Castellino (2021). "Phosphatase magnesium-dependent 1 δ (PPM1D), serine/threonine protein phosphatase and novel pharmacological target in cancer." Biochem Pharmacol **184**: 114362.
Neo, W. H., M. Lie-A-Ling, M. Z. H. Fadlullah and G. Lacaud (2021). "Contributions of Embryonic HSC-Independent Hematopoiesis to Organogenesis and the Adult Hematopoietic System." Frontiers in Cell and Developmental Biology **9**.
Nestorowa, S., F. K. Hamey, B. Pijuan Sala, E. Diamanti, M. Shepherd, E. Laurenti, N. K. Wilson, D. G. Kent and B. Göttgens (2016). "A single-cell resolution map of mouse hematopoietic stem and progenitor cell differentiation." Blood **128**(8): e20-31.
Newell, L. F. and R. J. Cook (2021). "Advances in acute myeloid leukemia." Bmj **375**: n2026.
Nijnik, A., L. Woodbine, C. Marchetti, S. Dawson, T. Lambe, C. Liu, N. P. Rodrigues, T. L. Crockford, E. Cabuy, A. Vindigni, T. Enver, J. I. Bell, P. Slijepcevic, C. C. Goodnow, P. A. Jeggo and R. J. Cornall (2007). "DNA repair is limiting for haematopoietic stem cells during ageing." Nature **447**(7145): 686-690.
Ning, Y., C. Wang, X. Liu, Y. Du, S. Liu, K. Liu, J. Zhou and C. Zhou (2019). "CK2-mediated CCDC106 phosphorylation is required for p53 degradation in cancer progression." J Exp Clin Cancer Res **38**(1): 131.
Noort, S., P. Wander, T. A. Alonzo, J. Smith, R. E. Ries, R. B. Gerbing, M. E. M. Dolman, F. Locatelli, D. Reinhardt, A. Baruchel, J. Stary, J. J. Molenaar, R. W. Stam, M. M. van den Heuvel-Eibrink, M. C. Zwaan and S. Meshinchi (2021). "The clinical and biological characteristics of NUP98-KDM5A in pediatric acute myeloid leukemia." Haematologica **106**(2): 630-634.
Obszański, P., A. Kozłowska, J. Wańcowiat, J. Twardowska, M. Lejman and J. Zawitkowska (2022). "Molecular-Targeted Therapy of Pediatric Acute Myeloid Leukemia." Molecules **27**(12).
Ogasawara, S., Y. Kiyota, Y. Chuman, A. Kowata, F. Yoshimura, K. Tanino, R. Kamada and K. Sakaguchi (2015). "Novel inhibitors targeting PPM1D phosphatase potently suppress cancer cell proliferation." Bioorg Med Chem **23**(19): 6246-6249.
Oka, M., S. Mura, K. Yamada, P. Sangel, S. Hirata, K. Maehara, K. Kawakami, T. Tachibana, Y. Ohkawa, H. Kimura and Y. Yoneda (2016). "Chromatin-prebound Crm1 recruits Nup98-HoxA9 fusion to induce aberrant expression of Hox cluster genes." Elife **5**: e09540.
Okeyo-Owuor, T., Y. Li, R. M. Patel, W. Yang, E. B. Casey, A. S. Cluster, S. N. Porter, D. Bryder and J. A. Magee (2019). "The efficiency of murine MLL-ENL-driven leukemia initiation changes with age and peaks during neonatal development." Blood Adv **3**(15): 2388-2399.
Orkin, S. H. (1995). "Hematopoiesis: how does it happen?" Curr Opin Cell Biol **7**(6): 870-877.
Orkin, S. H. (2000). "Diversification of haematopoietic stem cells to specific lineages." Nat Rev Genet **1**(1): 57-64.
Orkin, S. H. and L. I. Zon (2008). "Hematopoiesis: an evolving paradigm for stem cell biology." Cell **132**(4): 631-644.

Osawa, M., K. Hanada, H. Hamada and H. Nakauchi (1996). "Long-term lymphohematopoietic reconstitution by a single CD34-low/negative hematopoietic stem cell." Science **273**(5272): 242-245.
Ottersbach, K. (2019). "Endothelial-to-haematopoietic transition: an update on the process of making blood." Biochemical Society Transactions **47**(2): 591-601.
Pagano, L., A. Pulsoni, M. Vignetti, L. Mele, L. Fianchi, M. C. Petti, S. Mirto, P. Falcucci, P. Fazi, G. Broccia, G. Specchia, F. Di Raimondo, L. Pacilli, P. Leoni, S. Ladogana, E. Gallo, A. Venditti, G. Avanzi, A. Camera, V. Liso, G. Leone and F. Mandelli (2002). "Acute megakaryoblastic leukemia: experience of GIMEMA trials." Leukemia **16**(9): 1622-1626.
Palis, J. (2016). "Hematopoietic stem cell-independent hematopoiesis: emergence of erythroid, megakaryocyte, and myeloid potential in the mammalian embryo." FEBS Lett **590**(22): 3965-3974.
Papaemmanuil, E., M. Gerstung, L. Bullinger, V. I. Gaidzik, P. Paschka, N. D. Roberts, N. E. Potter, M. Heuser, F. Thol, N. Bolli, G. Gundem, P. Van Loo, I. Martincorena, P. Ganly, L. Mudie, S. McLaren, S. O'Meara, K. Raine, D. R. Jones, J. W. Teague, A. P. Butler, M. F. Greaves, A. Ganser, K. Döhner, R. F. Schlenk, H. Döhner and P. J. Campbell (2016). "Genomic Classification and Prognosis in Acute Myeloid Leukemia." N Engl J Med **374**(23): 2209-2221.
Patel, S. H., C. Christodoulou, C. Weinreb, Q. Yu, E. L. da Rocha, B. J. Pepe-Mooney, S. Bowling, L. Li, F. G. Osorio, G. Q. Daley and F. D. Camargo (2022). "Lifelong multilineage contribution by embryonic-born blood progenitors." Nature **606**(7915): 747-753.
Paul, F., Y. Arkin, A. Giladi, D. A. Jaitin, E. Kenigsberg, H. Keren-Shaul, D. Winter, D. Lara-Astiaso, M. Gury, A. Weiner, E. David, N. Cohen, F. K. Lauridsen, S. Haas, A. Schlitzer, A. Mildner, F. Ginhoux, S. Jung, A. Trumpp, B. T. Porse, A. Tanay and I. Amit (2015). "Transcriptional Heterogeneity and Lineage Commitment in Myeloid Progenitors." Cell **163**(7): 1663-1677.
Pecháčková, S., K. Burdová and L. Macurek (2017). "WIP1 phosphatase as pharmacological target in cancer therapy." J Mol Med (Berl) **95**(6): 589-599.
Pelcovits, A. and R. Niroula (2020). "Acute Myeloid Leukemia: A Review." R I Med J (2013) **103**(3): 38-40.
Pietras, E. M., D. Reynaud, Y. A. Kang, D. Carlin, F. J. Calero-Nieto, A. D. Leavitt, J. M. Stuart, B. Göttgens and E. Passegué (2015). "Functionally Distinct Subsets of Lineage-Biased Multipotent Progenitors Control Blood Production in Normal and Regenerative Conditions." Cell Stem Cell **17**(1): 35-46.
Pikman, Y., S. K. Tasian, M. L. Sulis, K. Stevenson, T. M. Blonquist, B. Apsel Winger, T. M. Cooper, M. Pauly, K. W. Maloney, M. J. Burke, P. A. Brown, N. Gossai, J. L. McNeer, N. N. Shukla, P. D. Cole, J. M. Kahn, J. Chen, M. J. Barth, J. A. Magee, L. Gennarini, A. A. Adhav, C. M. Clinton, N. Ocasio-Martinez, G. Gotti, Y. Li, S. Lin, A. Imamovic, C. E. Tognon, T. Patel, H. L. Faust, C. F. Contreras, A. Cremer, W. A. Cortopassi, D. Garrido Ruiz, M. P. Jacobson, N. V. Dharia, A. Su, A. L. Robichaud, A. Saur Conway, K. Tarlock, E. Stieglitz, A. E. Place, A. Puissant, S. P. Hunger, A. S. Kim, N. I. Lindeman, L. Gore, K. A. Janeway, L. B. Silverman, J. W. Tyner, M. H. Harris, M. L. Loh and K. Stegmaier (2021). "Matched Targeted Therapy for Pediatric Patients with Relapsed, Refractory, or High-Risk Leukemias: A Report from the LEAP Consortium." Cancer Discov **11**(6): 1424-1439.
Place, A. E., K. Goldsmith, J. P. Bourquin, M. L. Loh, L. Gore, D. A. Morgenstern, Y. Sanzgiri, D. Hoffman, Y. Zhou, J. A. Ross, B. Prine, M. Shebley, M. McNamee, T. Farazi, S. Y. Kim, M. Verdugo, L. Lash-Fleming, C. M. Zwaan and J. Vormoor (2018). "Accelerating drug development in pediatric cancer: a novel Phase I study design of venetoclax in relapsed/refractory malignancies." Future Oncol **14**(21): 2115-2129.
Popescu, D. M., R. A. Botting, E. Stephenson, K. Green, S. Webb, L. Jardine, E. F. Calderbank, K. Polanski, I. Goh, M. Efremova, M. Acres, D. Maunder, P. Vegh, Y. Gitton, J. E. Park, R. Vento-Tormo, Z. Miao, D. Dixon, R. Rowell, D. McDonald, J. Fletcher, E. Poyner, G. Reynolds, M. Mather, C. Moldovan, L. Mamanova, F. Greig, M. D. Young, K. B. Meyer, S. Lisgo, J. Bacardit, A. Fuller, B. Millar, B. Innes, S. Lindsay, M. J. T. Stubbington, M. S. Kowalczyk, B. Li, O. Ashenberg, M. Tabaka, D. Dionne, T. L. Tickle, M. Slyper, O. Rozenblatt-Rosen, A. Filby, P. Carey, A. C. Villani, A. Roy, A. Regev, A. Chédotal, I. Roberts, B. Göttgens, S. Behjati, E. Laurenti, S. A. Teichmann and M. Haniffa (2019). "Decoding human fetal liver haematopoiesis." Nature **574**(7778): 365-371.

Pronk, C. J., D. J. Rossi, R. Månsson, J. L. Attema, G. L. Norddahl, C. K. Chan, M. Sigvardsson, I. L. Weissman and D. Bryder (2007). "Elucidation of the phenotypic, functional, and molecular topography of a myeloerythroid progenitor cell hierarchy." Cell Stem Cell **1**(4): 428-442.
Pullarkat, V. A., N. J. Lacayo, E. Jabbour, J. E. Rubnitz, A. Bajel, T. W. Laetsch, J. Leonard, S. I. Colace, S. L. Khaw, S. A. Fleming, R. J. Mattison, R. Norris, J. T. Opferman, K. G. Roberts, Y. Zhao, C. Qu, M. Badawi, M. Schmidt, B. Tong, J. C. Pesko, Y. Sun, J. A. Ross, D. Vishwamitra, L. Rosenwinkel, S. Y. Kim, A. Jacobson, C. G. Mullighan, T. B. Alexander and W. Stock (2021). "Venetoclax and Navitoclax in Combination with Chemotherapy in Patients with Relapsed or Refractory Acute Lymphoblastic Leukemia and Lymphoblastic Lymphoma." Cancer Discov **11**(6): 1440-1453.
Quotti Tubi, L., C. Gurrieri, A. Brancalion, L. Bonaldi, R. Bertorelle, S. Manni, L. Pavan, F. Lessi, R. Zambello, L. Trentin, F. Adami, M. Ruzzene, L. A. Pinna, G. Semenzato and F. Piazza (2013). "Inhibition of protein kinase CK2 with the clinical-grade small ATP-competitive compound CX-4945 or by RNA interference unveils its role in acute myeloid leukemia cell survival, p53-dependent apoptosis and daunorubicin-induced cytotoxicity." J Hematol Oncol **6**: 78.
Radu, A., M. S. Moore and G. Blobel (1995). "The peptide repeat domain of nucleoporin Nup98 functions as a docking site in transport across the nuclear pore complex." Cell **81**(2): 215-222.
Ranzoni, A. M., A. Tangherloni, I. Berest, S. G. Riva, B. Myers, P. M. Strzelecka, J. Xu, E. Panada, I. Mohorianu, J. B. Zaugg and A. Cvejic (2021). "Integrative Single-Cell RNA-Seq and ATAC-Seq Analysis of Human Developmental Hematopoiesis." Cell Stem Cell **28**(3): 472-487.e477.
Rasche, M., M. Zimmermann, L. Borschel, J. P. Bourquin, M. Dworzak, T. Klingebiel, T. Lehrnbecher, U. Creutzig, J. H. Klusmann and D. Reinhardt (2018). "Successes and challenges in the treatment of pediatric acute myeloid leukemia: a retrospective analysis of the AML-BFM trials from 1987 to 2012." Leukemia **32**(10): 2167-2177.
Reece, K. M. and W. D. Figg (2010). "A novel regulator (USP10) of p53: Implications for tumor suppression and therapeutic targeting." Cancer Biol Ther **9**(8): 583-584.
Reimer, J., S. Knöß, M. Labuhn, E. M. Charpentier, G. Göhring, B. Schlegelberger, J. H. Klusmann and D. Heckl (2017). "CRISPR-Cas9-induced t(11;19)/MLL-ENL translocations initiate leukemia in human hematopoietic progenitor cells in vivo." Haematologica **102**(9): 1558-1566.
Reinhardt, D., E. Antoniou and K. Waack (2022). "Pediatric Acute Myeloid Leukemia-Past, Present, and Future." J Clin Med **11**(3).
Rieger, M. A. and T. Schroeder (2012). "Hematopoiesis." Cold Spring Harb Perspect Biol **4**(12).
Roberts, A. W., J. F. Seymour, J. R. Brown, W. G. Wierda, T. J. Kipps, S. L. Khaw, D. A. Carney, S. Z. He, D. C. Huang, H. Xiong, Y. Cui, T. A. Busman, E. M. McKeegan, A. P. Krivoshik, S. H. Enschede and R. Humerickhouse (2012). "Substantial susceptibility of chronic lymphocytic leukemia to BCL2 inhibition: results of a phase I study of navitoclax in patients with relapsed or refractory disease." J Clin Oncol **30**(5): 488-496.
Rosenbauer, F., B. M. Owens, L. Yu, J. R. Tumang, U. Steidl, J. L. Kutok, L. K. Clayton, K. Wagner, M. Scheller, H. Iwasaki, C. Liu, B. Hackanson, K. Akashi, A. Leutz, T. L. Rothstein, C. Plass and D. G. Tenen (2006). "Lymphoid cell growth and transformation are suppressed by a key regulatory element of the gene encoding PU.1." Nat Genet **38**(1): 27-37.
Rosselló-Tortella, M., G. Ferrer and M. Esteller (2020). "Epitranscriptomics in Hematopoiesis and Hematologic Malignancies." Blood Cancer Discovery **1**(1): 26-31.
Rossi, D. J., D. Bryder, J. M. Zahn, H. Ahlenius, R. Sonu, A. J. Wagers and I. L. Weissman (2005). "Cell intrinsic alterations underlie hematopoietic stem cell aging." Proc Natl Acad Sci U S A **102**(26): 9194-9199.
Roy, A., G. Wang, D. Iskander, S. O'Byrne, N. Elliott, J. O'Sullivan, G. Buck, E. F. Heuston, W. X. Wen, A. R. Meira, P. Hua, A. Karadimitris, A. J. Mead, D. M. Bodine, I. Roberts, B. Psaila and S. Thongjuea (2021). "Transitions in lineage specification and gene regulatory networks in hematopoietic stem/progenitor cells over human development." Cell Rep **36**(11): 109698.
San-Segundo, P. A. and G. S. Roeder (1999). "Pch2 links chromatin silencing to meiotic checkpoint control." Cell **97**(3): 313-324.

Schmoellerl, J., I. A. M. Barbosa, T. Eder, T. Brandstoetter, L. Schmidt, B. Maurer, S. Troester, H. T. T. Pham, M. Sagarajit, J. Ebner, G. Manhart, E. Aslan, S. Terlecki-Zaniewicz, C. Van der Veen, G. Hoermann, N. Duployez, A. Petit, H. Lapillonne, A. Puissant, R. Itzykson, R. Moriggl, M. Heuser, R. Meisel, P. Valent, V. Sexl, J. Zuber and F. Grebien (2020). "CDK6 is an essential direct target of NUP98 fusion proteins in acute myeloid leukemia." Blood **136**(4): 387-400.
Schwarzer, A., S. Emmrich, F. Schmidt, D. Beck, M. Ng, C. Reimer, F. F. Adams, S. Grasedieck, D. Witte, S. Käbler, J. W. H. Wong, A. Shah, Y. Huang, R. Jammal, A. Maroz, M. Jongen-Lavrencic, A. Schambach, F. Kuchenbauer, J. E. Pimanda, D. Reinhardt, D. Heckl and J. H. Klusmann (2017). "The non-coding RNA landscape of human hematopoiesis and leukemia." Nat Commun **8**(1): 218.
Seita, J. and I. L. Weissman (2010). "Hematopoietic stem cell: self-renewal versus differentiation." Wiley Interdiscip Rev Syst Biol Med **2**(6): 640-653.
Siegel, R., D. Naishadham and A. Jemal (2013). "Cancer statistics, 2013." CA Cancer J Clin **63**(1): 11-30.
Siegel, R. L., K. D. Miller and A. Jemal (2020). "Cancer statistics, 2020." CA Cancer J Clin **70**(1): 7-30.
Sievers, F., A. Wilm, D. Dineen, T. J. Gibson, K. Karplus, W. Li, R. Lopez, H. McWilliam, M. Remmert, J. Söding, J. D. Thompson and D. G. Higgins (2011). "Fast, scalable generation of high-quality protein multiple sequence alignments using Clustal Omega." Mol Syst Biol **7**: 539.
Skeltved, N., M. A. Nordmaj, N. T. Berendtsen, R. Dagil, E. M. R. Stormer, N. Al-Nakouzi, K. Jiang, A. Aicher, C. Heeschen, T. Gustavsson, S. Choudhary, I. Gögenur, J. P. Christensen, T. G. Theander, M. Daugaard, A. Salanti and M. A. Nielsen (2023). "Bispecific T cell-engager targeting oncofetal chondroitin sulfate induces complete tumor regression and protective immune memory in mice." J Exp Clin Cancer Res **42**(1): 106.
Sommarin, M. N. E., R. Olofzon, S. Palo, P. Dhapola, S. Soneji, G. Karlsson and C. Böiers (2023). "Single-cell multiomics of human fetal hematopoiesis define a developmental-specific population and a fetal signature." Blood Adv **7**(18): 5325-5340.
Spinozzi, G., V. Tini, L. Mincarelli, B. Falini and M. P. Martelli (2018). A comprehensive RNA-Seq pipeline includes meta-analysis, interactivity and automatic reporting, PeerJ Preprints.
Stemmer, M., T. Thumberger, M. Del Sol Keyer, J. Wittbrodt and J. L. Mateo (2015). "CCTop: An Intuitive, Flexible and Reliable CRISPR/Cas9 Target Prediction Tool." PLoS One **10**(4): e0124633.
Stubbins, R. J., A. Francis, F. Kuchenbauer and D. Sanford (2022). "Management of Acute Myeloid Leukemia: A Review for General Practitioners in Oncology." Curr Oncol **29**(9): 6245-6259.
Subramanian, A., P. Tamayo, V. K. Mootha, S. Mukherjee, B. L. Ebert, M. A. Gillette, A. Paulovich, S. L. Pomeroy, T. R. Golub, E. S. Lander and J. P. Mesirov (2005). "Gene set enrichment analysis: A knowledge-based approach for interpreting genome-wide expression profiles." Proceedings of the National Academy of Sciences **102**(43): 15545-15550.
Sudakin, V., G. K. Chan and T. J. Yen (2001). "Checkpoint inhibition of the APC/C in HeLa cells is mediated by a complex of BUBR1, BUB3, CDC20, and MAD2." J Cell Biol **154**(5): 925-936.
Szklarczyk, D., R. Kirsch, M. Koutrouli, K. Nastou, F. Mehryary, R. Hachilif, A. L. Gable, T. Fang, N. T. Doncheva, S. Pyysalo, P. Bork, L. J. Jensen and C. von Mering (2023). "The STRING database in 2023: protein-protein association networks and functional enrichment analyses for any sequenced genome of interest." Nucleic Acids Res **51**(D1): D638-d646.
Tabata, R., S. Chi, J. Yuda and Y. Minami (2021). "Emerging Immunotherapy for Acute Myeloid Leukemia." Int J Mol Sci **22**(4).
Takayama, K. I., T. Suzuki, T. Fujimura, S. Takahashi and S. Inoue (2018). "Association of USP10 with G3BP2 Inhibits p53 Signaling and Contributes to Poor Outcome in Prostate Cancer." Mol Cancer Res **16**(5): 846-856.
Takeda, A., N. J. Sarma, A. M. Abdul-Nabi and N. R. Yaseen (2010). "Inhibition of CRM1-mediated nuclear export of transcription factors by leukemogenic NUP98 fusion proteins." J Biol Chem **285**(21): 16248-16257.
Tan, H. L., C. Yong, B. Z. Tan, W. J. Fong, J. Padmanabhan, A. Chin, V. Ding, A. Lau, L. Zheng, X. Bi, Y. Yang and A. Choo (2018). "Conservation of oncofetal antigens on human embryonic stem cells enables discovery of monoclonal antibodies against cancer." Scientific Reports **8**(1): 11608.

Tao, Y., G. Yang, H. Yang, D. Song, L. Hu, B. Xie, H. Wang, L. Gao, M. Gao, H. Xu, Z. Xu, X. Wu, Y. Zhang, W. Zhu, F. Zhan and J. Shi (2017). "TRIP13 impairs mitotic checkpoint surveillance and is associated with poor prognosis in multiple myeloma." Oncotarget **8**(16).
Teichner, A., E. Eytan, D. Sitry-Shevah, S. Miniowitz-Shemtov, E. Dumin, J. Gromis and A. Hershko (2011). "p31comet Promotes disassembly of the mitotic checkpoint complex in an ATP-dependent process." Proc Natl Acad Sci U S A **108**(8): 3187-3192.
Terlecki-Zaniewicz, S., T. Humer, T. Eder, J. Schmoellerl, E. Heyes, G. Manhart, N. Kuchynka, K. Parapatics, F. G. Liberante, A. C. Müller, E. M. Tomazou and F. Grebien (2021). "Biomolecular condensation of NUP98 fusion proteins drives leukemogenic gene expression." Nat Struct Mol Biol **28**(2): 190-201.
Thiollier, C., C. K. Lopez, B. Gerby, C. Ignacimouttou, S. Poglio, Y. Duffourd, J. Guégan, P. Rivera-Munoz, O. Bluteau, V. Mabialah, M. Diop, Q. Wen, A. Petit, A. L. Bauchet, D. Reinhardt, B. Bornhauser, D. Gautheret, Y. Lecluse, J. Landman-Parker, I. Radford, W. Vainchenker, N. Dastugue, S. de Botton, P. Dessen, J. P. Bourquin, J. D. Crispino, P. Ballerini, O. A. Bernard, F. Pflumio and T. Mercher (2012). "Characterization of novel genomic alterations and therapeutic approaches using acute megakaryoblastic leukemia xenograft models." J Exp Med **209**(11): 2017-2031.
Till, J. E. and C. E. Mc (1961). "A direct measurement of the radiation sensitivity of normal mouse bone marrow cells." Radiat Res **14**: 213-222.
Umeda, M., J. Ma, T. Westover, Y. Ni, G. Song, J. L. Maciaszek, M. Rusch, D. Rahbarinia, S. Foy, B. J. Huang, M. P. Walsh, P. Kumar, Y. Liu, W. Yang, Y. Fan, G. Wu, S. D. Baker, X. Ma, L. Wang, T. A. Alonzo, J. E. Rubnitz, S. Pounds and J. M. Klco (2024). "A new genomic framework to categorize pediatric acute myeloid leukemia." Nature Genetics **56**(2): 281-293.
Vader, G. (2015). "Pch2TRIP13: controlling cell division through regulation of HORMA domains." Chromosoma **124**(3): 333-339.
Vélez-Cruz, R., S. Manickavinayaham, A. K. Biswas, R. W. Clary, T. Premkumar, F. Cole and D. G. Johnson (2016). "RB localizes to DNA double-strand breaks and promotes DNA end resection and homologous recombination through the recruitment of BRG1." Genes Dev **30**(22): 2500-2512.
Velten, L., S. F. Haas, S. Raffel, S. Blaszkiewicz, S. Islam, B. P. Hennig, C. Hirche, C. Lutz, E. C. Buss, D. Nowak, T. Boch, W. K. Hofmann, A. D. Ho, W. Huber, A. Trumpp, M. A. Essers and L. M. Steinmetz (2017). "Human haematopoietic stem cell lineage commitment is a continuous process." Nat Cell Biol **19**(4): 271-281.
Vidal-Calvo, E. E., A. Martin-Salazar, S. Choudhary, R. Dagil, S. S. R. Raghavan, L. Duvnjak, M. A. Nordmaj, T. M. Clausen, A. Skafte, J. Oberkofler, K. Wang, M. Ø. Agerbæk, C. Løppke, A. M. Jørgensen, D. Ropac, J. Mujollari, S. Willis, A. Garcias López, R. L. Miller, R. T. G. Karlsson, F. Goerdeler, Y.-H. Chen, A. R. Colaço, Y. Wang, T. Lavstsen, A. Martowicz, I. Nelepcu, M. Marzban, H. Z. Oo, M. S. Ørum-Madsen, Y. Wang, M. A. Nielsen, H. Clausen, M. Wierer, D. Wolf, I. Gögenur, T. G. Theander, N. Al-Nakouzi, T. Gustavsson, M. Daugaard and A. Salanti (2024). "Tumor-agnostic cancer therapy using antibodies targeting oncofetal chondroitin sulfate." Nature Communications **15**(1): 7553.
Vogler, M., H. S. Walter and M. J. S. Dyer (2017). "Targeting anti-apoptotic BCL2 family proteins in haematological malignancies - from pathogenesis to treatment." Br J Haematol **178**(3): 364-379.
Wang, G. G., L. Cai, M. P. Pasillas and M. P. Kamps (2007). "NUP98-NSD1 links H3K36 methylation to Hox-A gene activation and leukaemogenesis." Nat Cell Biol **9**(7): 804-812.
Wang, G. G., J. Song, Z. Wang, H. L. Dormann, F. Casadio, H. Li, J. L. Luo, D. J. Patel and C. D. Allis (2009). "Haematopoietic malignancies caused by dysregulation of a chromatin-binding PHD finger." Nature **459**(7248): 847-851.
Wang, J. C., M. Doedens and J. E. Dick (1997). "Primitive human hematopoietic cells are enriched in cord blood compared with adult bone marrow or mobilized peripheral blood as measured by the quantitative in vivo SCID-repopulating cell assay." Blood **89**(11): 3919-3924.
Wang, Y., J. Huang, B. Li, H. Xue, G. Tricot, L. Hu, Z. Xu, X. Sun, S. Chang, L. Gao, Y. Tao, H. Xu, Y. Xie, W. Xiao, D. Yu, Y. Kong, G. Chen, X. Sun, F. Lian, N. Zhang, X. Wu, Z. Mao, F. Zhan, W. Zhu and J. Shi (2020). "A Small-Molecule Inhibitor Targeting TRIP13 Suppresses Multiple Myeloma Progression." Cancer Res **80**(3): 536-548.

Weijts, B., L. Yvernogeau and C. Robin (2021). "Recent Advances in Developmental Hematopoiesis: Diving Deeper With New Technologies." Frontiers in Immunology **12**.
Wilson, A., E. Laurenti, G. Oser, R. C. van der Wath, W. Blanco-Bose, M. Jaworski, S. Offner, C. F. Dunant, L. Eshkind, E. Bockamp, P. Lió, H. R. Macdonald and A. Trumpp (2008). "Hematopoietic stem cells reversibly switch from dormancy to self-renewal during homeostasis and repair." Cell **135**(6): 1118-1129.
Wilson, N. K., D. G. Kent, F. Buettner, M. Shehata, I. C. Macaulay, F. J. Calero-Nieto, M. Sánchez Castillo, C. A. Oedekoven, E. Diamanti, R. Schulte, C. P. Ponting, T. Voet, C. Caldas, J. Stingl, A. R. Green, F. J. Theis and B. Göttgens (2015). "Combined Single-Cell Functional and Gene Expression Analysis Resolves Heterogeneity within Stem Cell Populations." Cell Stem Cell **16**(6): 712-724.
Wu, Y. and K. K. Hirschi (2021). "Regulation of Hemogenic Endothelial Cell Development and Function." Annu Rev Physiol **83**: 17-37.
Xu, H., Z. Ma, X. Mo, X. Chen, F. Xu, F. Wu, H. Chen, G. Zhou, H. Xia and C. Zhang (2022). "Inducing Synergistic DNA Damage by TRIP13 and PARP1 Inhibitors Provides a Potential Treatment for Hepatocellular Carcinoma." J Cancer **13**(7): 2226-2237.
Xu, H., D. G. Valerio, M. E. Eisold, A. Sinha, R. P. Koche, W. Hu, C. W. Chen, S. H. Chu, G. L. Brien, C. Y. Park, J. J. Hsieh, P. Ernst and S. A. Armstrong (2016). "NUP98 Fusion Proteins Interact with the NSL and MLL1 Complexes to Drive Leukemogenesis." Cancer Cell **30**(6): 863-878.
Yamamoto, R., Y. Morita, J. Ooehara, S. Hamanaka, M. Onodera, K. L. Rudolph, H. Ema and H. Nakauchi (2013). "Clonal analysis unveils self-renewing lineage-restricted progenitors generated directly from hematopoietic stem cells." Cell **154**(5): 1112-1126.
Yang, L., D. Bryder, J. Adolfsson, J. Nygren, R. Månsson, M. Sigvardsson and S. E. Jacobsen (2005). "Identification of Lin(-)Sca1(+)kit(+)CD34(+)Flt3- short-term hematopoietic stem cells capable of rapidly reconstituting and rescuing myeloablated transplant recipients." Blood **105**(7): 2717-2723.
Yang, Y.-L., T.-H. Jaing, S.-H. Chen, H.-C. Liu, I.-J. Hung, D.-T. Lin, C.-P. Yang, C.-T. Peng, K.-H. Lin, C.-C. Hsiao, S.-T. Jou, J.-S. Chen, M.-T. Lin, S.-C. Wang, T.-K. Chang, F.-L. Huang, C.-N. Cheng, K.-H. Wu, J.-M. Sheen, S.-H. Chen, M.-Y. Lu, G.-Y. Hung, H.-J. Yen, Y.-L. Hsieh, J.-L. Wang, Y.-H. Chang, H.-H. Chang, T.-C. Yeh, T.-F. Weng, J.-Y. Hou, B.-W. Chen, R.-L. Chen, L.-Y. Wang, W.-L. Ho, Y.-C. Chen, S.-N. Cheng, Y.-H. Chao, S.-H. Yang, T.-H. Huang, S.-W. Chou, C.-Y. Lin, H.-Y. Chen, Y.-M. Y. Chao, D.-C. Liang and T.-T. Chang (2021). "Treatment outcomes of pediatric acute myeloid leukemia: a retrospective analysis from 1996 to 2019 in Taiwan." Scientific Reports **11**(1): 5893.
Yang, Z., X. S. Wu, Y. Wei, S. A. Polyanskaya, S. V. Iyer, M. Jung, F. P. Lach, E. R. Adelman, O. Klingbeil, J. P. Milazzo, M. Kramer, O. E. Demerdash, K. Chang, S. Goodwin, E. Hodges, W. R. McCombie, M. E. Figueroa, A. Smogorzewska and C. R. Vakoc (2021). "Transcriptional Silencing of ALDH2 Confers a Dependency on Fanconi Anemia Proteins in Acute Myeloid Leukemia." Cancer Discovery **11**(9): 2300-2315.
Yassin, E. R., A. M. Abdul-Nabi, A. Takeda and N. R. Yaseen (2010). "Effects of the NUP98-DDX10 oncogene on primary human CD34+ cells: role of a conserved helicase motif." Leukemia **24**(5): 1001-1011.
Yu, D. C., X. Y. Chen, H. Y. Zhou, D. Q. Yu, X. L. Yu, Y. C. Hu, R. H. Zhang, X. B. Zhang, K. Zhang, M. Q. Lin, X. D. Gao and T. W. Guo (2022). "TRIP13 knockdown inhibits the proliferation, migration, invasion, and promotes apoptosis by suppressing PI3K/AKT signaling pathway in U2OS cells." Mol Biol Rep **49**(4): 3055-3064.
Yu, L., Y. Xiao, X. Zhou, J. Wang, S. Chen, T. Peng and X. Zhu (2019). "TRIP13 interference inhibits the proliferation and metastasis of thyroid cancer cells through regulating TTC5/p53 pathway and epithelial-mesenchymal transition related genes expression." Biomed Pharmacother **120**: 109508.
Yuan, J., K. Luo, L. Zhang, J. C. Cheville and Z. Lou (2010). "USP10 regulates p53 localization and stability by deubiquitinating p53." Cell **140**(3): 384-396.
Zaidi, S. K., S. E. Frietze, J. A. Gordon, J. L. Heath, T. Messier, D. Hong, J. R. Boyd, M. Kang, A. N. Imbalzano, J. B. Lian, J. L. Stein and G. S. Stein (2017). "Bivalent Epigenetic Control of Oncofetal Gene Expression in Cancer." Mol Cell Biol **37**(23).

Zamalloa, L. G., M. M. Pruitt, N. M. Hermance, H. Gali, R. L. Flynn and A. L. Manning (2023). "RB loss sensitizes cells to replication-associated DNA damage by PARP inhibition." bioRxiv.
Zanjirband, M., S. Rahgozar and N. Aberuyi (2023). "miR-16-5p enhances sensitivity to RG7388 through targeting PPM1D expression (WIP1) in Childhood Acute Lymphoblastic Leukemia." Cancer Drug Resist **6**(2): 242-256.
Zhang, C. C. and H. F. Lodish (2008). "Cytokines regulating hematopoietic stem cell function." Curr Opin Hematol **15**(4): 307-311.
Zhang, G., Y. Guan, Y. Zhao, T. van der Straaten, S. Xiao, P. Xue, G. Zhu, Q. Liu, Y. Cai, C. Jin, J. Yang, S. Wu and X. Lu (2017). "ERCC2/XPD Lys751Gln alter DNA repair efficiency of platinum-induced DNA damage through P53 pathway." Chem Biol Interact **263**: 55-65.
Zhang, G., Q. Zhu, G. Fu, J. Hou, X. Hu, J. Cao, W. Peng, X. Wang, F. Chen and H. Cui (2019). "TRIP13 promotes the cell proliferation, migration and invasion of glioblastoma through the FBXW7/c-MYC axis." Br J Cancer **121**(12): 1069-1078.
Zhang, W., M. A. Sartori, T. Makhnevych, K. E. Federowicz, X. Dong, L. Liu, S. Nim, A. Dong, J. Yang, Y. Li, D. Haddad, A. Ernst, D. Heerding, Y. Tong, J. Moffat and S. S. Sidhu (2017). "Generation and Validation of Intracellular Ubiquitin Variant Inhibitors for USP7 and USP10." J Mol Biol **429**(22): 3546-3560.
Zhao, W., D. Lu, L. Liu, J. Cai, Y. Zhou, Y. Yang, Y. Zhang and J. Zhang (2017). "Insulin-like growth factor 2 mRNA binding protein 3 (IGF2BP3) promotes lung tumorigenesis via attenuating p53 stability." Oncotarget **8**(55): 93672-93687.
Zhou, K., W. Zhang, Q. Zhang, R. Gui, H. Zhao, X. Chai, Y. Li, X. Wei and Y. Song (2017). "Loss of thyroid hormone receptor interactor 13 inhibits cell proliferation and survival in human chronic lymphocytic leukemia." Oncotarget **8**(15): 25469-25481.
Zhu, J. and S. G. Emerson (2002). "Hematopoietic cytokines, transcription factors and lineage commitment." Oncogene **21**(21): 3295-3313.

9. Appendix

9.1. List of figures

Figure 1 Tree-like hierarchy model 5
Figure 2 The developmental timeline of hematopoiesis in the CS15 (Carnegie stages 15) human embryo. 7
Figure 3 The unique features of fetal and adult HSPCs identified by transcriptomic, epigenetic, proteomic, and functional studies 9
Figure 4 Leukemic fusions in AML by age..... 12
Figure 5 Pediatric and adult AMKL patients are genomically distinct..... 15
Figure 6 Survival of NUP98::KDM5A$^+$ AML 18
Figure 7 Structure of NUP98, KDM5A, and NUP98::KDM5A proteins. 19
Figure 8 A schematic representation of the domain organization of TRIP13. 20
Figure 9 Model describing the role of TRIP13/Pch2 in the regulation of the spindle assembly checkpoint (SAC). 21
Figure 10 Model describing the role of TRIP13/Pch2 in meiotic G2/prophase. 22
Figure 11 Modeling NUP98-KDM5A$^+$ AMKL in murine system..... 47
Figure 12 NUP98::KDM5A induces an aggressive leukemia in fetal HSPCs in vitro. 48
Figure 13 NUP98::KDM5A fusion protein is expressed at very low level in murine primary cells..... 49
Figure 14 NUP98::KDM5A oncoprotein induces a more aggressive leukemia in mFL-HSPCs in vivo. .. 50
Figure 15 NUP98::KDM5A induces transformation only in human fetal HSPCs in vitro. 51
Figure 16 hFL NUP98::KDM5A cells are dependent on low expression of NUP98::KDM5A fusion protein. 52
Figure 17 Identification of Trip13 as selective candidate in fetal NUP98::KDM5A model..... 53
Figure 18 TRIP13/Trip13 expression is upregulated by NUP98::KDM5A oncoprotein retaining the fetal-enrichment 54
Figure 19 Loss of Trip13 induces apoptosis and arrests cell cycle of fetal NUP98::KDM5A$^+$ cells in vitro. 55
Figure 20 Loss of Trip13 do not affect DNA damage response of fetal NUP98::KDM5A$^+$ cells..... 56
Figure 21 Trip13 knockout activates TP53 signaling pathway in fetal NUP98::KDM5A$^+$ cells. 57
Figure 22 Trip13 depletion leads to increased TP53 protein level..... 57
Figure 23 Rescue experiments confirm the mechanism acting through TRIP13/TP53 axis..... 58
Figure 24 TRIP13 might interact with PPM1D/WIP1 and promote TP53 pathway activation. 59
Figure 25 PPM1D/WIP1 mimics TRIP13 60
Figure 26 TRIP13 interacts with PPM1D/WIP1 to repress TP53 60
Figure 27 Loss of Trip13 shows sensitivity in fetal NUP98::KDM5A$^+$ model in vivo. 61
Figure 28 Pharmacological TRIP13 inhibition as treatment of NUP98::KDM5A$^+$ AMKL in vitro 62
Figure 29 Targeting TRIP13 in combination with MDM2 inhibitor as therapeutic strategy for AMKL. 63
Figure 30 Targeting TRIP13 in combination with MDM2 inhibitor as therapeutic strategy for AMKL. 64
Figure 31 Rescue experiments confirm the mechanism acting through TRIP13/TP53 axis..... 65
Figure 32 TP53 pathway based CRISPR-Cas9 in vitro screening combined with Trip13 knockout identifies synthetic-lethal dependencies for combinatorial therapeutic approaches..... 66
Figure 33 Fetal NUP98::KDM5A$^+$ cells are responsive to Navitoclax and 5-Azacytidine..... 67
Figure 34 Triple combination of Idasanutlin, Navitoclax and 5-Azacytidine has high synergistic effect in NUP98::KDM5A models..... 68
Figure 35 Proposed mechanism of TRIP13/PPM1D/TP53 vulnerability in NUP98-KDM5A-driven leukemia. 70

9.2. List of tables

Table 1: List of technical devices 25
Table 2: List of molecular biology reagents 27
Table 3: List of proteomics reagents 28
Table 4: List of cell culture reagents 28
Table 5:List of antibiotics 30
Table 6: Drugs used for *in vitro* experiments 30
Table 7: Antibodies used for flow cytometry and Western Blot 30
Table 8: Cell lines used for *in vitro* experiments 32
Table 9: Vectors used for the experiments 33
Table 10 : sequencing primers used to assess inserted cDNAs and sgRNAs after cloning 35
Table 11 : Single strand oligonucleotides for sgRNA cloning. 36
Table 12: primers used to assess the sgRNA cutting efficiency 38
Table 13: PCR protocol for amplicon sequencing 40
Table 14: Mix used for transfection 43

9.3. List of abbreviations

Hematopoietic stem and progenitor cells (HSPCs); murine fetal liver hematopoietic stem and progenitor cells (mFL-HSPCs); murine bone marrow hematopoietic stem and progenitor cells (mBM-HSPCs); myeloid leukemia associated with Down Syndrome (ML-DS); familial platelet disorder with predisposition to AML (FPD-AML); human fetal liver hematopoietic stem and progenitor cells (hFL-HSPCs); gene set expression analysis (GSEA); hematopoietic stem cells (HSCs); long-term hematopoietic stem cells (LT-HSCs); short-term hematopoietic stem cells (ST-HSCs); bone marrow (BM); multipotent progenitors (MPPs); lymphoid common progenitors (CLPs); myeloid common progenitors (CMPs); granulocyte-monocyte progenitors (GMPs); megakaryocyte-erythrocyte progenitors (MEPs); Carnegie stages (CS); multipotent erythroid-myeloid progenitors (EMPs); aorta-gonad-mesonephros (AGM); aortic hematopoietic clusters (IAHC); endothelial-to-hematopoietic transition (EHT); hemogenic endothelium (HE); transcription factors (TFs); Acute myeloid leukemia (AML); World Health Organization (WHO); acute megakaryoblastic leukemia (AMKL); acute lymphoblastic leukemia (ALL); antibody-drug conjugates (ADCs); Food and Drug Administration (FDA); Chimeric antigen receptor (CAR); Down-syndrome (DS); Nucleoporin 98 (NUP98); nuclear pore complex (NPC); Anaphase-Promoting Complex (APC); phenylalanine-glycine (FG); glycine-leucine-phenylalanine-glycine (GLFG); Gle2-binding-sequence (GLEBS); intrinsically disordered regions (IDRs); Jumonji catalytic domain (JMJ); plant homeodomain (PHD); autoproteolytic cleavage sites (APD); histone 3 lysin 4 methylation (H3K4me); mitotic checkpoint complex (MCC); spindle assembly checkpoint (SAC); anaphase promoting complex/cyclosome (APC/C); synaptonemal complex (SC); DNA strand break (DSB); homology-directed repair (HDR); homologues recombination (HR); nonhomologous end-joining (NHEJ); chromosome instability (CIN); event-free survival (EFS); overall survival (OS); multiple myeloma (MM); squamous cell carcinoma of the head and neck cells (SCCHN); chronic lymphocytic leukemia (CLL); deubiquitinase (DUBs); immunoprecipitation-mass spectrometry (IP/MS); Fanconi anemia

(FA); proteolysis-targeting chimera (PROTAC); hemagglutinin (HA); normalized enrichment scores (NES).

9.4. List of publications and conferences

Cifarelli, L. N., H. Issa, K. Schuschel, K. Menge, L. Gack, C. Ihling, A. Sinz, J.-H. Klusmann and D. Heckl (2023). "TRIP13 Is a Fetal-Enriched Therapeutic Target in NUP98-JARID1A^{+} Pediatric Non-Down Syndrome AMKL." Blood 142(Supplement 1): 711-711.

Cifarelli, L. N., H. Issa, K. Schuschel, K. Menge, L. Gack, C. Ihling, A. Sinz, J.-H. Klusmann and D. Heckl (20xx). "The activation of TP53 pathway is a therapeutic vulnerability in NUP98::KDM5A^{+} pediatric Acute Megakaryoblastic Leukemia " *Manuscript in preparation*

Attended conferences as speaker:

1. August 2024 Frankfurt Cancer Conference
2. June 2024 Kind-Philipp-Meeting
3. December 2023 American Society of Hematology
4. June 2023 Kind-Philipp-Meeting
5. June 2022 Kind-Philipp-Meeting

9.5. Curriculum Vitae

Personal information

Luca Nunzio Cifarelli

Nationality: Italian

Awards:

2023 ASH Abstract Achievement Awards

Academic education

2019-2025	"*The activation of TP53 pathway is a therapeutic vulnerability in NUP98::KDM5A⁺ pediatric Acute Megakaryoblastic Leukemia*" (PhD Thesis) Department of Pediatric Hematology and Oncology, Martin-Luther-University Halle-Wittenberg Scientific employee and PhD Student at the Department of Pediatrics I Supervisors: Prof Heckl and Prof. Jan-Henning Klusmann
2018-2019	"*Minimal Residual Disease (MRD) in Multiple Myeloma and Ph-negative Acute Lymphoblastic Leukemia*" Institute of Hematology and Oncology "L.A Seragnoli"- Sant' Orsola Hospital, Bologna Scientific employee Supervisor: PhD Carolina Terragna
2018	Lower Saxony International Summer Academy (LISA) Certificate Medical Hannover School, Hannover
2015-2017	Master of Science in Functional Genomics and Genetics University of Trieste AND University of Paris VII- Denis-Diderot
2017	"*The role of RAD21 cohesin complex subunit during megakaryopoiesis*" (Master thesis) Gustave Roussy Cancer Campus Grand Paris, Paris, France Master of Science in Functional Genomics and Genetics Supervisor: MD William Vainchenker
2012-2015	Bachelor of Science in Biological Sciences University of Bologna
2015	"*The role of Tp53 mutations on response to first-line TKI treatment in EGFR-mutated NSCLC patients*" (Bachelor Thesis) IRCCS Istituto Scientifico Romagnolo per lo Studio e la Cura dei Tumori (I.R.S.T.), Meldola, Italy Bachelor of Science in Biological Sciences Supervisor: MD Paola Ulivi

9.6. Declaration

I hereby affirm that I wrote the present dissertation independently and without outside help. I have not used any sources or resources other than those indicated by me. The written version of the thesis submitted corresponds to that on the electronic storage medium.

With this thesis, I am applying for the first time to obtain the doctoral degree doctor rerum naturalium.

Frankfurt, November 2024

_____

Luca Nunzio Cifarelli